DELINEATING MIDBRAIN CIRCUITS UNDERLYING MOTIVATED BEHAVIORS

Alice Stamatakis

A dissertation submitted to the faculty at the University of North Carolina at Chapel Hill in partial fulfillment of the requirements for the degree of Doctor of Philosophy in the Graduate School (Neurobiology Curriculum).

Chapel Hill
2014

Approved by:

Garret D. Stuber

Thomas L. Kash

Regina M. Carelli

Spencer L. Smith

Fulton T. Crews

ABSTRACT

Alice Stamatakis: Delineating midbrain circuits underlying motivated behaviors
(Under the direction of Garret Stuber)

Lateral habenula (LHb) neurons convey aversive and negative reward conditions through potent indirect inhibition of ventral tegmental area (VTA) dopaminergic neurons. Although the LHb and VTA reciprocally project to each other, the electrophysiological properties and the behavioral consequences associated with selective manipulations of this circuit are unknown. We found that exposure to aversive stimuli in mice increased LHb excitatory drive onto RMTg neurons. Furthermore, optogenetic activation of this pathway promoted active, passive and conditioned behavioral avoidance. Thus, activity of LHb efferents to the midbrain is aversive, but can also serve to negatively reinforce behavioral responding. Aspects of this behavioral phenotype were recapitulated by optogenetically activating lateral hypothalamic (LH) glutamatergic inputs to the LHb, suggesting that the LH may be an important upstream contributor to aversive signaling of LHb neurons. Optogenetic activation of VTA dopaminergic inputs to the LHb resulted in no detectable dopamine release in LHb brain slices. Instead, stimulation produced GABA-mediated inhibitory synaptic transmission, which suppressed the firing of postsynaptic LHb neurons in brain slices and increased the spontaneous firing rate of VTA dopaminergic neurons in vivo. Furthermore, in vivo activation of this pathway produced reward-related

phenotypes that were dependent on intra-LHb $GABA_A$ receptor signaling. These results suggest that noncanonical inhibitory signaling by these hybrid dopaminergic-GABAergic neurons acts to suppress LHb output under rewarding conditions. Collectively, these data demonstrate that the LHb and midbrain interact in a reciprocal manner and implicate the VTA's projection to the LHb as a key node in the classical midbrain reward circuit.

ACKNOWLEDGEMENTS

First and foremost I would like to thank my mentor, Garret Stuber, for his guidance, patience, and brilliant scientific insight. I would like to thank all of the members of the Stuber lab, past and present, especially Dennis Sparta, Grace Blair, Shanna Resendez, and Josh Jennings. Josh, your inherent curiosity, resilient work ethic, and passion for science are out of this world and truly inspiring. I would also like to thank my dissertation committee, Regina Carelli, Fulton Crews, Thomas Kash, and Spencer Smith, for their time, mentorship, and excellent feedback. Finally, this process could not be possible without the support from all of my family and friends.

TABLE OF CONTENTS

LIST OF FIGURES

LIST OF ABBREVIATIONS

3V	Third ventricle
AAV	Adeno-associated virus
aCSF	Artificial cerebral spinal fluid
Arch	Archaerhodopsin
BAC	Bacterial artificial chromosome
BLA	Basolateral amygdala
BNST	Bed nucleus of the stria terminalis
CamKIIα	Calcium/calmodulin-dependent protein kinase II α
CART	Cocaine- and amphetamine-regulated transcript
CHAT	Choline acetyltransferase
ChR2	Channelrhodopsin-2
DA	Dopamine
DAT1	Dopamine transporter
DG	Dentate gyrus
DMH	Dorsal medial hypothalamus
DRD2	Dopamine receptor D2
DRN	Dorsal raphe nucleus
EN	Entopenduncular nucleus
eYFP	Enhanced yellow fluorescent protein
FSCV	Fast scan cyclic voltammetry

Fx	Fornix
GABA	Gamma-Aminobutyric acid
GAD	Glutamate decarboxylase
GFP	Green fluorescent protein
Hsyn	human synapsin
I_h	Hyperpolarization-activated inward rectifying current
LDT	Lateraldorsal thalamus
LDTg	Lateraldorsal tegmental nuclei
LH	Lateral hypothalamus
LHb	Lateral Habenula
MCH	Melanin-concentrating hormone
MDT	Medial dorsal thalamus
MHb	Medial habenula
mPFC	Medial prefrontal cortex
MSN	Medium spiny neuron
NAc	Nucleus Accumbens
NpHR	Halorhodopsin
OFC	Orbital frontal cortex
PPTg	Pedunculopontine tegmental nucleus
PVN	Paraventricular hypothalamus
Slc17a6	Vesicular glutamate transporter-2
Slc18a2	Vesicular monoamine transporter-2
Slc32a1	Vesicular GABA transporter

TH	Tyrosine hydroxylase
TH$^{VTA-LHb}$	LHb-projecting VTA dopaminergic neurons
TH$^{VTA-NAc}$	NAc-projecting VTA dopaminergic neurons
RMTg	Rostromedial tegmental nucleus
Vgat	Vesicular GABA transporter
VGlut2	Vesicular glutamate transporter-2
VMat2	Vesicular glutamate transporter-2
VMH	Ventral medial hypothalamus
VTA	Ventral Tegmental Area

CHAPTER 1. GENERAL INTRODUCTION[1]

HISTORY AND FUNCTION OF DOPAMINE

Animals are constantly faced with the necessity to seek out rewards, such as food and mates, while at the same time avoid dangerous and harmful situations. Therefore, motivated behaviors directed towards reward seeking and avoidance have evolved to promote survival across species (O'Connell and Hofmann, 2011). The brain reward system has been identified as an essential regulator for processing appetitive and aversive stimuli as well as generating appropriate motivated behaviors directed towards such stimuli. Specifically, dopaminergic neurons arising from the ventral tegmental area (VTA) and substantia nigra are integral for diverse neural functions including sensorimotor functions, motor control, motivation, reward seeking, salience detection, and novelty (Bromberg-Martin et al., 2010a; Schultz, 2007; Wise, 2004).

The notion that reward seeking is driven by neurological functions was first demonstrated by Olds and Milner in a seminal 1954 study (OLDS and MILNER, 1954). Olds and Milner demonstrated that rats would press a lever for electrical stimulation of "pleasure centers" in the brain. This study fostered numerous

[1]Sections from this chapter previously appeared in a book chapter published in the book *Addiction.* The original citation is as follows. Stamatakis, A.M., and Stuber, G.D. (2012) Optogenetic strategies to dissect the neural circuits that underlie reward and addiction. Cold Spring Harb Perspect med. *11*, a011924.

subsequent investigations to determine the exact neurotransmitter and neural circuits that underlie this phenomenon. Successive electrophysiological, pharmacological, and behavioral studies identified dopamine as the neurotransmitter that was critical for reward seeking and motivated behaviors (Wise, 2008).

While it is clear that dopamine signaling contributes to reward, a debate has ensued over the precise role of dopamine to reward. Two prominent theories have emerged: reward prediction error and incentive salience. Studies supporting the role for dopamine in reward prediction have found that dopamine computes the difference between an expected outcome and the actual outcome, and thus can act as a teaching signal (Cohen et al., 2012; Schultz et al., 1997; Wise, 2005). Incentive salience argues that dopamine functions to promote reward seeking by attributing an incentive salience to reward-predictive cues (Berridge, 2007). However, these two hypotheses should not be viewed as mutually exclusive, and it is likely that dopaminergic neurons have multiple roles in reward behavior, and can act as both a teaching signal and to signal incentive salience.

In addition to reward processing, dopaminergic neurons have also been identified as a key neural substrate in processing aversion. VTA neurons respond to aversive stimuli, and the cues that predict these stimuli, in a complex and diverse pattern (Bromberg-Martin et al., 2010a). It is likely that much of this diversity and complexity arises from the heterogeneity of VTA neurons, as well as the connectivity of the VTA with a multitude of different inputs and outputs. Therefore, discerning the precise role of dopamine in reward and aversion requires intense investigation of the

function of select subpopulations of dopaminergic neurons, and the precise control and manipulation of specific VTA afferents and efferents.

COMPOSITION AND HETEROGENEITY OF THE VTA

Anatomy and Cellular Composition of the VTA

The VTA is a midbrain structure that houses the A10 group of dopaminergic neurons (Dahlstroem and Fuxe, 1964). Cytoarchitectonic identification of the VTA is difficult, due to the lack of clear borders, and thus the VTA is often identified by it's location to neighboring structures (Fields et al., 2007). The VTA is located posterior to the hypothalamus, anterior to the brainstem reticular formation, medial to the substantia nigra, and ventral to the red nucleus.

The VTA is comprised of a heterogeneous population of neuronal subtypes containing approximately 65% dopaminergic neurons, 30% GABAergic neurons, and 5% glutamatergic neurons (Van Bockstaele and Pickel, 1995; Carr and Sesack, 2000a; Dobi et al., 2010; Margolis et al., 2006). However, a more detailed analysis of the composition of VTA neurons reveals that it is more complicated. Recent studies have demonstrated that midbrain VTA dopaminergic neurons are capable of co-transmitting both GABA and glutamate (Stuber et al., 2010; Tecuapetla et al., 2010; Tritsch et al., 2012). Consequently, it is not completely accurate to describe the VTA as a population of discrete dopaminergic, glutamatergic, and GABAergic neurons. It should be noted, though, that it is unclear what percentage of VTA neurons are co-releasing multiple classical neurotransmitters. The cellular composition of the VTA also varies along the anterior-posterior and medial-lateral

axis. VTA non-dopaminergic glutamatergic neurons are located more densely in the medial and anterior portions of the VTA (Yamaguchi et al., 2007). While GABAergic neurons are located throughout the VTA, more posterior regions of the VTA tend to have a higher percentage of GABAergic neurons than the anterior regions (Jhou et al., 2009a; Kaufling et al., 2009).

Heterogeneity of VTA dopaminergic neurons

A number of recent studies have demonstrated that VTA dopaminergic neurons themselves are heterogeneous in terms of their electrophysiological properties, their molecular profile, anatomical location, and projection field. In brain slices, dopaminergic neurons have traditionally been identified based on the presence of a hyperpolarization-activated inward rectifying current (I_h)(Margolis et al., 2006; Mercuri et al., 1995). Recently, however, studies have demonstrated that not all dopaminergic neurons have I_h currents (Lammel et al., 2008; Margolis et al., 2006). While basolateral amygdala (BLA)- and nucleus accumbens (NAc)-projecting VTA dopaminergic neurons have an I_h current, medial prefrontal cortex (mPFC)-projecting VTA dopaminergic neurons do not (Ford et al., 2006; Lammel et al., 2008). A pharmacological marker of a subset of dopaminergic neurons *in vitro* is inhibition in response to a D2 dopamine autoreceptor activation (Beckstead et al., 2004). While NAc- and BLA-projecting VTA dopaminergic neurons have functional D2 autoreceptors, mPFC-projecting VTA dopaminergic neurons do not show inhibitions to D2 autoreceptor activation, and thus do not appear to have functional D2 autoreceptors on the soma (Lammel et al., 2008). Consequently, previous

studies examining dopaminergic neurons using these electrophysiological criteria in brain slices may have excluded mPFC-projecting dopaminergic neurons.

Dopaminergic neurons, and likely VTA neurons in general, are heterogeneous with respect to their connectivity. In general, VTA dopaminergic neurons do not collateralize to other regions of the brain, and thus separate populations of dopamine neurons project to nonoverlapping target structures (Ford et al., 2006; Lammel et al., 2008; Swanson, 1982). Therefore, VTA dopaminergic neurons can be categorized based on their projection target. It is also likely, although less clear, that dopaminergic neurons receive unique inputs. Supporting this idea, the lateral habenula (LHb) projects predominantly onto mPFC-projecting dopaminergic neurons, while the laterodorsal tegmentum (LDT) synapses primarily onto NAc-projecting dopaminergic neurons (Lammel et al., 2012). Dopaminergic neurons are also anatomically segregated. BLA-projecting VTA dopaminergic neurons are located in the anterior-lateral portions of the VTA (Ford et al., 2006), NAc-projecting VTA dopaminergic neurons are located in the posterior-medial VTA (Ford et al., 2006; Lammel et al., 2008), and mPFC-projecting VTA dopaminergic neurons are located in the anterior-medial regions of the VTA (Nair-Roberts et al., 2008; Yamaguchi et al., 2007).

Finally, depending on projection target, VTA dopaminergic neurons have heterogeneous molecular profiles. BLA-, mPFC-, NAc core-, and NAc medial shell-projecting VTA dopaminergic neurons have small dopamine transporter (DAT)/ tyrosine hydroxylase (TH) mRNA expression ratios compared to VTA dopaminergic

neurons projecting to the lateral shell of the NAc, and SN neurons projecting to the dorsal striatum (Lammel et al., 2008).

VTA CIRCUITRY

Interconnectivity within the VTA

Along with receiving a multitude of inputs from across the brain, which is discussed in detail below, the VTA is also locally controlled by GABAergic, glutamatergic, and dopaminergic neurons. VTA GABAergic neurons locally inhibit VTA dopaminergic neurons, and activation of VTA GABAergic neurons decreases electrically-evoked dopamine release in the NAc (van Zessen et al., 2012), suggesting that VTA GABAergic neurons synapse onto NAc-projecting VTA dopaminergic neurons. However, it remains unclear whether VTA GABAergic neurons inhibit other subpopulations of VTA dopaminergic neurons. *In vivo* electrophysiological recordings from optically-tagged VTA GABAergic neurons demonstrate that these neurons show increases in firing when a reward is expected, and in response to aversive stimuli (Cohen et al., 2012; Tan et al., 2012). Additionally, optogenetic activation of VTA GABAergic neurons is aversive and disrupts reward consumption (Tan et al., 2012; van Zessen et al., 2012). Combined, these studies implicate a significant role for VTA GABAergic signaling in reward and aversion. However, it is unclear if these effects are due to local inhibition of VTA dopaminergic neurons, or due to inhibition of a downstream target of VTA GABAergic neurons. It is also currently unknown whether local VTA GABAergic

neurons collateralize and project to other brain structures, or if there is a population of GABAergic interneurons separate from GABAergic projection neurons.

The rostromedial tegmental nucleus (RMTg) is a GABAergic structure located immediately posterior of the VTA. Also called the tail end of the VTA, the RMTg is considered a GABAergic posterior extension of the VTA (Kaufling et al., 2009). GABAergic RMTg neurons also directly inhibit VTA dopaminergic neurons (Matsui and Williams, 2011). Similar to VTA GABAergic neurons, RMTg neurons also show increases in firing in response to noxious stimuli (Hong et al., 2011; Jhou et al., 2009b). While VTA GABAergic neurons and RMTg neurons show similar responses to aversive stimuli, the two structures appear to be distinct in terms of connectivity. The VTA sends GABAergic projections to the forebrain, while the RMTg lacks these projections (Van Bockstaele and Pickel, 1995; Carr and Sesack, 2000a; Jhou et al., 2009a; Kaufling et al., 2010; Taylor et al., 2014). Additionally, while the VTA and RMTg both receive LHb afferents, the LHb projection to the RMTg is notably more robust (Balcita-Pedicino et al., 2011).

Dopaminergic neurons also release dopamine locally via somatodendritic release (Björklund and Lindvall, 1975; Geffen et al., 1976). Dopamine receptor D2 autoreceptors are expressed on the soma and dendrites of midbrain dopaminergic neurons. These D2 receptors are coupled to G protein-coupled potassium channels (GIRK2), and thus activation of D2 receptors hyperpolarizes dopaminergic neurons (Beckstead et al., 2004). Dopaminergic neurons also release dopamine spontaneously within the VTA, resulting in a G protein-couple receptor-mediated inhibitory postsynaptic currents (Gantz et al., 2013; Jaffe et al., 1998).

Glutamatergic neurons in the VTA also release glutamate locally to control the activity of VTA dopaminergic and non-dopaminergic neurons (Dobi et al., 2010), although the function of this local glutamatergic release is uncertain.

Optogenetic activation of dopaminergic neurons

It has been clear for nearly 40 years that dopamine underlies aspects of reward and motivation (Wise, 2008). However, due to technical restraints, the exact causal relationship between dopamine and reward was difficult to ascertain. Within the last six years a number of studies have utilized optogenetics to selectively excite, inhibit, and record from dopaminergic neurons to help establish a causal relationship between dopamine and behavior.

Optogenetic activation of VTA dopaminergic neurons has confirmed that phasic activation of dopaminergic neurons is sufficient to produce behavioral conditioning and promote reward (Tsai et al., 2009). In addition, activation of dopaminergic neurons is also reinforcing, as mice and rats will self-administer optical activation of VTA dopaminergic neurons, and projections to the NAc, demonstrating that reinforcement and reward can arise solely within the dopaminergic system (Kim et al., 2012; Steinberg et al., 2014; Witten et al., 2011). Finally, phasic activation of dopaminergic neurons to mimic a reward prediction error is sufficient to cause long-lasting reward-seeking behavior (Steinberg et al., 2013). Collectively, these data demonstrate a causal role for dopamine in reinforcement learning.

Dopamine has also been thought to contribute to the pathophysiology of psychiatric disorders such as depression. Importantly, using optogenetics, two

recent studies have begun to address this hypothesis and found that dopaminergic neurons mediate aspects of depression (Chaudhury et al., 2013; Tye et al., 2013). Interestingly, Tye et al. found that activation of VTA dopaminergic neurons could alleviate symptoms of depression, while Chaudhury et al. demonstrated that activation of dopaminergic neurons promoted aspects of depression. These paradoxical findings could be the result of the different techniques the authors used to produce the depressive-like symptoms. While Tye et al. used a milder form of stress to induce depressive-like symptoms, Chaudhury et al. used a more intense chronic social-defeat stressor. Nonetheless, these studies provide a direct link between dopaminergic firing and depression and underscore the complexity of neuropsychiatric diseases and the circuitry underlying these diseases.

Inputs to the VTA

VTA dopaminergic neurons are phasically excited by rewards, and the cues that predict these rewards, and are phasically inhibited by the omission of rewards (Cohen et al., 2012; Schultz et al., 1997). And, as discussed above, dopaminergic neurons show heterogeneous responses to aversive events, and the cues that predict these aversive events. The VTA receives diverse afferents from throughout the brain, but the precise brain areas that provide input to VTA neurons and communicate reward- and aversive-related information remains relatively unknown. Recent studies using optogenetics have begun to provide insight into which inputs are controlling aspects of motivated behaviors. Using an elegant and novel monosynaptic tracing study Watabe-Uchida et al. identified VTA afferents throughout

the brain (Watabe-Uchida et al., 2012). Importantly, this study was able to identify monosynaptic inputs directly to VTA dopaminergic neurons. This study identified well-known inputs to VTA dopaminergic neurons, such as the bed nucleus of the stria terminalis (BSNT), lateral hypothalamus (LH), LHb, dorsal raphe (DRN), and laterodorsal tegmental nucleus (LDT). However, the study also identified novel dopaminergic afferents, such as the NAc and paraventricular hypothalamus (PVN).

Lateral hypothalamus

A variety of limbic regions project to the VTA and affect various components of motivated behaviors. One of the most well studied limbic input to the VTA arises from the LH. The LH is a heterogeneous structure that regulates aspects of homeostasis and is critical for a variety of motivated behaviors (Sternson, 2013). Therefore, the connection between the LH and the VTA may be necessary for guiding motivated behavior directed towards maintaining homeostasis. Anatomical and electrophysiological evidence suggests that the LH sends glutamatergic, GABAergic, and peptidergic projections to the VTA, where they make connections onto both dopaminergic and non-dopaminergic VTA neurons (Edinger et al., 1977; Geisler et al., 2007; Hernandez and Hoebel, 1988; Korotkova et al., 2003; Maeda and Mogenson, 1981). Peptidergic projections from the LH include orexin, neurotensin, dynorphin, melanin-concentrating hormone (MCH) and cocaine- and amphetamine-regulated transcript (CART) (Bittencourt et al., 1992; Dallvechia-Adams et al., 2002; Fadel and Deutch, 2002; Woulfe and Beaudet, 1992). Mice will self-administer optical stimulation of LH fibers in the VTA and the rewarding effects

of activation of the LH-to-VTA pathway is attenuated by blockade of endogenous neurotensin and NDMA receptor signaling (Kempadoo et al., 2013). However, given the complexity of the projections from the LH to the VTA, the precise integration and segregation of LH afferents, and their role in motivated behavior and homeostatic regulation will require further investigation.

Striatum

Although the VTA-to-NAc circuit has received much attention for it's role in motivation and reward seeking (discussed below), the NAc also sends a reciprocal projection back to the VTA (Heimer et al., 1991; Kalivas et al., 1993; Lu et al., 1998; Nauta et al., 1978; Tripathi et al., 2010; Usuda et al., 1998). Dopamine receptor D1-expressing GABAergic medium spiny neurons (MSNs) in the NAc synapse onto GABAergic neurons in the VTA (Bocklisch et al., 2013; Xia et al., 2011). Selective activation of D1-expressing neurons in the NAc is highly reinforcing (Kravitz et al., 2012). Thus, the circuit mechanism by which activation of D1-expressing MSNs is reinforcing could be through inhibition of VTA GABAergic neurons, and thus disinhibition of VTA dopaminergic neurons. Although the NAc also sends a direct projection to dopaminergic neurons (Watabe-Uchida et al., 2012), the connection onto GABAergic neurons is markedly more robust and profuse (Bocklisch et al., 2013; Xia et al., 2011).

Amygdala and extended amygdala

The VTA also receives a dense projection from the BNST. Both glutamatergic and GABAergic neurons in the BNST project to the VTA, where they synapse primarily onto GABAergic VTA neurons, although they also project to dopaminergic neurons as well (Jennings et al., 2013a; Kudo et al., 2012). Interestingly, activation of these parallel circuits affects behavior in an opposing fashion (Jennings et al., 2013a). Activation of the glutamatergic inputs to the VTA is anxiogenic and aversive, while activation of the GABAergic inputs to the VTA is anxiolytic, positively reinforcing, and rewarding. Since BNST neurons project primarily onto GABAergic neurons in the VTA, it is thought that these opposing behavioral responses are due to indirect inactivation (via BNST glutamatergic neurons) or activation (via BNST GABAergic neurons) of VTA dopaminergic neurons.

The BLA is also an important afferent to dopaminergic neurons. Although the BLA does not send appreciable projections directly to the VTA, glutamatergic BLA neurons project to the NAc, where they modulate presynaptic dopamine release, likely through an axo-axonic mechanism (Howland et al., 2002). Consistent with these observations, optogenetic activation of BLA glutamatergic inputs to the NAc is reinforcing, and dependent on dopamine signaling in the NAc (Stuber et al., 2011).

Lateral Habenula

Recently, a lot of attention has been focused on the projection from the LHb to the midbrain. The LHb is a well-conserved glutamatergic epithalamic structure.

LHb neurons tend to fire in a manner opposite to dopaminergic neurons. While dopaminergic neurons show excitations to reward-predictive cues, and inhibitions to cues that predict no rewards, LHb neurons show excitations to cues that predict the absence of rewards and are inhibited by reward-predictive cues (Matsumoto and Hikosaka, 2007). LHb neurons also show excitations to aversive stimuli and the cues that predict them (Matsumoto and Hikosaka, 2009a). Interestingly, the excitation of LHb neurons to the cue that predicts the absence of a reward precedes the inhibition of dopaminergic neurons, suggesting that LHb neurons are providing dopaminergic neurons with a negative reward signal (Matsumoto and Hikosaka, 2007). Since LHb neurons are primarily glutamatergic, this reward information is likely relayed to dopaminergic neurons via GABAergic neurons. The LHb sends a robust glutamatergic projection to the RMTg, a GABAergic hindbrain structure that directly inhibits VTA dopaminergic neurons (Jhou et al., 2009b; Matsui and Williams, 2011), and thus the RMTg has been identified as the likely intermediary structure through which LHb neurons signal negative reward information to dopaminergic neurons (Hong et al., 2011). However, the behavioral and functional relevance of this circuit is unclear, and is one of the main goals of this dissertation, as discussed in the **Dissertation** section below.

Cortex

The VTA receives cortical afferents from the mPFC, orbital frontal cortex (OFC), somatosensory cortex, and cingulate cortex (Geisler et al., 2007; Sesack and Pickel, 1992; Watabe-Uchida et al., 2012). The PFC projects to NAc-projecting VTA

GABAergic neurons and PFC-projecting VTA dopaminergic neurons (Carr and Sesack, 2000b). The orbital frontal cortex sends a modest projection to the VTA (Watabe-Uchida et al., 2012). No studies to date have selectively activated this circuit; however, an inactivation study demonstrated that both the VTA and OFC are necessary for learning unexpected outcomes. Although it is possible that this could be mediated by an intermediary structure, it is clear that either direct or indirect connectivity between the VTA and OFC are necessary for reward prediction error (Takahashi et al., 2009).

Hindbrain

Burst firing of dopaminergic neurons results in phasic dopamine release in the NAc (Gonon, 1988; Overton and Clark, 1992), and is thought to be essential for reward prediction error. Several studies have demonstrated that burst firing in dopaminergic neurons is likely driven by inputs from the mesopontine tegmentum. Nuclei of the mesopontine tegmentum that project to the VTA include the pedunculopontine (PPTg), laterodorsal (LDTg), and the RMTg. While the RMTg is likely the main candidate for providing dopaminergic neurons with negative reward prediction error (Hong et al., 2011), the LDT and PPTg contribute to phasic burst firing in dopaminergic neurons (Floresco et al., 2003; Lodge and Grace, 2006a, 2006b). The mechanism by which the PPTg and LDT affects burst firing is unclear, as both of these regions send glutamatergic, cholinergic, and GABAergic projections to the VTA (Geisler et al., 2007; Mena-Segovia et al., 2008; Oakman et al., 1995; Wang and Morales, 2009; Winn et al., 1997). LDT neurons send a glutamatergic

projection to NAc-projecting VTA dopaminergic neurons, and optogenetic activation of this projection elicits conditioned place preference, and promotes a rewarding phenotype that is dependent on dopamine signaling in the NAc (Lammel et al., 2012). Collectively, these data demonstrate that hindbrain afferents, in particular from the mesopontine tegmentum are a likely candidate for providing dopaminergic neurons with reward prediction error.

Another prominent VTA hindbrain afferent arises from the DRN, which provides the majority of serotonergic input to the forebrain (Jacobs and Azmitia, 1992). Along with the VTA, the DRN also projects to several reward-related brain regions such as the NAc and PFC (Vertes, 1991). However, the investigation of the role of serotonin and reward has yielded conflicting results. For example, while some studies have demonstrated a positive correlation between serotonin neurotransmission and reward (Kranz et al., 2010), others have suggested that serotonin may encode aversion and oppose the actions of dopamine in reward (Abler et al., 2012; Schweimer and Ungless, 2010). A recent study that selectively targeted serotoninergic neurons, and their projections to the VTA, demonstrated that activation of serotonin neurons results in a robust rewarding phenotype (Liu et al., 2014). DRN serotoninergic neurons also release glutamate in the VTA. Therefore, it is unclear whether this appetitive phenotype is mediated by serotonin or glutamate release (Liu et al., 2014).

Unexplored circuits

The VTA also receives several other afferents that have been yet to be functionally or behaviorally dissected. These include GABAergic projections from the ventral pallidum, preoptic area of the hypothalamus projections, inputs from the superior colliculus, periaqueductal gray, and projections from several nuclei in the pontine, cerebellum and medulla (Geisler and Zahm, 2005). It will be important for future studies to continue to tease apart how each of these inputs onto VTA dopaminergic neurons contribute to appetitive and aversive processing of stimuli, as well as the subsequent generation of motivated behavioral responses.

Outputs of the VTA

In general, regions of the brain that receive input from the VTA, send projections back to the VTA (Geisler and Zahm, 2005; Taylor et al., 2014; Watabe-Uchida et al., 2012). Dopaminergic neurons in the VTA send widespread projections throughout the forebrain, including the mPFC, NAc, LHb BLA, and hippocampus (Swanson, 1982). VTA GABAergic and glutamatergic neurons also send extensive connections to both overlapping VTA dopaminergic target regions, as well as distinct regions of the brain that receive little to no dopaminergic input. Since dopaminergic neurons project to largely non overlapping regions (Ford et al., 2006; Lammel et al., 2008; Swanson, 1982), and since dopamine appears to be involved in a variety of aspects of motivated behavior, it is likely that the precise role of dopamine in various behaviors is a function of projection target.

Striatum

The most well studied dopaminergic output is to the NAc. Along with dopaminergic afferents, the NAc also receives glutamatergic afferents from limbic regions such as the BLA, prefrontal cortex, and hippocampus. The NAc projects to motor areas such as the VTA and ventral pallidum, and is thus situated to interface and process motivation and reward information to then promote goal directed behaviors (Mogenson et al., 1980).

The study of dopamine release in the NAc using electrochemistry, and in particular fast scan cyclic voltammetry (FSCV), has allowed for the quantification of dopamine release with unparalleled temporal and spatial resolution (Phillips et al., 2003a). In addition, these studies have complemented previous electrophysiological, genetic, and pharmacological studies implicating dopamine signaling in the NAc in appetitive and aversive behaviors (Wanat et al., 2009). Supporting the role of dopamine as a teaching signal, FSCV studies have demonstrated that as a rodent learns to associate a reward-predictive cue with a reward, dopamine transients in the NAc shift from occurring during the onset of the reward, to the onset of the cue (Day et al., 2007). Electrochemical studies have also demonstrated dopamine release in the NAc in response to novel stimuli, aversive stimuli, during sexual behavior, and in response to cues predicting drugs of abuse such as cocaine (Badrinarayan et al., 2012; Phillips et al., 2003b; Rebec et al., 1997; Robinson et al., 2001; Stuber et al., 2005; Young et al., 1993).

Selective activation of dopaminergic inputs to the ventral striatum is rewarding and drives positive reinforcement (Witten et al., 2011). However, in light of recent

studies demonstrating that dopaminergic neurons can co-release both GABA and glutamate in the striatum (Stuber et al., 2010; Tecuapetla et al., 2010; Tritsch et al., 2012), results from the aforementioned studies may not be exclusively attributed to the effects of dopamine release. While many studies have established a central role for dopamine in reinforcement (Berridge and Robinson, 1998; Ikemoto and Panksepp, 1999; Wise, 2004), it remains unclear if the co-release of glutamate and GABA from dopaminergic neurons mediates aspects of reinforcement.

GABAergic neurons in the VTA also project to the striatum (Van Bockstaele and Pickel, 1995; Brown et al., 2012; van Zessen et al., 2012). Surprisingly, these neurons project specifically to cholinergic interneurons, and activation of these inputs decreases the spontaneous firing rate of postsynaptic cholinergic neurons, similar to the pause seen during reinforcement training (Brown et al., 2012). When the authors mimicked this pause in vivo, by activating the VTA GABAergic inputs to the striatum, mice were better able to discriminate a salient stimulus that predicted an aversive event. These data demonstrate that GABAergic afferents to cholinergic interneurons are important in modifying behavioral responses to conditioned stimuli. Finally, non-dopaminergic glutamatergic VTA neurons also project to the NAc (Hnasko et al., 2012), but the precise function of this circuit is yet to be determined.

Cortex

Dopaminergic, GABAergic, and glutamatergic VTA neurons project to the mPFC (Carr and Sesack, 2000a; Swanson, 1982; Taylor et al., 2014). And, as discussed above, the PFC projects back to the VTA, where it synapses onto PFC-

projecting dopaminergic neurons and NAc-projecting GABAergic neurons (Carr and Sesack, 2000b). Recent studies have suggested that the VTA-to-mPFC circuit may processes aversive and stressful stimuli. mPFC-projecting VTA dopaminergic neurons show increases in AMPA/NMDA ratio following exposure to an aversive stimulus (Lammel et al., 2011). Therefore, mPFC-projecting VTA dopaminergic neurons may be the neurons that are showing phasic excitations to aversive stimuli (Brischoux et al., 2009; Matsumoto and Hikosaka, 2009b). Interestingly, optical inhibition of the VTA-to-mPFC circuit in mice with a history of social defeat decreased social interaction, suggesting that inputs to the mPFC arising from the VTA may be involved in promoting aspects of depression (Chaudhury et al., 2013).

Limbic regions

VTA dopaminergic neurons also project to the hippocampus, where they preferentially target the subiculum, hilus, and the CA1 region (Lisman and Grace, 2005). The VTA-to-hippocampus circuit is thought to signal novelty and enhance learning. Exposure to a novel environment increases dopamine release in the hippocampus (Ihalainen et al., 1999) and enhances D1-dependent long term potentiation in the CA1 (Li et al., 2003). In addition, dopamine agonists in the hippocampus tend to enhance learning and memory (Bach et al., 1999; Bernabeu et al., 1997; Packard and White, 1991), while antagonists impair memory (Bernabeu et al., 1997; Gasbarri et al., 1996). The VTA also receives indirect connections from the hippocampus through a subiculum-accumbens-ventral pallidum – VTA circuit (Lisman and Grace, 2005). The VTA also sends projections to parts of the amygdala

and extended amygdala, including the BLA, central amygdala, and BNST (Swanson, 1982).

While these studies demonstrate a functional circuit from the VTA to limbic regions, future studies are clearly needed to determine the causal role of the dopaminergic projection to these areas.

Unexplored Circuits

While optogenetic techniques have been employed to investigate the behavioral and functional role of the VTA-to-NAc and VTA-to-mPFC circuits, a number of dopaminergic circuits have yet to be fully defined. Importantly, although the existence of a mesohabenular pathway has been identified (Gruber et al., 2007; Phillipson and Griffith, 1980; Skagerberg et al., 1984; Swanson, 1982), the behavioral or functional significance of this circuit remains unclear, which is the topic for the second part of this dissertation, as discussed below in the **Dissertation** section. Additionally, projection targets of VTA glutamatergic and GABAergic neurons of the VTA remain widely unexplored. VTA GABAergic neurons project to the NAc, PFC, ventral pallidum, preoptic nuclei, LH, and LHb (Fields et al., 2007; Taylor et al., 2014). VTA glutamatergic neurons project to the NAc, LHb, amygdala, ventral pallidum and mPFC (Hnasko et al., 2012; Taylor et al., 2014; Yamaguchi et al., 2011). Interestingly, while VTA non-dopaminergic GABAergic and glutamatergic neurons project to areas that also receive dopaminergic innervation, they also send projections to areas that receive little to no dopaminergic innervation.

ROLE OF THE LATERAL HABENULA IN MOTIVATED BEHAVIORS

The habenula is a bilateral epithalamic structure located on both sides of the third ventricle. The habenula is subdivided into the lateral (LHb) and medial (MHb) portions, which are anatomically, genetically, morphologically, and functionally distinct (Klemm, 2004; Nair et al., 2012). The LHb receives converging inputs from the cortex, basal ganglia, and limbic systems (Geisler and Trimble, 2008). While the LHb sends weak projections back to a few of these regions, the primary output of the LHb is to midbrain monoamanergic nuclei, including the VTA and DRN (Araki et al., 1988; Geisler and Trimble, 2008). Electrical stimulation of the LHb inhibits midbrain dopaminergic neurons, while lesions of the LHb result in activation of midbrain dopaminergic neurons (Lisoprawski et al., 1980; Nishikawa et al., 1986). Similarly, inhibition of the LHb increases dopamine release in the striatum (Lecourtier et al., 2008).

Seminal studies conducted in monkeys revealed that LHb neurons encode negative reward prediction errors (Matsumoto and Hikosaka, 2007). While midbrain dopaminergic neurons show excitations to reward predictive cues and inhibitions to cues that predict reward omissions, LHb neurons show excitations to cues that predict no reward and inhibitions to reward predictive cues (Matsumoto and Hikosaka, 2007). The excitation to the reward omission in the LHb neurons preceded the inhibition of dopaminergic firing, suggesting that the LHb is inhibiting midbrain dopaminergic neurons to suppress behaviors directed towards a non-rewarding stimulus.

The LHb is comprised of almost entirely glutamatergic neurons (Geisler and Trimble, 2008), and sends projections to GABAergic neurons in the RMTg (Balcita-Pedicino et al., 2011; Hikosaka et al., 2008), a discrete population of neurons posterior to the VTA, which inhibits VTA dopaminergic neurons (Matsui and Williams, 2011). VTA-projecting RMTg neurons show Fos induction after exposure to aversive stimuli, such as foot shock and food deprivation. Collectively, these data suggest that the LHb negatively modulates midbrain dopaminergic neurons during the presentation of aversive stimuli or omission of rewards through connections with the RMTg.

The LHb has also been recently implicated as a key brain nuclei in the pathophysiology of depression. Neuroimaging studies have revealed increased activity in the habenula in models of depression in humans and rodents (Caldecott-Hazard et al., 1988; Morris et al., 1999; Shumake et al., 2003). A recent study aimed at uncovering the molecular mechanisms in the LHb mediating core symptoms of depression, found that increasing beta-CamKII increased synaptic efficacy and output of the LHb and was sufficient in producing depressive-like symptoms (Li et al., 2013).

RELATIONSHIP BETWEEN NEURAL CIRCUITS UNDERLYING MOTIVATED BEHAVIORS AND NEUROPSYCHIATRIC DISEASES

Disruption in dopaminergic signaling in the VTA, as well as dysfunction in VTA afferent and efferent connectivity, are thought to underlie aspects of addiction, mood disorders, attention disorders, and schizophrenia (Bonci et al., 2003; Nestler and Carlezon, 2006; Tye and Deisseroth, 2012). A number of studies have

demonstrated that nearly every drug of abuse either directly or indirectly increases dopamine neurotransmission (Di Chiara and Imperato, 1988; Nestler, 2005). Further, both short term and long term exposures to drugs of abuse can have long lasting changes on dopaminergic function and afferent and efferent plasticity (Lüscher and Malenka, 2011). In addition to the role of midbrain function and connectivity on drug addiction, recent optogenetic investigations have also implicated the VTA in mediating aspects of depression, as discussed above in the **VTA Circuitry** section.

Recent studies have implicated the LHb in neuropsychiatric diseases such as depression (as discussed above) and drug addiction. Drugs of abuse have both rewarding and aversive components, and it is thought that both the negative and positive reinforcing properties of drug taking contribute to drug addiction (Koob, 2013). In vivo electrophysiology in rats have demonstrated that exposure to cocaine produces biphasic responses in aversive-responding LHb neurons (Jhou et al., 2013). LHb neurons showed initial inhibition to intravenous cocaine, followed by delayed excitation, mirroring the shift from the rewarding to aversive aspects of cocaine. Lesions of LHb efferents, lesions of the RMTg, and optogenetic inhibition of the RMTg all abolished cocaine-induced avoidance behaviors (Jhou et al., 2013).

OVERVIEW OF OPTOGENETICS

Determining causal relationships between neural function and behavior is crucial to understand the neuropathology underlying neuropsychiatric diseases. As reviewed above, both the LHb and VTA have been implicated in a number of

neuropsychiatric diseases, and thus I utilized a novel technique called optogenetics to investigate the functional and behavioral significance of the reciprocal connectivity between the LHb and VTA. Because this technique is used throughout all of the subsequent chapters, below I have outlined the technical aspects of optogenetics, as well as *in vitro* and *in vivo* applications. Further, at the end of this dissertation I discuss a few of the important limitations and considerations associated with optogenetic experiments.

The functional complexity and genetic heterogeneity of the brain has historically prevented researches from investigating the causal link between neural circuits and behavior. Relationships between function and behavior have traditionally been accomplished by tissue lesioning techniques, electrical stimulation, or pharmacological activation or inactivation. Whereas these methods have uncovered the basic neuroanatomical pathways that mediate reward-related behavior, they often fail to determine pathway or genetic specificity mediating a behavioral response. Site-directed pharmacological manipulations can sometimes be used to address genetically defined pathways (if only a given population of neurons locally express a specific receptor), but these manipulations are often over longer timescales, which do not allow for determining how neural activity is required for discrete behavioral events, which can often times last for less than 1 s. To investigate causal relationships between genetically defined populations of neurons and reward-seeking behavior, techniques allowing for precise control of neural circuitry with millisecond precision are required. Optogenetics allows for pathway-specific manipulation of brain circuitry over a range of timescales, which circumvents

many of the technical limitations associated with electrical, lesioning, and pharmacological manipulations. Finally, combining optogenetics with slice electrophysiology and *in vivo* behavioral paradigms allows for an unprecedented insight into the neural circuitry involved in motivated behaviors.

Opsins and hardware to control specific neuronal pathways with light

For a full description of the different opsins currently used to study neural circuits see Yizhar et al. (Yizhar et al., 2011a). The most commonly used opsin to activate neural circuits is channelrhodopsin (ChR2). ChR2 is a light-gated cation channel that was originally isolated from blue-green algae (Nagel et al., 2003). ChR2 is maximally activated by a blue, 450-490 nm light. When activated, absorbed photons cause a light-induced isomerization of the all-trans retinal protein, which opens the channel allowing sodium and other cations to flow through the cell. When expressed in a neuron, this influx of cations causes depolarization of the cell membrane at resting membrane potentials, which will lead to the opening of endogenously expressed voltage-gated sodium channels to initiate an action potential.

Optogenetic inactivation of neural circuits is most commonly accomplished using the light gated chloride pump, halorhodopsin (NpHR), which was first discovered in arachabacteria (Matsuno-Yagi and Mukohata, 1977). Introduction of wildtype NpHR into neurons demonstrated that while photoinhibition was possible, exogenous NpHR protein was not initially sufficiently expressed at neuronal membranes for consistent results in vivo (Gradinaru et al., 2010). Further

modification of NpHR, with an added endoplasmic reticulum export signal and membrane trafficking peptide sequence, results in robust expression at neuronal membranes, which facilitated its use *in vivo* for neuronal circuit element inhibition (Gradinaru et al., 2010). NpHR is maximally activated by a yellow/orange, ~590 nm wavelength of light, but can response to a broad wavelength range from ~520 – 620 nm. When activated, NpHR pumps chloride from the extracellular space into the cytoplasm of the cell. When expressed in a neuron, this results in hyperpolarization of the cell membrane, and can decrease neuronal firing rates (Fenno et al., 2011). Optical inhibition can also be achieved by the use of outward proton pumps, such as archaerhodopsin (Arch) (Fenno et al., 2011). Arch is maximally activated by a 560 nm wavelength of light, and activation of Arch has been shown to result in robust currents at relatively low light outputs (Chow et al., 2010). Although proton pumps such as Arch show robust inhibition of neuronal membranes, it remains undetermined the deleterious effects these proteins have in neuronal tissues and if they show any non cell-type specific effects (Fenno et al., 2011).

Expressing opsin proteins under the control of cell type specific promoters is one method of targeted manipulations of genetically defined neuronal subtypes. Using this technique, optogenetic manipulation of glutamatergic BLA neurons to the NAc have been investigated (Stuber et al., 2011). Calcium-calmodulin-dependent protein kinase IIα (CamKIIα) is preferentially expressed in glutamatergic projection neurons in the BLA (McDonald, 1992). ChR2 or NpHR3.0 was introduced into these glutamatergic neurons using an adeno-associated virus (AAV) vector with ChR2 under the control of a CamKIIα promoter. Stereotaxic injection of this construct into

the BLA results in ChR2 positive neurons constrained to glutamatergic projection neurons within the BLA. As discussed in detail below, implantation of an optical fiber into the NAc, allows for precise control over excitatory BLA inputs into the NAc. Other studies using the CamKIIα promoter have investigated BLA afferents to other regions of interest such as the central amygdala (Tye et al., 2011) and to study cortical pyramidal neurons (Aravanis et al., 2007; Sohal et al., 2009; Yizhar et al., 2011b).

A transgenic approach is also a common method to achieve targeted manipulation of genetically defined cells. There now exist a number of transgenic mouse lines that selectively express ChR2 or NpHR in specific subtypes of neurons (Arenkiel et al., 2007; Zhao et al., 2011). Whereas this method ensures that virtually all neurons of a specific genetically defined population will express opsin proteins, it oftentimes do not provide anatomical specificity of expression to a discrete brain region of interest. Thus, to reliably target neuronal populations within specific brain nuclei, cre recombinase-inducible expression systems have been used in conjunction with transgenic animals expressing cre in specific populations of neurons. Using this method, cre-inducible opsins are stereotaxically injected into transgenic mice expressing cre recombinase in genetically identified neuronal populations (Atasoy et al., 2008; Cardin et al., 2009; Sohal et al., 2009; Tsai et al., 2009; Witten et al., 2011). Cre-inducible AAV vectors contain DNA cassettes with two pairs of incompatible lox sites (LoxP and lox2722) with an opsin inserted between the two lox sites in the reverse orientation. Cre recombinase catalyzes recombination between the two lox sites, resulting in the opsin reversing its

orientation, allowing the opsin to be transcribed. Thus, delivery of these cre-inducible opsins into a specific brain region results in opsin expression in only the genetically identified cell-type in the brain region of interest. Cholinergic interneurons in the NAc have been targeted using this method (Witten et al., 2010). Here, bacterial artificial chromosome (BAC) transgenic Choline Acetyltransferase (ChAT)::Cre mice are injected with a cre-inducible double floxed recombinant AAV vector coding for ChR2 or NpHR3.0 into the NAc. Dopaminergic neurons in the VTA have also been targeted using a transgenic approach in which TH-cre (Tsai et al., 2009) in mice or rats (Witten et al., 2011) or DAT-cre mice (Cohen et al., 2012; Stuber et al., 2010) are injected with a double floxed cre-inducible opsin vector. The use of cre-mice paired with double-floxed opsins, or the use of cell-type promoters, allows for precise control over genetically defined populations of neurons.

Different hardware setups have been utilized to deliver light *in vitro* and *in vivo*. The most common *in vitro* light delivery systems include filtered light from mercury arc lamps (Boyden et al., 2005; Gunaydin et al., 2010), lasers, (Cardin et al., 2010; Kravitz et al., 2012), and LEDs (Adesnik and Scanziani, 2010; Wang and Morales, 2009). *In vivo*, lasers coupled to optical fibers are most commonly used to deliver light into the brain (Cardin et al., 2010; Stuber et al., 2011; Tye et al., 2011). For a more in depth description of *in vivo* light delivery to the brain, see the section entitled ***In Vivo Optogenetic Strategies***.

Finally, interfacing lasers with behavioral equipment allows for optogenetics to be employed in a wide-range of reward-related behavioral paradigms including conditioned place preference (Lobo et al., 2010; Tsai et al., 2009), operant

conditioning (Adamantidis et al., 2011) and Pavlovian conditioning (Stuber et al., 2011). Combining these paradigms with optogenetics allows for sub second precision control of neural circuitry time locked to discrete behavioral events. Behavioral paradigms associated with other neuropsychiatric diseases, such as open field test and elevated plus maze, have also been interfaced with in vivo optogenetics (Tye et al., 2011). This can be achieved using real-time video tracking hardware and software to restrict optical stimulation when the animal enters a specific area of a behavioral arena.

Slice electrophysiology paired with optogenetics to parcel out local circuits

Anatomical tracing studies and electrophysiological techniques using electrical stimulation are often used to study the synaptic connectivity within neural circuits. However, there are significant limitations associated with both of these techniques. Anatomical tracing studies often fail to address the strength and functionality of the synaptic connections. Electrophysiological studies using electrical stimulation can address functionality, but they often fail to determine cell-type specific projections. Because of the heterogeneity of most neural tissues, electrical stimulation will typically non-specifically activated all afferents to a given neuron. Patch clamp electrophysiology paired with optogenetics circumvents the limitations associated with both of these methods because it allows for cell-type specific activation and assessment of the strength and functionality of these connections. Using this method, it is possible to record from postsynaptic neurons (using mice expressing fluorescent proteins in specific neurons or by post hoc

immunohistochemistry), while optically stimulating site-specific or genetically defined afferents that are expressing ChR2. These techniques have been successful in parsing out neural circuits involved in addiction. In one example of this application, Chuhma et al (2011) used optogenetics in NAc brain slices to define the functional connectivity of MSNs. By conditionally expressing ChR2 in MSNs, these authors were able to investigate connections within the striatum and projections to the globus pallidus and substantia nigra (Chuhma et al., 2011), as well as examine how striatal cholinergic interneurons can regulate function of other populations of striatal neurons.

Optogenetics paired with slice electrophysiology has also been used to examine the possibility of neurotransmitter co-release. Dopamine and glutamate coincident signaling is crucial for a variety of motivated behaviors including responding to motivationally significant stimuli. A subset of TH positive dopaminergic neurons in the VTA also express vesicular glutamate transporter-2 (VGluT2), indicating that these dopaminergic neurons are capable of packaging glutamate into synaptic vesicles (Hnasko et al., 2010). Furthermore, pharmacological and electrophysiological studies have suggested that dopaminergic neurons co-release glutamate (Bourque and Trudeau, 2000; Chuhma et al., 2009; Sulzer et al., 1998); however, these studies only provided indirect evidence as a result of the technical limitations. Selective optogenetic stimulation of ChR2-positive dopaminergic terminals in the NAc shell results in excitatory postsynaptic currents (Stuber et al., 2010; Tecuapetla et al., 2010), confirming that midbrain dopaminergic neurons are capable of co-releasing glutamate in the NAc. Similar studies have now

confirmed that other neurons that release neuromodulators, such as acetylcholine, are also capable of glutamate corelease, such as projection neurons in the MHb (Ren et al., 2011). Utilizing optogenetic approaches to study neurotransmitter release will likely yield a plethora of novel information on the intraneuronal signaling dynamics of defined neural circuits.

In vivo optogenetic strategies

In vivo optogenetic approaches can be used for a variety of different experiments from targeted manipulations of genetically defined cells to manipulation of specific neural pathways on a physiologically relevant time-scale. Furthermore, utilizing these *in vivo* optogenetic approaches in awake and behaving animals allows for precise control over neural circuitry time locked to discrete events, necessary for determining a causal relationship between structure and cue or reward-related behavior.

Delivering light into the brain is most often accomplished by implanting an acute or chronic optical fiber into the region of interest (Sparta et al., 2012; Zhang et al., 2010). Using the acute optical fiber method, a guide cannula is chronically implanted in either the virus-targeted region or the projection region of interest. Then, the optical fiber is acutely implanted immediately prior to the experiment. One benefit of employing an acute fiber is the ability to combine local pharmacology through the cannula before implantation of the fiber. However, a major caveat to this method is the risk of tissue damage and fiber breakage due to repeated insertion and removal of the fiber. This is especially of concern when working with behavioral

paradigms that involve weeks of training and testing. Chronic fibers, on the other hand, are cemented into the skull during stereotaxic surgery and allow for multiple testing sessions over an extended time period with minimal light loss (Sparta et al., 2012).

Chronic or acute optical fibers can be placed in the same brain area as the virus injection to examine the effects of optical stimulation or inhibition on genetically targeted cell bodies of interest. For example, optical activation of D2 positive neurons in the NAc expressing ChR2 suppresses cocaine reward, while activation of D1 positive neurons increases cocaine reward (Lobo et al., 2010). Optical fibers can also be placed in projection targets to investigate the effects of altering pathway-specific circuits on behavior. Opsins are trafficked across the membrane and a few weeks after transduction of cell bodies, opsins tagged to fluorescent proteins can be visualized in axons and terminals (Yizhar et al., 2011a). This technique has mainly been employed to look at BLA afferent projections to different brain regions (see below) (Stuber et al., 2011; Tye et al., 2011), but can be utilized to look other neural circuits important in addiction such as dopaminergic afferents in the NAc and mPFC. In addition, this strategy can identify neural circuit elements or genetically defined populations of neurons that are necessary or sufficient for a discrete behavior such as conditioned approach behavior to a reward-predictive cue. For example, BLA glutamatergic afferents to the NAc have been hypothesized to be important in cue-triggered motivated behavior, but because of the inability to specifically modulate this pathway during time-locked cues, the causal functional role of this pathway in cue-reward behavior was preciously not well defined. Using optogenetics, activation

and inactivation of BLA terminals in the NAc demonstrated that this circuitry is both necessary and sufficient for cue-driven motivated behavior (Stuber et al., 2011).

Optogenetic manipulations of the neural circuitry involved in motivated behaviors have aided in supporting and refuting many hypotheses that were previously untestable as a result of technical limitations associated with traditional techniques. Many of the optogenetic studies to date investigating these circuits have used optogenetic stimulation of neurons, but optogenetic inhibition is likely to prove to be an even more powerful tool to determine both necessity and sufficiency of neural circuits for mediating reward-related behaviors. In addition, combining optogenetics with *in vivo* monitoring techniques such as *in vivo* electrophysiology, and neurochemical techniques such as microdyalisis and voltammetry, allows for actuation of neural circuits, while simultaneously measuring the neurophysiological output. The ever-increasing methods for targeted genetic manipulations of neurons as well as the continued development and refinement of optogenetic methods are unprecedented.

DISSERTATION

Neurons in the LHb are excited by aversive stimuli and are thought to inhibit midbrain dopaminergic neurons during the presentation of an aversive stimulus or the omission of a reward through synapses onto RMTg neurons. However, little is known about the electrophysiological properties of LHb excitatory inputs onto postsynaptic neurons in the RMTg. Further, although correlative evidence suggests that the LHb neurons convey anti-reward and aversive information, the behavioral

consequences of LHb-to-RMTg activation remain unknown. To address this, I use *ex vivo* and *in vivo* optogenetic strategies to investigate how aversive stimuli alter LHb-to-RMTg glutamatergic transmission and how direct manipulation of this pathway affects behavior.

Following thorough investigation of the LHb-to-midbrain circuit I next investigated various LHb afferents. Inputs to the LHb arise from forebrain regions including the LH, entopenduncular nucleus (EN) and prefrontal cortex (Kim and Lee, 2012; Poller et al., 2013; Shabel et al., 2012; Warden et al., 2012). Although the majority of LHb afferents arise from the forebrain, the LHb also receives a substantial projection from the VTA, with an estimated 30-50% of LHb-projecting VTA neurons being dopaminergic (Gruber et al., 2007; Phillipson and Griffith, 1980; Skagerberg et al., 1984). Electrical stimulation of the midbrain decreases the firing rate of LHb neurons (Shen et al., 2012), but the functional and behavioral significance of synaptic inputs to the LHb arising from VTA dopaminergic neurons remains unknown. I utilized a combination of optogenetic manipulations, electrophysiology, and viral tracing techniques to investigate the molecular, anatomical, and genetic profiles of LHb-projecting VTA dopaminergic neurons. I next used electrophysiology combined with electrochemical techniques to determine which neurotransmitters these dopaminergic neurons release in the LHb, and how this connection affects downstream reward circuitry. Finally, I combined optogenetics with behavior to determine the behavioral significance of this circuit.

In the last aim of this dissertation I investigated another LHb afferent from the LH. The LH is involved with promoting behaviors to maintain homeostasis, such as

reward-seeking and feeding. The LHb receives a robust glutamatergic projection from the LH (Poller et al., 2013), and thus may serve as a prominent connection between homeostatic and reward circuits. However, the precise function of this circuit is unclear. To investigate this, I utilized optogenetics in combination with a genetic ablation method to determine the behavioral and functional relevance of this circuit.

Collectively, data generated from these aims will increase our understanding of the neural circuits involved in processing aversive and rewarding stimuli, and may aid in the identification of novel targets for the treatment of addiction and other neuropsychiatric diseases.

CHAPTER 2: ACTIVATION OF LATERAL HABENULA INPUTS TO THE VENTRAL MIDBRAIN PROMOTES BEHAVIORAL AVOIDANCE[2]

INTRODUCTION

The neural circuitry that mediates behavioral responses to rewarding and aversive stimuli become disrupted in neuropsychiatric diseases such as drug addiction, anxiety disorders, and depression (Koob and Volkow, 2010; Shin and Liberzon, 2010). Ventral tegmental area (VTA) dopaminergic neurons show changes in firing patterns in response to both rewarding and aversive associated stimuli (Brischoux et al., 2009; Schultz et al., 1997). While dopaminergic neurons encode salient stimuli and predictive cues, the neural circuit elements that provide dopamine neurons with reward- and aversive-related information are not well defined.

The lateral habenula (LHb) has been shown to signal punishment and prediction errors, as LHb neurons are excited by aversive stimuli and inhibited by rewarding stimuli (Bromberg-Martin and Hikosaka, 2011). In addition, excitatory inputs to LHb neurons are potentiated in a learned helplessness model of depression (Li et al., 2011). The LHb sends excitatory projections to GABAergic neurons in midbrain limbic structures such as the VTA and rostromedial tegmental nucleus (RMTg) (Jhou et al., 2009b; Matsui and Williams, 2011; Perrotti et al.,

[2]This chapter previously appeared as an article in the journal *Nature Neuroscience.* The original citation is as follows: Stamatakis, A.M., and Stuber, G.D. (2012) Activation of lateral habenula inputs to the ventral midbrain promotes behavioral avoidance. Nature Neuroscience. *8*. 1105-1107.

2005), which act to inhibit dopaminergic neuron output (Ji and Shepard, 2007; van Zessen et al., 2012). While correlative evidence suggests that the LHb neurons convey negative reward-related information, whether selective activation of LHb efferents to the midbrain has behaviorally relevant consequences remains elusive. Here, we used *ex vivo* and *in vivo* optogenetic strategies to investigate whether neurotransmission at LHb-to-RMTg glutamatergic synapses is altered by acute exposure to unpredictable aversive stimuli, and how direct manipulation of this pathway affects behavior.

METHODS

Experimental subjects and stereotaxic surgery

We grouped housed adult (25–30 g) male C57BL/6J mice (Jackson Laboratory) until surgery. We anesthetized the mice with ketamine (150 mg per kg of body weight) and xylazine (50 mg per kg) and placed the mice in a stereotaxic frame (Kopf Instruments). We bilaterally microinjected 0.4 µl of purified and concentrated adeno-associated virus (AAV, ~10^{12} infections units per ml, packaged and titered by the UNC Vector Core Facility) into the LHb (coordinates from bregma: −1.7 anterior/posterior, ±0.48 medial/lateral, −3.34 dorsal/ventral). LHb neurons were transduced with virus encoding ChR2-EYFP or EYFP under the control of the human synapsin (*SYN1*) promoter. Following surgery, we individually housed the mice. For behavioral experiments, we also implanted mice with a unilateral chronic fiber directed above the RMTg (coordinates from bregma: −3.9 AP, ±0.3 ML, −4.8 DV). We performed all experiments 6–8 weeks after surgery. We conducted all

procedures in accordance with the Guide for the Care and Use of Laboratory Animals, as adopted by the US National Institutes of Health, and with approval of the UNC Institutional Animal Care and Use Committees.

Histology, immunohistochemistry and microscopy

We anesthetized mice with pentobarbital and killed them by perfusion with phosphate-buffered saline followed by 4% paraformaldehyde (wt/vol) in phosphate-buffered saline. We subjected 40-μm brain sections to immunohistochemical staining for neuronal cell bodies and/or tyrosine hydroxylase (Pel Freeze, made in sheep; Neurotrace: Invitrogen, 640-nm excitation/660-nm emission or 435-nm excitation/455-nm emission) as previously described (van Zessen et al., 2012). We mounted sections and captured *z* stack and tiled images on a Zeiss LSM Z10 confocal microscope using a 20× or 63× objective. For determination of optical fiber placements, we imaged tissue at 10× on an upright fluorescent microscope. We recorded optical stimulation sites as the location in tissue where visible optical fiber tracks terminated.

Slice preparation for patch-clamp electrophysiology

We prepared brain slices for patch-clamp electrophysiology as previously described (Stuber et al., 2011; van Zessen et al., 2012). Briefly, we anesthetized mice with pentobarbital and perfused transcardially with modified artificial cerebrospinal fluid. We then rapidly removed the brains and placed them in the same solution that we used for perfusion at ~0° C. We cut sagittal midbrain slices containing the RMTg (200 μm) or horizontal midbrain slices containing the VTA and

RMTg (200 μm) on a vibratome (VT-1200, Leica Microsystems), placed the slices in a holding chamber and allowed them to recover for at least 30 min before recording.

Patch-clamp electrophysiology

We made whole-cell voltage-clamp recordings of RMTg neurons as previously described (Stuber et al., 2011). Briefly, we back-filled patch electrodes (3.0–5.0 MΩ) for current-clamp recordings, with a potassium-gluconate internal solution (van Zessen et al., 2012). For voltage-clamp recordings, we back-filled patch electrodes with a cesium methanesulfonic acid internal solution (Stuber et al., 2010). For optical stimulation of EPSCs, we used light pulses from an LED coupled to a 40× microscope objective (1-ms pulses of 1–2 mW, 473 nm) to evoke presynaptic glutamate release from LHb projections to RMTg. For mEPSCs and optically evoked EPSCs, we voltage-clamped RMTg neurons at −70 mV. For AMPA and NMDA receptor experiments, the holding potential was +40 mV. We added picrotoxin (100 μM) to the external solution to block $GABA_A$ receptor–mediated inhibitory postsynaptic currents for all experiments. For mEPSCs, we added tetrodotoxin (500 nM) to the external solution to suppress action potential driven release. We calculated the AMPA/NMDA ratio and paired pulse ratio as previously described18. We averaged six sweeps together to calculate both the AMPA/NMDA ratio and the paired pulse ratio. We collected mEPSCs for 5 min or until 300 mEPSCs were collected. To determine where, anterior-posterior, midbrain neurons were light responsive, we injected *TH-IRES-GFP* mice with *SYN1-ChR2-EYFP* into the LHb. We voltage-clamped (–70mV) GFP-positive (tyrosine hydroxylase positive) and GFP-negative (tyrosine hydroxylase negative) midbrain neurons and

categorized the cells as light-responsive if a light pulse resulted in an average evoked current across six sweeps of >20 pA.

Shock procedure for patch-clamp electrophysiology

We placed mice expressing ChR2-EYFP in the LHb-to-RMTg pathway into standard mouse behavioral chambers (Med Associates) equipped with a metal grid floor capable of delivery foot shocks for 20 min. Mice received either 19 or 0 unpredictable foot shocks (0.75 mA, 500 ms). We presented shocks with a pseudo-random interstimulus interval of 30, 60 or 90 s. We anesthetized mice for patch-clamp electrophysiology 1 h after the session ended (described above).

***In vivo* optogenetic excitation**

For all behavioral experiments, we injected mice with a ChR2-EYFP or EYFP virus and implanted them with a chronic unilateral custom-made optical fiber targeted to the RMTg as described previously (Sparta et al., 2012). We connected mice to a 'dummy' optical patch cable 3 d before the experiment each day for 30–60 min to habituate them to the tethering procedure. Following the tethering procedure, we then ran mice in the behavioral procedures (see below). We used a 10-mW laser with a stimulation frequency of 60 Hz and a 5-ms light pulse duration for all behavioral experiments.

Real-time place preference

We placed mice in a custom-made behavioral arena (50 × 50 × 25 cm black plexiglass) for 20 min. We assigned one counterbalanced side of the chamber as the

stimulation side. We placed the mouse in the nonstimulated side at the onset of the experiment and delivered a 60-Hz constant laser stimulation each time the mouse crossed to the stimulation side of the chamber until the mouse crossed back into the nonstimulation side. We recorded behavioral data via a CCD camera interfaced with Ethovision software (Noldus Information Technologies). We defined an escape attempt as each time a mouse attempted to climb out of the apparatus. We only scored an attempt if no paws were on the ground.

Conditioned place preference

The conditioned place preference apparatus (Med Associates) consisted of a rectangular cage with a left black chamber (17 cm × 12.5 cm) with a vertical metal bar floor, a center gray chamber (15 cm × 9 cm) with a smooth gray floor and a right white chamber (17 cm × 12.5 cm) with a wire mesh floor grid. We monitored mouse location in the chamber using a computerized photo-beam system. The conditioned place preference test consisted of 4 d. Day 1 consisted of a preconditioning test that ensured that mice did not have a preference for one particular side20. On days 2 and 3, we placed the mice into either the black or white side of the chamber (counterbalanced across all mice) and delivered either 0.5 s of 60-Hz stimulation with an interstimulus interval of 1 s for 20 min, or no stimulation. Approximately 4 h later, we placed the mice into the other side of the chamber and the mice received the other treatment. We placed the mice back into the chamber 24 h after the last conditioning session with all three chambers accessible to assess preference for the stimulation and nonstimulation paired chambers. To assess long-term associations between the stimulation and context, we placed the mice back in the chambers 7 d

later.

Negative and positive reinforcement procedures

Behavioral training and testing occurred in mouse operant chambers interfaced with optogenetic stimulation equipment as described previously (Sparta et al., 2012). For the negative reinforcement procedure, we placed mice into the chamber and delivered 500 ms of 60-Hz optical stimulation with an interstimulus interval of 1 s. We trained mice on a fixed ratio (FR1) training schedule, in which each nose poke resulted in 1 20-s period in which the laser was shut off and the LHb-to-RMTg pathway was not optogenetically activated. In addition, a tone and houselight cue turned on for the entire 20 s and turned off when the laser stimulation returned. For the positive reinforcement procedure, we food restricted a separate group of mice to 90% of their free-feeding bodyweight. We then trained mice for one session per day for 1 h in the operant chambers on a FR1 schedule (in which each nose poke resulted in 20 µl of a 15% sucrose solution, wt/vol). In addition, a tone and houselight cue turned on for 2 s. Once the mice reached stable behavioral responding (as determined by 3 d of over 100 active nose pokes that did not vary by more than 20% from the first of the 3 d), mice received 2 s of 60-Hz optical stimulation time-locked to the cue following each active nose poke. For both behaviors, we recorded inactive nose pokes, but these had no programmed consequences. In addition, we collected and time-stamped the number of active and inactive nose pokes.

Data analysis

We used *t* tests and one- or two-way analyses of variance to analyze all behavioral and electrophysiological data when applicable. When we obtained significant main effects, we performed Tukey's HSD *post hoc* tests for group comparison. For all behavioral experiments, we analyzed the data in Ethovision, Matlab, Excel and Prism. We used six mice per group for the real-time place preference and negative reinforcement experiments and eight mice per group for the conditioned place preference and positive reinforcement experiments. We used no more than two neurons from a given animal for patch-clamp electrophysiology in the aversive stimuli exposure experiments.

RESULTS

Optogenetic Targeting of LHb Neurons and Innervation to the RMTg

To selectively activate LHb efferents to the RMTg, we introduced channelrhodopsin-2 fused to an enhanced yellow fluorescent protein (ChR2-eYFP) in the LHb of mice using viral methods (**Figure 2.1 A-C**). We observed LHb terminal expression of ChR2-eYFP in midbrain structures, including the VTA and RMTg (**Figure 2.1 D-F**). Whole cell recordings from RMTg neurons in brain slices revealed that light pulses, to selectively stimulate LHb ChR2-expressing efferent fibers, resulted in inward currents that were blocked by the glutamatergic receptor antagonist DNQX (**Figure 2.1 G,H**).

We then determined the anterior-posterior distribution of LHb-to-midbrain functional connectivity by recording from dopaminergic and non-dopaminergic

neurons following optical stimulation of LHb efferents in *th-ires-GFP* transgenic mice. Fibers originating from the LHb were predominantly localized to the posterior VTA and RMTg and the majority of light-responsive neurons were non-dopaminergic neurons located in the RMTg and posterior VTA (**Figure 2.1 E,I,J**).

Acute unpredictable foot shock exposure enhances LHb-to-RMTg glutamate release

Since neurotransmission by LHb neurons may encode information related to aversive stimuli processing (Matsumoto and Hikosaka, 2009a), we explored whether exposure to an aversive stimulus altered excitatory neurotransmission at LHb-to-RMTg synapses. We exposed mice expressing ChR2-eYFP in LHb-to-RMTg fibers to either 0 or 19 unpredictable foot shocks in a single 20-min session. One hour later, we performed whole-cell recordings from RMTg neurons in close proximity to LHb-to-RMTg ChR2-eYFP-positive fibers. Voltage clamp recordings from RMTg neurons from foot shock-exposed mice displayed an increase in the frequency of miniature excitatory postsynaptic currents (mEPSCs) compared to non-shocked controls (**Figure 2.2 A-C**). Furthermore, LHb-to-RMTg glutamate release probability was significantly enhanced following shock exposure, as indexed by a reduction in the optically-evoked paired pulse ratio (**Figure 2.2 D,E**). We observed no differences in mEPSC amplitude or optically-evoked AMPA/NMDA ratios, measurements of postsynaptic glutamate receptor number or function (**Figure 2.2 A,C,F,G**). These data suggest that aversive stimuli exposure enhances presynaptic transmission from LHb inputs to RMTg neurons.

Activation of LHb inputs to the RMTg produces active, passive, and conditioned behavioral avoidance

To determine whether optogenetic stimulation of LHb-to-RMTg fibers has behavioral consequences, we optogenetically stimulated this pathway in behaving mice at 60-Hz as this was the mean light-evoked firing rate of LHb neurons in brain slices (**Figure 2.1 B,C**). To determine if optogenetic stimulation of LHb-to-RMTg fibers resulted in passive avoidance behavior, we tested mice in a real-time place preference chamber. When an experimental mouse crossed over into a counter-balanced stimulated-designated, contextually indistinct side of an open field, light stimulation was constantly pulsed until the mouse crossed back into the non-stimulated designated side. Mice expressing eYFP spent equal times on both sides of the chamber, whereas mice expressing ChR2-eYFP spent significantly less time on the stimulated side (**Figure 2.3 A,B**) and made significantly more escape attempts (**Figure 2.3 C**). There were no differences in total distance traveled or average velocity between ChR2-eYFP and eYFP mice across the entire session (**Figure 2.3 D,E**). These data suggest that acute activation of LHb-to-RMTg fibers promotes location-specific passive avoidance behavior.

While activation of the LHb-to-RMTg pathway induced acute avoidance, we next determined if activation of this pathway produced conditioned avoidance using a standard nonbiased conditioned place preference paradigm. 24 hrs after the last conditioning session, where optogenetic stimulation was paired with a distinct context, ChR2-eYFP-expressing mice showed a significant conditioned place aversion for the stimulation-paired chamber, while the eYFP-expressing mice showed no preference or aversion (**Figure 2.3 F**). This conditioned place aversion

was maintained in the ChR2-eYFP-expressing mice 7 days following the last conditioning session (**Figure 2.3 G**) demonstrating that activity in this pathway also promotes conditioned avoidance. To determine if mice would perform an operant response to actively avoid activation of LHb-to-RMTg fibers, ChR2-eYFP or eYFP expressing mice were placed in chambers where they could nose-poke to terminate optogenetic stimulation of LHb-to-RMTg fibers (**Figure 2.4 A**). ChR2-eYFP-expressing mice learned to nose-poke to terminate laser stimulation over 3 daily training sessions (**Figure 4 B,C**). Following training, ChR2-eYFP-expressing mice made significantly more active nose-pokes to terminate LHb-to-RMTg activation compared to eYFP-expressing mice (**Figure 4 D,E**), resulting in a significant increase in the percentage of time the stimulation was off (percent time stimulation was off: ChR2-eYFP: 47.5 ± 7.1 %; eYFP: 2.8 ± 0.9 %; $t(10) = 6.28$, $p < 0.0001$). These data demonstrate that LHb-to-RMTg activity can negatively reinforce behavioral responding.

Next, we examined whether LHb-to-RMTg activation disrupted positive reinforcement. We trained a separate group of mice to nose-poke to earn liquid sucrose rewards. Following stable responding, nosepokes to earn sucrose in subsequent test sessions where paired with a 2s, 60-Hz LHb-to-RMTg stimulation (**Figure 2.5 A**). ChR2-eYFP-expressing mice receiving stimulations made significantly fewer nose-pokes compared to eYFP-expressing mice and took significantly longer to retrieve and consume the rewards (**Figure 2.5 B-G**). Importantly, there were no significant differences between the two groups in the session prior when nosepokes were not paired with LHb-to-RMTg stimulation ($t(14)$

= 1.64, p = 0.12), suggesting that stimulation of this pathway time-locked to an operant response served as a punishment.

DISCUSSION

We found that activation of LHb terminals in the RMTg promotes active, passive, and conditioned behavioral avoidance, suggesting that endogenous activity of LHb glutamatergic inputs to the RMTg conveys information related to aversion. The data presented here suggest that the LHb's connection with midbrain GABA neurons is crucial for promoting these behaviors. Consistent with this, direct excitation of VTA GABA neurons disrupts reward-related behaviors (van Zessen et al., 2012) and stimulation of VTA GABA neurons or inhibition of VTA dopamine neurons promotes aversion (Tan et al., 2012). Importantly, optogenetic stimulation of LHb terminals in the RMTg suppressed positive reinforcement and supported negative reinforcement, demonstrating this pathway can bidirectionally effect the same behavioral response (nose-poking) depending on the task. Dopamine signaling in the nucleus accumbens (NAc) promotes positive reinforcement (Koob and Volkow, 2010; Schultz et al., 1997). Thus, motivated behavior to suppress activation of the LHb-to-RMTg pathway may also depend on dopamine signaling in the NAc. Although encoding negative consequences requires multiple neural circuits, activation of glutamatergic presynaptic inputs to the LHb (Li et al., 2011; Shabel et al., 2012) or LHb inputs to the midbrain alone produces aversion. Since

LHb projections are phylogenetically well-conserved (Stephenson-Jones et al., 2012), neurotransmission in this pathway is likely essential for survival by promoting learning and subsequent behavior to avoid stimuli associated with negative consequence.

FIGURES

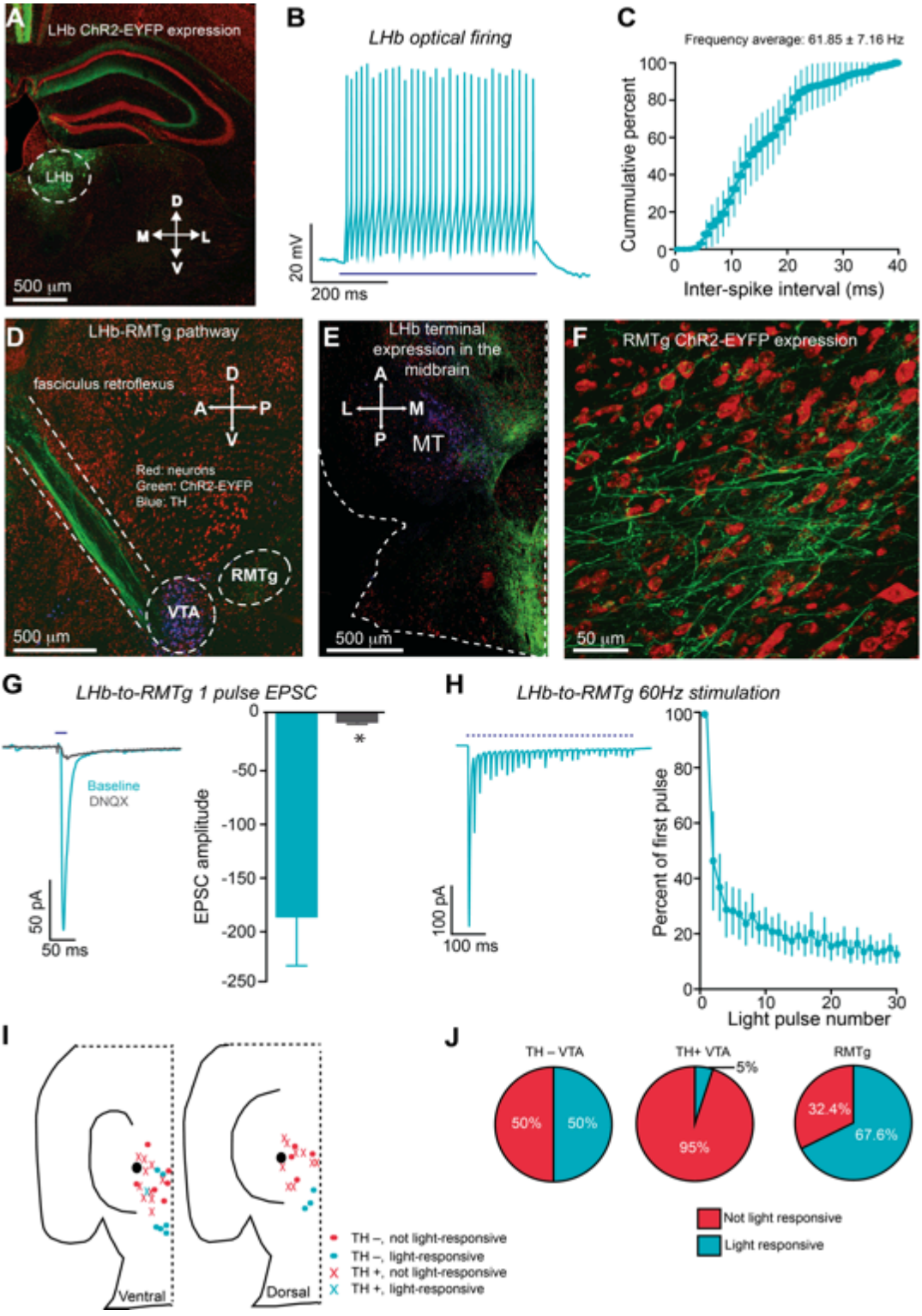

Figure 2.1. The LHb sends a functional glutamatergic projection to the RMTg.

(**A**) Expression of ChR2-eYFP (green) following injection of the viral construct into

the LHb. Neurons were counter-stained using a red fluorescent Nissl stain. D, Dorsal; V, Ventral; M, Medial; L, Lateral. (**B**,**C**) Activation of ChR2 expressed in LHb cell bodies in brain slices resulted in sustained high frequency activation during the 500 ms stimulation (n=7 cells). (**D**) Sagittal confocal image showing expression of ChR2-eYFP in the LHb-to-midbrain pathway via the fasciculus retroflexus fiber bundle following injection of the viral construct into the LHb. Midbrain TH+ dopaminergic neurons are shown in blue. A, Anterior; P, Posterior. (**E**) Horizontal confocal image showing the distribution of LHb terminals in the midbrain. (**F**) Confocal compressed z-stack showing that ChR2-eYFP is expressed in LHb projection fibers in the RMTg after virus injection into the LHb. (**G**) Postsynaptic optically-evoked EPSCs recorded from RMTg neurons were significantly attenuated following bath application of 10μM DNQX ($t_6 = 3.94$, $p = 0.07$, n = 4 cells). (**H**) LHb efferents to the RMTg were stimulated at 60 Hz for all behavioral tasks. Optically-evoked EPSCs at this frequency for 500 ms show a significant reduction in amplitude across the pulse train stimulation ($F_{2,29} = 60.21$, $p < 0.001$, n = 5 cells). All error bars for all figures correspond to the s.e.m. *indicates $p < 0.05$ and ** indicates $p < 0.01$ for all figures.

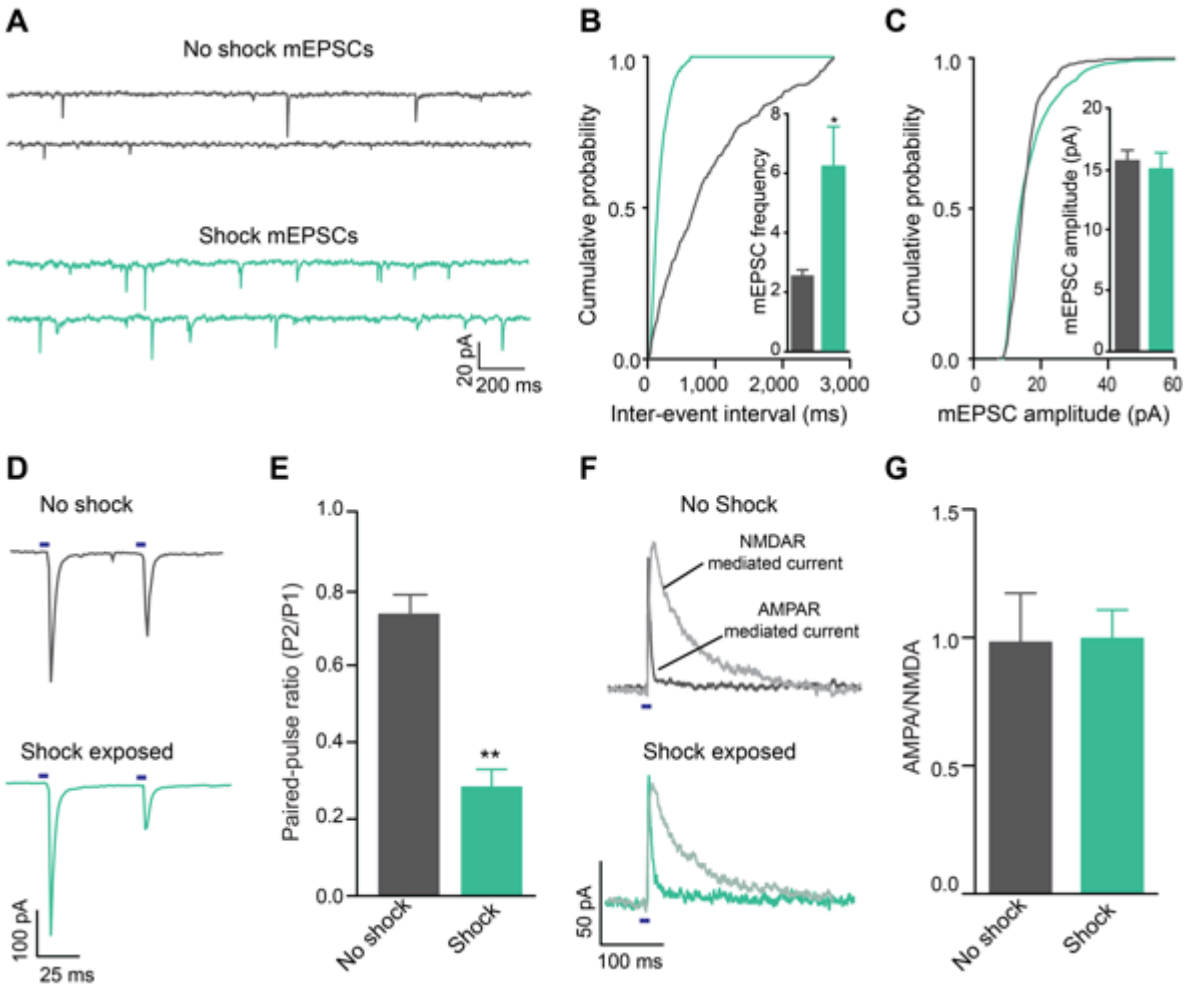

Figure 2.2: Acute unpredictable foot shock exposure enhances LHb-to-RMTg glutamate release. (**A**) Representative mEPSC traces recorded from neurons from mice immediately following either 0 or 19 unpredictable foot shocks. (**B**) Representative cumulative mEPSC inter-event interval probability plot. Inset: Average mEPSC frequent was significantly increased in neurons from shock exposed mice (t_{13} = 2.88, p = 0.01) (**C**) Representative cumulative mEPSC amplitude probability plot. Inset: Average mEPSC amplitude was not altered in RMTg neurons from shock-exposed mice (t_{13}= 0.12, p = 0.19). (**D**) Representative optically evoked paired-pulse ratios from LHb efferents onto RMTg neurons. (**E**) Average paired-pulse ratios showing that paired-pulse ratios at LHb-to-RMTg

synapses were significantly depressed from mice that received foot shocks (t_{14} = 3.56, p = 0.003, n = 8 cells/group). (**F**) Representative optically evoked AMPA/NMDA ratios at LHb-to-RMTg synapses following 0 or 19 foot shocks. (**G**) Optically evoked AMPA/NMDA ratios were not significantly different between the groups t_{14} = 0.36, p = 0.86, n = 8 cells/group).

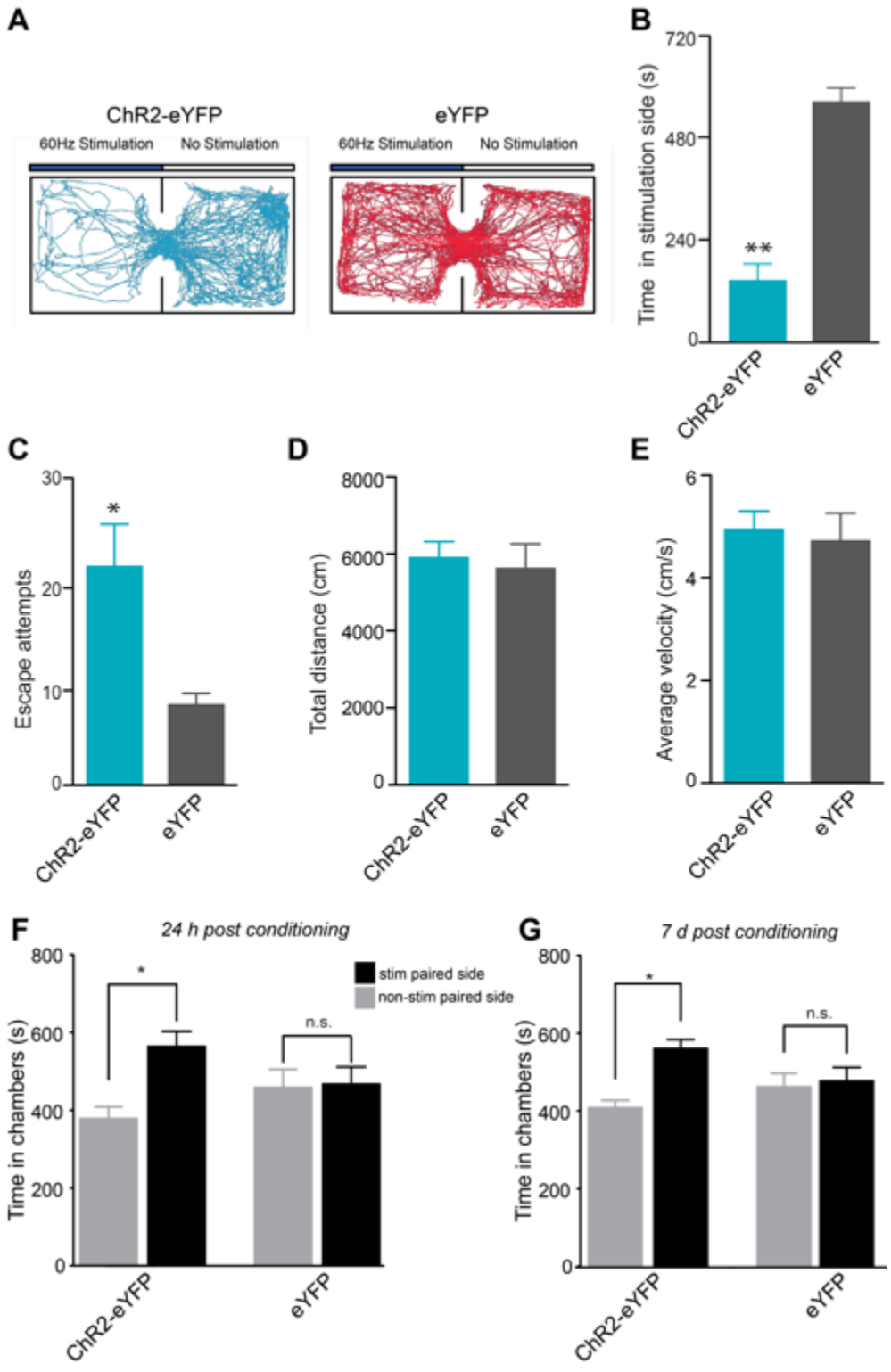

Figure 2.3: Activation of LHb inputs to the RMTg produces active and conditioned behavioral avoidance. (**A**) Real-time place preference location plots

from two representative mice showing the animal's position over the course of the 20-min session. (**B**) ChR2-eYFP-expressing mice spent significantly less time on the stimulated-paired side (t_{10} = 7.90, p < 0.0001, n = 6 mice/group for real-time place preference. (**C**) ChR2-eYFP-expressign mice made significantly more escape attempts during the real-time place preference session than eYFP-expressing mice (t_{10} = 2.82, p = 0.018). (**D**) Total distance (cm) during the real time place preference experiment across the entire arena was not significantly different between groups (t_{10} = 0.37, p = 0.72). (**E**) Average velocity across the entire 20-min session across the entire arena was not significantly different between groups (t_{10} = 0.34, p = 0.74, n = 6 mice per group). (**F**) ChR2-eYFP-expressing mice spent significantly less time in the stimulation=paired chamber compared with the nonstimulation-paired chamber 24 h after the last stimulation conditioning session (t_7 = 3.54, p = 0.01). eYFP expressing mice did not show a preference (t_7 = 0.57, p = 0.58). (**G**) ChR2-eYFP-expressing mice spent significantly less time in the stimulation=paired chamber compared with the nonstimulation-paired chamber 7 d after the last stimulation conditioning session (t_7 = 3.24, p = 0.01). eYFP expressing mice did not show a preference (t_7 = 0.17, p = 0.86). n = 8 mice per group for conditioned place preference. Error bars represent s.e.m.

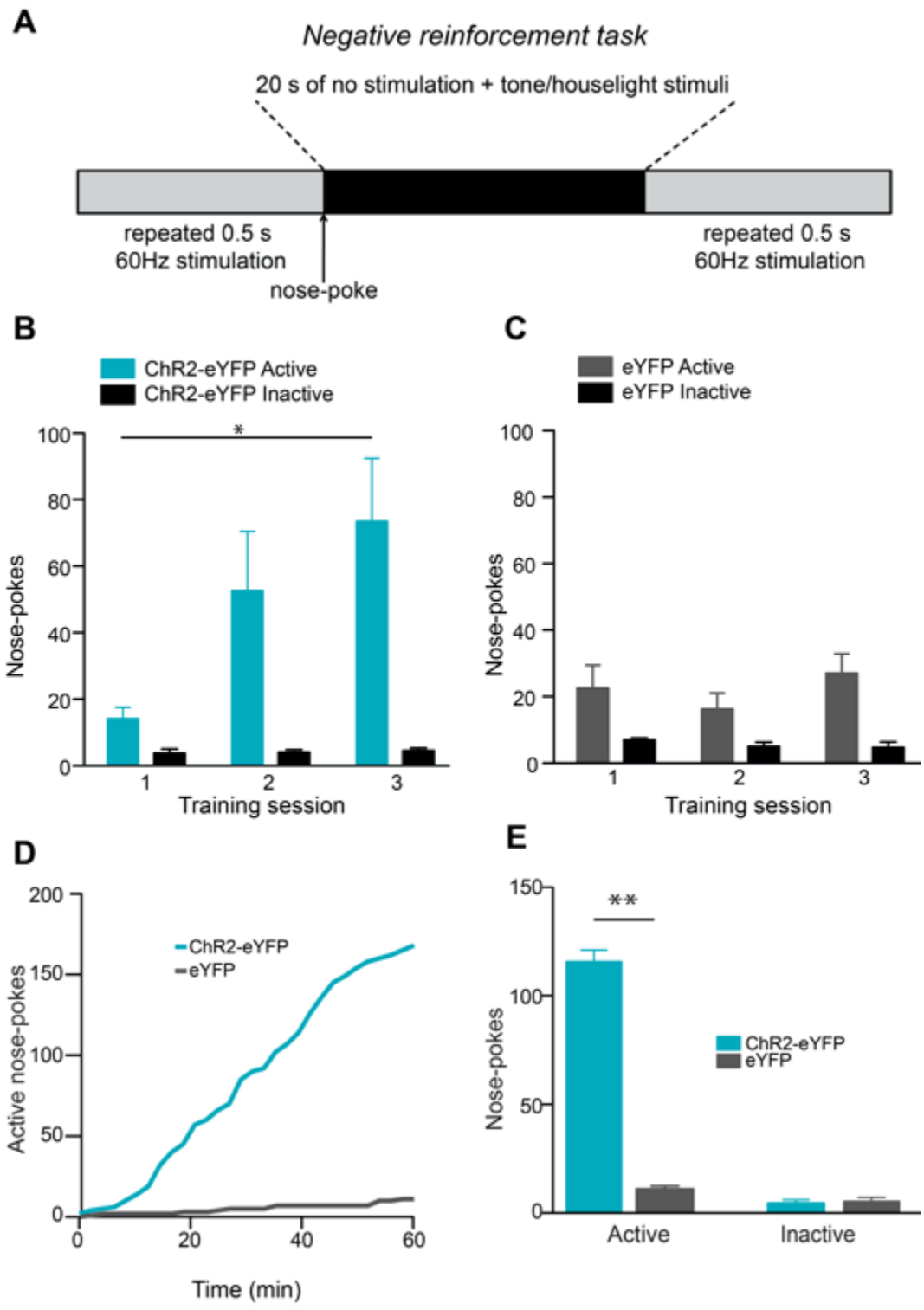

Figure 2.4: Activation of LHb inputs to the RMTg promotes negative reinforcement. (**A**) Behavioral schematic for the 1-hr negative reinforcement session. (**B**) Active and inactive nose-poke responses from ChR2-eYFP-expressing

mice over the first 3 days of training. There was a significant interaction between active lever presses and days ($F_{2,10}$ = 3.86, p = 0.03). (**C**) Active and inactive nose-poke responses from eYFP-expressing mice over the first 3 days of training. There was no significant interaction between active lever presses and days ($F_{2,10}$ = 0.84, p = 0.44) (**D**) Example cumulative records of active nose-pokes made by a ChR2-eYFP and eYFP-expressing mouse to terminate LHb-to-RMTg optical activation. (**E**) Average number of active nose-pokes from one behavioral session in following training (> 4 days; t_{10} = 20.52, p < 0.0001). There was no difference in inactive nose pokes between the two groups (t_{10} = 0.29, p = 0.78). n = 6 mice per group. Error bars represent s.e.m.

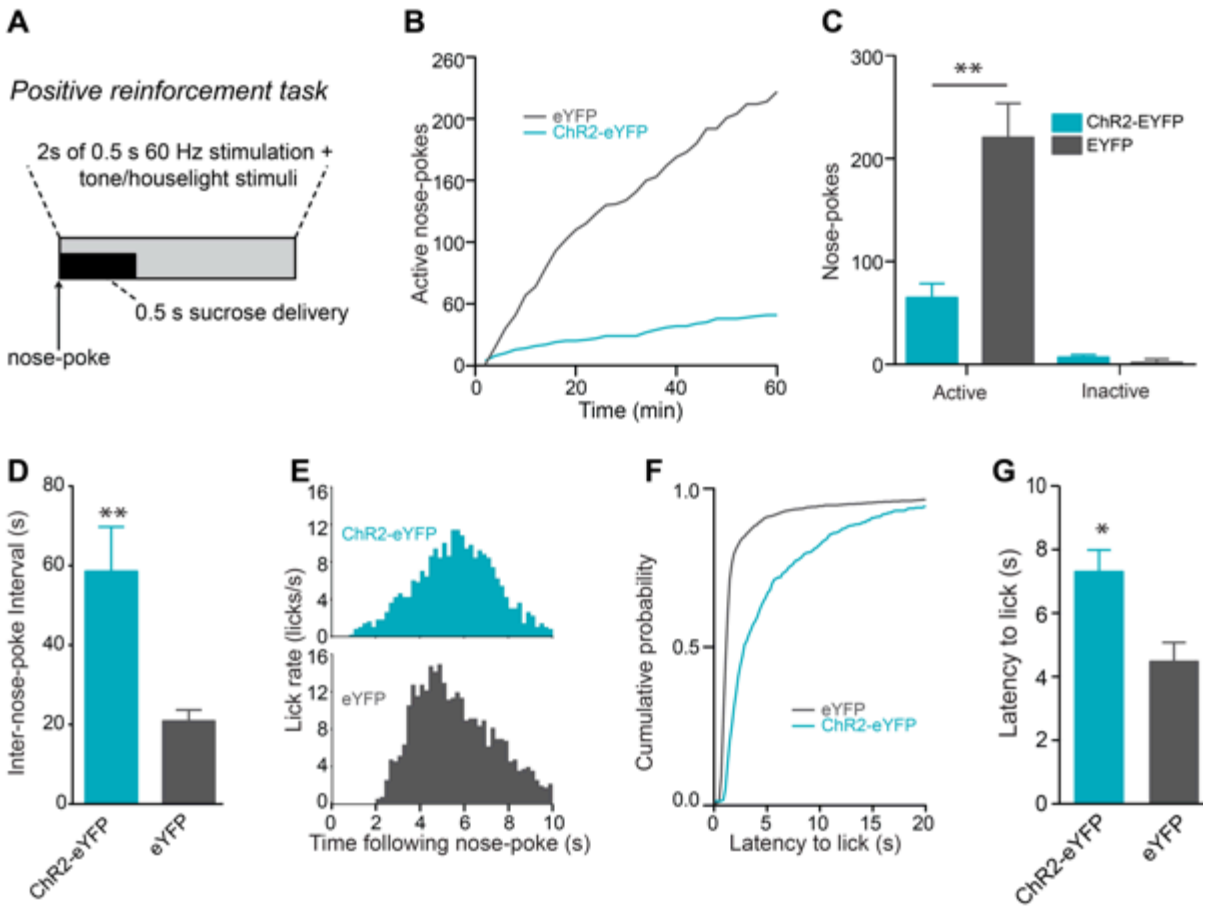

Figure 2.5: Activation of LHb inputs to the RMTg disrupts positive reinforcement (**A**) Behavioral schematic for the 1-hr positive reinforcement session. (**B**) Example cumulative records of active nose pokes made by a ChR2-eYFP-expressing mouse and an eYFP-expressing mouse when optical stimulation was paired with the nose poke to receive a sucrose reward. (**C**) Average number of active and inactive nose pokes during positive reinforcement ($t_{14} = 4.01$, $p < 0.01$). There was no difference in inactive nose pokes between the two groups (t14 = 1.22, p = 0.24) (**D**) The inter nose-poke interval (time between each nose-poke averaged across the session) was significantly higher in ChR2-eYFP-expressing mice ($t_{3577} = 10.8$, $p < 0.001$). (**E**) Example histograms of licks time-locked to active nose-pokes for ChR2-eYFP-expressing mouse (top) and ChR2-eYFP-expressing mouse

(bottom). (**F**) Cumulative probability of the latency to lick following stimulation for ChR2-eYFP and eYFP—expressing mice. (**G**) Average latency to lick following stimulation for ChR2-eYFP and eYFP-expressing mice (t_{2032} = 2.5, p = 0.01) n = 8 mice per group. Error bars represent s.e.m.

CHAPTER 3: A UNIQUE POPULATION OF VENTRAL TEGMENTAL AREA NEURONS INHIBITS THE LATERAL HABENULA TO PROMOTE REWARD[3]

INTRODUCTION

Dopaminergic neurons in the ventral tegmental area (VTA) are thought to encode reward prediction error—the difference between an expected reward and actual reward. Consistent with this, dopaminergic neurons are phasically excited by reward and the cues that predict them and are phasically inhibited by the omission of reward and aversive stimuli (Cohen et al., 2012; Matsumoto and Hikosaka, 2007; Pan and Hyland, 2005; Schultz et al., 1997; Tobler et al., 2005; Ungless et al., 2004). Increased firing rate of dopaminergic neurons in response to salient stimuli causes phasic dopamine release in the nucleus accumbens (NAc), a signaling event thought to be critical for initiation of motivated behaviors (Day et al., 2007; Grace, 1991; Oleson et al., 2012; Phillips et al., 2003b; Stuber et al., 2008).

The lateral habenula (LHb) is a key neuroanatomical regulator of midbrain reward circuitry. Although dopaminergic neurons are excited by rewarding stimuli and inhibited by the omission of reward, neurons in the LHb display contrary responses: they are inhibited by cues that predict reward and excited by the

[3]This chapter previously appeared as an article in the journal *Neuron.* The original citation is as follows: Stamatakis, A.M., Jennings, J.H., Ung, R.L., Blair, G.A., Weinberg, R.J., Neve, R.L., Boyce, F., Mattis, J., Ramakrishnan, C., Deisseroth, K., and Stuber, G.D. (2013) A unique population of ventral tegmental area neurons inhibits the lateral habenula to promote reward. Neuron. *4*. 1039-1053.

omission of reward (Matsumoto and Hikosaka, 2007). Importantly, in response to the omission of reward, excitation of the LHb neurons precedes the inhibition of dopaminergic neurons, suggesting that LHb neurons may modulate VTA dopaminergic neurons. Further supporting this claim, electrical stimulation of the LHb inhibits midbrain dopaminergic neurons (Christoph et al., 1986; Ji and Shepard, 2007), whereas pharmacological inhibition of the LHb increases dopamine release in the striatum (Lecourtier et al., 2008). Collectively, these data suggest that LHb neurons encode negative reward prediction errors and may negatively modulate midbrain dopaminergic neurons in response to aversive events.

The LHb sends a functional glutamatergic projection to the rostromedial tegmental nucleus (RMTg, also referred to as the tail of the VTA), a population of GABAergic neurons located posterior to the VTA (Brinschwitz et al., 2010; Jhou et al., 2009b; Stamatakis and Stuber, 2012). *In vivo* activation of VTA-projecting LHb neurons (Lammel et al., 2012), or LHb glutamatergic terminals in the RMTg, produces aversion and promotes motivated behavior to avoid further activation of the LHb-to-RMTg pathway (Stamatakis and Stuber, 2012), demonstrating a causal role for this pathway in controlling aversive behavior. Because GABAergic RMTg neurons inhibit midbrain dopaminergic neurons (Matsui and Williams, 2011), the RMTg is likely the intermediary structure through which the LHb inhibits midbrain dopaminergic neurons.

Although the LHb-to-midbrain circuit has been dissected both functionally and behaviorally, less is known about the importance of the various LHb afferents. Inputs to the LHb arise from forebrain regions including the lateral hypothalamus,

entopenduncular nucleus (EN), and prefrontal cortex (Kim and Lee, 2012; Poller et al., 2013; Shabel et al., 2012; Warden et al., 2012). A recent study suggests that aversive signaling by the LHb is mediated in part from the EN, as *in vivo* activation of these afferents in the LHb is aversive (Shabel et al., 2012). Although the majority of LHb afferents arise from the forebrain, the LHb also receives a substantial projection from the VTA (Gruber et al., 2007; Phillipson and Griffith, 1980; Skagerberg et al., 1984), with an estimated 30%–50% of LHb-projecting VTA neurons being dopaminergic (Gruber et al., 2007; Skagerberg et al., 1984). Electrical stimulation of the midbrain decreases the firing rate of LHb neurons (Shen et al., 2012), but the functional and behavioral significance of synaptic inputs to the LHb arising from VTA dopaminergic neurons remains unknown. Here, we demonstrate that selective activation of this projection inhibits LHb neurons by the actions of synaptically released GABA, which disinhibits VTA dopaminergic neurons to promote reward-related behavior.

METHODS

Subjects and Stereotactic Surgery

Adult (25–30 g) mice were group housed until surgery and maintained on a reverse 12 hr light cycle (lights off at 8:00) with ad libitum access to food and water. Mice were anesthetized with ketamine (150 mg/kg of body weight) and xylazine (50 mg/kg) and placed in a stereotactic frame (Kopf Instruments). For all slice electrophysiology and fast-scan cyclic voltammetry experiments, except for the retrobeads experiments, male and female TH-IRES-Cre backcrossed to C57BL/6J

were bilaterally microinjected with 0.5 µl of purified and concentrated adeno-associated virus serotype 5 (AAV5; ~10^{12} infections units per ml, packaged and titered by the UNC Vector Core Facility) into the VTA. Each VTA was injected with an AAV5 coding Cre-inducible ChR2 under control of the EF1α promoter to transduce VTA dopaminergic neurons (TH^{VTA}::ChR2). For the retrobead slice electrophysiology and PCR retrobead experiments, male and female TH-IRES-GFP mice received quadruple injections of 0.3 µl of red retrobeads (Lumafluor) into either the NAc or LHb. For the retrobead mapping and quantification experiments, male C57BL/6J mice (Jackson Laboratory) received quadruple injections with 0.3 µl of red retrobeads into the NAc. In the same surgery, the mice also received quadruple injections of 0.3 µl with green retrobeads (Lumafluor) into the LHb. For tracing experiments, TH-IRES-Cre mice were bilaterally injected with 0.5 µl of HSV-EF1α-LS1L-flp into the LHb or NAc and bilaterally injected with 0.5 µl of AAV5-EF1α-fdhChR2(H134R)-eYFP into the VTA. For behavioral experiments, male TH-IRES-Cre positive ($TH^{VTA\text{-}LHb}$::ChR2) and negative ($TH^{VTA\text{-}LHb}$::Control) littermates were bilaterally injected with Cre-inducible ChR2 and also implanted with bilateral chronic fibers directed above the LHb. For the LHb microinjection experiments, a 26G steel tube cannula (McMasters-Carr) that terminated 0.5 mm above the tip of the optical fiber was epoxied to an optical fiber and bilaterally aimed at the LHb. Retrobead experiments were performed 7–21 days after surgery. All other experiments were performed 6–8 weeks after surgery. All procedures were conducted in accordance with the Guide for the Care and Use of Laboratory Animals, as adopted by the US National Institutes of Health, and with approval of the UNC Institutional Animal Care

and Use Committees.

Stereotactic coordinates

VTA coordinates (in mm from bregma): −3.1 anterior/posterior, ±0.4 medial/lateral, −5.0 dorsal/ventral. NAc coordinates (quadruple injections) at four different sites (in mm from bregma): +1.0 and 1.5 anterior/posterior, ±1.0 medial/lateral, −4.4 dorsal/ventral. LHb coordinates (quadruple injections) at four different sites (in mm from bregma): -1.3 and -1.9 anterior/posterior, ±0.44 medial/lateral, -3.44 dorsal/ventral. LHb fiber coordinates (in mm from bregma at 15º): -1.7 anterior/posterior, ±1.25 medial/lateral, -3.24 dorsal/ventral.

HSV vector construction

To optimize Adult the transcriptional cassette in the ST HSV vector backbone, thereby creating LT HSV, the entire CMV-transgene-SV40 polyadenylation (pA) signal cassette in ST HSV was replaced with an optimized cassette that had been previously assembled. The ST HSV and LT HSV have different promoters. The hCMV-IE1 promoter in the ST HSV was derived from pEGFP-C1 (Clontech), whereas it has been replaced with the EF1α promoter in LT HSV. The LT HSV vector also contains base pairs 1064-1750 of the Woodchuck Hepatitis Virus post-transcriptional response element (WPRE; (Donello et al., 1998)) which contributes to stabilization of expression. The promoter is flanked on the 5' side by the HSV oriS and IE4/5 promoter, which are followed by a SV40 A signal. The 3' pA signal in ST HSV is the SV40 late pA signal, and was derived from pCI (Promega), whereas the 3' pA signal in LT HSV is the SV40 early pA signal.

Histology, immunohistochemistry, and confocal microscopy

Mice were anesthetized with pentobarbital, and transcardially perfused with PBS followed by 4% (w/v) paraformaldehyde in PBS. Brains were then removed and submerged in 4% paraformaldehyde for 24 hr and transferred to 30% sucrose in ddH2O for 48 hr. 40 mm brain sections were obtained and subjected to immunohistochemical staining for neuronal cell bodies (NeuroTrace Invitrogen; 640-nm excitation/660-nm emission or 435-nm excitation/455-nm emission), and/or tyrosine hydroxylase (Pel Freeze; made in sheep, 1:500). Brain sections were mounted, and z-stack and tiled images were captured on a Zeiss LSM 710 confocal microscope using a 20x, 40x, or 63x objective and analyzed using ZEN 2009 and ImageJ software. To quantify fluorescence intensity, images were acquired using identical pinhole, gain, and laser settings for all brain regions. Intensity was then quantified using a scale from 0-255 in Image J to determine mean intensity. For co-localization analysis, Coloc2 software (Fiji) was used. To determine optical fiber placement, tissue was imaged at 10X and 20X on an upright conventional fluorescent microscope.

Electron Microscopy

TH$^{VTA\text{-}LHb}$::ChR2 mice were deeply anesthetized and intracardially perfused with PBS followed by a mixture of 4% paraformaldehyde and 1% glutaraldehyde in 0.1 M phosphate buffer, pH 7.2 (PB). Brains were removed and postfixed overnight in the same fixative. 50 µm-thick coronal sections throughout the LHb were cut on a Vibratome and collected in PB. Epifluorescence screening of wet sections was

performed to confirm appropriate fluorescent label of fibers in LHb. Sections were incubated at room temperature on a shaker in 1% hydrogen peroxide for 10 min (to block endogenous peroxidases), 30 min in 10% normal donkey serum (to block nonspecific antibody binding), and then overnight in chicken anti-GFP IgG (1:5,000). The next day sections were rinsed, blocked in 2% normal donkey serum, and treated with biotinylated secondary antibody against chicken IgG (Jackson ImmunoResearch, 1:200). After one hour incubation, sections were rinsed and incubated in ExtrAvidin (Sigma, 1:5,000) followed by standard diaminobenzidine histochemistry (for pre-embedding immunoperoxidase), or Nanogold-conjugated streptavidin (Nanoprobes, 1:100) followed by silver enhancement with IntenSE M (Amersham) for visualization of pre-embedding immunogold. Immunoprocessed sections were incubated 1 h in osmium tetroxide solution (0.1-0.5% in PB), rinsed in maleate buffer (0.1 M, pH 6.0), then 1 h in uranyl acetate (1% in maleate). Sections were dehydrated through graded ethanol, infiltrated in Spurr's resin, and sandwiched between two sheets of ACLAR plastic. They were then flat embedded between glass slides and heat-polymerized at 60° C for 48 hours. After polymerization, bits of tissue were cut from LHb and glued to plastic blocks. Thin sections (~70 nm) were cut with a diamond knife and collected on 300 mesh nickel grids (Ted Pella) for further processing. For single-label analysis, sections were post-stained with uranyl acetate and Sato's lead; for double-label study, sections first processed for postembedding immunogold labeling for GABA, as previously described (Phend et al., 1992), before post-staining. Grids were examined in a Tecnai F12 transmission EM (FEI); images were collected with a Gatan 12-bit cooled CCD. Images were

cropped and contrast adjusted using Adobe Photoshop.

Slice Preparation for Single-Cell RT-PCR, Fast-Scan Cyclic Voltammetry, and Patch-Clamp Electrophysiology

Mice were anesthetized with pentobarbital and perfused transcardially with modified artificial cerebrospinal fluid. Brains were then rapidly removed and placed in the same solution that was used for perfusion at ~0°C. For the PCR experiments, horizontal slices containing the VTA (200 μm) were cut on a Vibratome (VT-1200, Leica Microsystems). For fast-scan cyclic voltammetry, coronal slices containing either the NAc (250 μm), (BNST 250 μm), or LHb (250 μm) were obtained. For patch-clamp electrophysiology, coronal slices containing the LHb (200 μm), or horizontal slices containing the VTA (200 μm) were obtained. Following slicing, brain slices were placed in a holding chamber and were allowed to recover for at least 30 min before being placed in the recording chamber and superfused with bicarbonate-buffered solution saturated with 95% O_2 and 5% CO_2.

Patch-clamp Electrophysiology

Modified artificial cerebral spinal fluid contained (in mM): 225 sucrose, 119 NaCl, 1.0 NaH2PO4, 4.9 MgCl2, 0.1 CaCl2, 26.2 NaHCo3, 1.25 glucose. Bicarbonate-buffered solution contained (in mM): 119 NaCl, 2.5 KCl, 1.0 NaH2PO4, 1.3 MgCl2, 2.5 CaCl2, 26.2 NaHCO3, and 11 glucose (at 32-34°C). Potassium chloride internal solution contained (in mM): 135 KCl, 0.5 EGTA, 10 HEPES, 1.5 MgCl2, in RNAse- and DNAse-free water (Millipore). Methanesulfonic acid contained (in mM): 117 Cs methanesulfonic acid, 20 HEPES, 0.4 EGTA, 2.8 NaCl, 5 TEA, 2 ATP, 0.2 GTP. Cesium chloride internal solution contained (in mM): 130

CsCl, 1 EGTA, 10 HEPES, 2 ATP, 0.2 GTP. Potassium gluconate internal solution contained (in mM): 130 K-gluconate, 10KCl, 10 HEPES, 10 EGTA, 2 MgCl2, 2ATP, 0.2 GTP. pH = 7.35, 270-285 mOsm for all internal solutions. For voltage-clamp recordings, patch electrodes (3-5 MW) were back-filled with either a cesium methanesulfonic acid or cesium chloride internal solution. Cells were visualized using infrared differential contrast and fluorescence microscopy. For current-clamp and cell-attached recordings, patch electrodes (3-5 MW for current-clamp, 2-4 MW for cell-attached) were back-filled with a potassium gluconate internal solution. Whole-cell voltage-clamp, current-clamp, and cell-attached recordings of LHb or VTA dopaminergic neurons were made using an Axopatch 700B amplifier (Molecular Devices). For all optical stimulations, blue light (1 mW, 473 nm) was delivered through a 40X objective via a LED. Series resistance (15-25 MW) and/or input resistance were monitored online with a 5-mV hyperpolarizing step delivered between stimulation sweeps. All data were filtered at 2kHz, digitized at 5-10kHz, and collected using pClamp10 software (Molecular Devices). For the autoreceptor experiment, following 5-10 min of baseline recording, 3 μm of the D2 agonist quinpirole was bath-applied for 5 min. For IPSCs, following 5-10 min of baseline recording, 1 mM of the K^+ channel blocker 4AP, and 1 μM of the Na^+ channel blocker TTX was bath-applied for 10 min, followed by a 10 min bath application of 10 μM of the $GABA_A$ receptor antagonist, SR-95531 (gabazine). IPSC and EPSC amplitudes were calculated by measuring the peak current from the average response from 6 sweeps during baseline and during each drug application. Cells that showed a > 20% change in the holding current or access resistance were excluded

from analysis. To inhibit vesicular monoamine transporters *TH*^{VTA}::ChR2 mice were injected intraperitoneally with the irreversible *Vmat2* inhibitor reserpine (5 mg/kg) 24 h prior to slicing (Tritsch et al., 2012). Brain slices from these mice were prepared as described above, but were incubated in aCSF containing 1 μM reserpine. For the cell-attached recordings, following 5-10 min baseline recording, 10 μM of the D1 antagonist SCH23390 and 10 μM of the D2 antagonist raclopride were washed on for 10 min, followed by a 10 min bath application of 10 μM of the $GABA_A$ receptor antagonist, SR-95531 (gabazine). For the retrobeads experiments, whole-cell voltage clamp and cell-attached recordings were made from GFP+ neurons containing red retrobeads in the VTA. I_h current was measured by voltage-clamping the cell and stepping from −70 mV to −105 mV in 5 mV steps. For voltage-clamp recordings in LHb neurons, membrane potentials were maintained at −70 mV, and light pulses were delivered every 20 s to evoke neuronal firing. For cell-attached recordings, a 20-Hz optical stimulation was delivered for 1 s every 20 s for 20 sweeps. Firing rate was averaged across all 20 sweeps.

RT-PCR

Autoclaved patch electrodes (2.0–2.5 MΩ) were backfilled with ~3–5 μl of a potassium chloride internal solution. Two microliters of RNase inhibitor (ANTI-RNase, Life Technologies) were added per 1 ml of the potassium chloride internal solution. Holding current was measured for no more than 3 min to minimize potential mRNA degradation. The cytoplasm was then aspirated by applying negative pressure and the integrity of the seal was monitored during aspiration to prevent

extracellular contamination. Cells that showed more than a 100-pA change in holding current during aspiration were discarded. Immediately following aspiration, the pipette was removed from the tissue and the tip was broken into an RNase-free PCR tube. The solution inside the pipette was then injected into the RNase-free tube using positive pressure. Between each cell recording, the silver wire located inside the recording pipette was wiped thoroughly with 70% alcohol to minimize cross sample contamination. Finally, to control for pipette contamination, after each five consecutive recordings, a recording pipette was lowered into the tissue with positive pressure, but without aspiration (tissue-stick control) and was then processed for quantitative PCR.

Single-cell gene expression profiling

Extracted intracellular samples were profiled using the Single Cell-to-C_t Kit (Life Technologies). Briefly, intracellular contents were prepared individually in lysis solution containing DNase. The volume of lysis and DNase solution was reduced from the normal protocol to compensate for the added volume of internal solution from each sample (approximately 3-5 μL). Reverse transcription of RNA to complementary DNA (cDNA) was then performed, followed by a multiplexed preamplification of all target genes using TaqMan Gene Expression Assays (Life Technologies). The assays used to detect the target genes in the VTA were the recommended exon-spanning assays for *Slc17a6* (vesicular glutamate transporter-2, *Vglut2*), *Slc32a1* (vesicular GABA transporter, *Vgat*), *GAD1/GAD2* (glutamate decarboxylase 1 and 2), *Slc18a2* (vesicular monoamine transporter-2, *Vmat2*),

DRD2, (dopamine receptor D2), *DAT1* (dopamine transporter), *TH* (tyrosine hydroxylase), and *Rn18s* (Control). The house-keeping gene, *Rn18s*, is highly abundant in all cells, and was thus not preamplified in order to avoid a reduction of amplification of other cDNAs in the multiplexed sample. Next, qPCR was performed to obtain the C_t values of each target gene by using a StepOnePlus qPCR instrument (Life Technologies) using recommended amplification parameters for TaqMan based probes. Technical replicates from each individual biological sample were performed as well as those from tissue-stick control on the same 96-well plate. Thus, each 96 well plate contained 5 consecutively recorded cells and their 1 subsequent tissue-stick control sample.

Single-cell gene analysis

qPCR data obtained from a given cell were not included for analysis if their qPCR amplification curves were not consistent across technical replicates or if they did not display a predicted sigmoidal amplification curve. Additionally, tissue-stick controls did not display any expression of the profiled target genes following qPCR. Gene expression for each neuron was normalized to the sample's Rn18s expression in order to account for the volume of each collected sample ($\Delta C_t = C_t^{gene} - C_t^{Rn18s}$). Gene expression for each neuron was then normalized and calculated as the difference between normalized gene expression of each gene and normalized average expression of that gene in $TH^{VTA\text{-}NAc}$ neurons ($\Delta\Delta C_t = \Delta C_t - \text{Avg. } \Delta C_{t,VTA\text{-}NAc}$). These fold expression values for each gene were log transformed (Normalized gene amount relative to $TH^{VTA\text{-}NAc} = 2^{-DDCt}$; (Livak and Schmittgen, 2001)) and

analyzed with a non-parametric t test (Mann-Whitney). Only data from TH-GFP neurons that expressed TH were included in the analysis.

Fast-Scan Cyclic Voltammetry

T-650 carbon fiber microelectrodes (100–200 μm in length) were used for detection of dopamine in brain slices. Electrodes were placed in the NAc core, dorsal lateral BNST, or LHb of TH^{VTA}::ChR2 brain slices. Every 100 ms, the potential applied to the electrode was ramped from −0.4 V to +1.3 V to −0.4 V versus a Ag/AgCl reference wire at a rate of 400 V/s. To increase the sensitivity to detect dopamine with fast-scan cyclic voltammetry, slices were prepared as described above, but were incubated in aCSF containing 1 μM GBR12909 and 10 μM raclopride for at least 1 hr before recording. Prior to recording, slices were preperfused with L-Dopa (10 μM) for 10 min. Additionally, the electrode was ramped from −0.6 to 1.4 V to −0.6 V versus a Ag/AgCl reference wire at a rate of 400 V/s. Electrochemical data were acquired using a custom-written software in LabVIEW and filtered at 1 kHz offline. 5-ms, 473-nm, 1-mW light pulses were delivered through a 40X objective via a high-powered LED (Thorlabs) to evoke dopamine release. 5 light pulses were delivered at 1, 2, 5, 10, and 20 Hz. At 20 Hz, 1, 2, 4, 8, 16, and 32 light pulses were delivered. Immediately after optical stimulation of the slice, background-subtracted cyclic voltammograms were generated, which were characteristic of dopamine (peak oxidation potential of 600-700 mV).

In Vivo Circuit Activity Mapping of the $TH^{VTA\text{-}LHb}$ Pathway

For monitoring RMTg and VTA neural firing during optical stimulation of the

$TH^{VTA\text{-}LHb}$ pathway, the recording electrode was lowered separately into the RMTg (−3.9 mm posterior to bregma, ±0.9 mm lateral to midline, and –3.6 mm ventral to skull surface) and VTA (−3.1 mm posterior to bregma, ±0.4 mm lateral to midline, and −5.0 mm ventral to skull surface) by a motorized micromanipulator (Scientifica). To optically stimulate $TH^{VTA\text{-}LHb}$ terminals, an optical fiber coupled to a solid state laser (473 nm) was situated within a guide cannula and placed directly above the LHb at a 15° angle (−1.7 mm posterior to bregma, ±1.25 mm lateral to midline, and –3.24 mm ventral to skull surface). Train pulses of light (20 Hz) were delivered to the LHb every 3 s for 20 trials (each trial having 2 s prestimulation, 2 s stimulation, and 1 s poststimulation periods; Off, On, Off). To optically stimulate RMTg and VTA cell bodies, an optical fiber was fed through the side port of the electrode holder to terminate near the tip of the glass recording electrode. Recorded units were classified as light-responsive neurons if reliable light-evoked spikes were detected during the presentation of 2-ms light pulses (20 trials each).

TH^{VTA}::ChR2 mice were anesthetized with choral hydrate (4% w/v. 480 mg/kg i.p.) and supplemental doses were provided as needed (4% w/v, 120 mg/kg i.p.) (Sigma). A homeothermic heating blanket (Harvard Apparatus, Holliston, MA) was used to maintain body temperature at ~ 37°C and lidocaine (2%) was applied to the incision site (Akorn). A reference electrode was fixed within brain tissue and extracellular neural activity was recorded using glass recording electrodes (5-10 MΩ: and filled with 0.5 M NaCl). All recordings were amplified (Multiclamp 700B, Molecular Devices), bandpass filtered between 300 Hz and 16 kHz and sampled up to 40 kHz. Data acquisition and analysis was performed using pCLAMP software

(Molecular Devices) and placements of recording electrode tips within the RMTg and VTA were verified with histological examination of brain tissue following the experiments.

Real-time place preference

TH$^{VTA-LHb}$::ChR2 and *TH*$^{VTA-LHb}$::Control mice bilaterally implanted with optical fibers aimed at the LHb were placed in a custom-made behavioral arena (50 × 50 × 25 cm black plexiglass) for 20 min. One counterbalanced side of the chamber was assigned as the stimulation side. At the start of the session, the mouse was placed in the non-stimulated side of the chamber. Every time the mouse crossed to the stimulation side of the chamber, 20-Hz constant laser stimulation was delivered until the mouse crossed back into the non-stimulation side. Percent time spent on the stimulation-paired and velocity was recorded via a CCD camera interfaced with Ethovision software (Noldus Information Technologies).

Intra-LHb injection of antagonist and photostimulation during RTPP test

TH$^{VTA-LHb}$::ChR2 mice bilaterally implanted with a 26-gauge cannula coupled to an optical fiber aimed above the LHb were placed in the place-preference chamber and were run in the RTPP task to achieve a baseline measurement. 24 hr following the baseline measurement, mice received intra-LHb bilateral 0.3 μL microinjections of vehicle (saline), a dopamine receptor antagonist cocktail (600 ng of SCH23390 to block D1 receptors and 100 ng raclopride to block D2 receptors in saline), or gabazine (5 ng in saline) counterbalanced across days. The injector needles (33-gauge steel tube, McMasters-Carr) extended approximately 1 mm past

the cannula to ensure drug delivery 0.5 mm below the optical fiber. All drugs were infused at a rate of 1.5 μL/min. The injector remained in place for 2 min after infusion to ensure diffusion of drug into the LHb. Immediately after the infusion procedure, mice were placed into the RTPP chamber. Mice had at least 24 hours without manipulation between each LHb microinjection.

Systemic injection of antagonist and photostimulation during the RTPP test

7 days following the intra-LHb microinjections, *TH*$^{VTA\text{-}LHb}$::ChR2 mice were given i.p. injections of either vehicle (saline) or a dopamine receptor antagonist cocktail (0.04 mg/kg SCH23390 and 0.075 mg/kg raclopride). 20 min following the injection, mice were placed into the RTPP chamber. Mice had at least 24 hr without manipulation between each injection.

Optical self-stimulation

TH$^{VTA\text{-}LHb}$::ChR2 and *TH*$^{VTA\text{-}LHb}$::Control mice bilaterally implanted with optical fibers aimed at the LHb were given daily, 1 hr access to operant chambers (Med Associates) interfaced with optogenetic stimulation equipment. Mice were trained on a fixed-ratio 1 training schedule to nose-poke for optical stimulation of *TH*$^{VTA\text{-}LHb}$::ChR2 fibers. Each nose-poke in the active port resulted in a 3-s 20-Hz optical pulse train that was paired with a 3-s tone and houselight cue.

5-choice optical self-stimulation

At least 24 hr following optical self-stimulation, *TH*$^{VTA\text{-}LHb}$::ChR2 and *TH*$^{VTA\text{-}LHb}$::Control mice bilaterally implanted with optical fibers aimed at the LHb were given one, 1-hr session in an operant chamber containing 5 nose-poke ports. A nose-poke in each port would result in a 1-, 5-, 10-, 20-, or 40-Hz optical stimulation. The pairing of the port with the frequency was counterbalanced between mice.

RESULTS

Optogenetic Targeting of VTA Dopaminergic Neurons and Innervation to the LHb

To selectively target VTA dopaminergic neurons, we introduced a Cre-inducible viral construct coding for channelrhodopsin-2 fused to an enhanced yellow fluorescent protein (ChR2-eYFP) bilaterally into the VTA of tyrosine hydroxylase (TH)-internal ribosome entry site-Cre (TH^{VTA}::ChR2) adult mice as previously described (Tsai et al., 2009).

Three to four weeks following surgery, we observed robust ChR2-eYFP expression in the VTA (**Figure 3.1 A,B**). To ensure the specificity of ChR2-eYFP for dopaminergic neurons, we quantified the number of VTA neurons that were TH-positive (TH$^+$) and eYFP-positive (eYFP$^+$). We found that 62.4% ± 3.4% of VTA neurons were TH$^+$, 48.6% ± 0.9% were eYFP$^+$, and 99.2% ± 0.4% of the eYFP$^+$ neurons were also labeled with TH (**Figure 3.1 C**), consistent with previous results (Tsai et al., 2009). Six weeks following surgery, we observed eYFP expression that was largely restricted to the LHb relative to neighboring structures (**Figure 3.1 D,E**).

Fluorescence quantification analysis in brain slices containing the LHb revealed that axonal fibers originating from VTA dopaminergic neurons densely innervated the LHb, but only sparsely innervated surrounding structures, such as the medial habenula, thalamus, and hippocampus (**Figure 3.1 F**).

LHb-Projecting VTA Dopaminergic Neurons Do Not Send Axon Collaterals to Other Reward-Related Brain Structures

We next determined whether LHb-projecting VTA dopaminergic neurons ($TH^{VTA\text{-}LHb}$) collateralize and project to other brain regions. To accomplish this, we utilized an intersectional genetic approach to selectively label TH^+ neurons in the VTA that project to the LHb. We bilaterally injected the LHb of TH-Cre mice with a retrogradely transducing herpes simplex virus (Chaudhury et al., 2013) encoding a Cre-inducible flippase recombinase (flp) under control the of an Ef1α promoter fragment (HSV-EF1α-LS1L-flp) (**Figure 3.2 A**; see **METHODS** for more detail) (Kuhlman and Huang, 2008). In the same surgery, we bilaterally injected a flp-inducible ChR2-eYFP (AAV5-EF1α-fdhChR2(H134R)-eYFP; a construct designed with the same structure as the Cre-inducible viral construct coding for ChR2 (Tsai et al., 2009) into the VTA (**Figure 3.2 B**). This resulted in the selective labeling of the somas and processes of VTA TH^+ neurons that project to the LHb. If $TH^{VTA\text{-}LHb}$ neurons collateralize to other target regions, we would expect to see $eYFP^+$ fibers in these regions as well as the LHb. However, 6 weeks following this procedure, we observed $eYFP^+$ fibers in the LHb, but not in other terminal regions of VTA dopaminergic neurons, such as the medial prefrontal cortex (mPFC), NAc (**Figure 3.2 B**; n = 6 slices from n = 3 mice), basolateral amygdala (BLA), or bed nucleus of

the stria terminalis (BNST, data not shown), suggesting that $TH^{VTA\text{-}LHb}$ neurons only project to the LHb and do not send collaterals to these other target structures. Additionally, in a separate group of TH-Cre mice, we bilaterally injected the HSV-EF1α-LS1L-flp virus into the NAc and the AAV5-EF1α-fdhChR2(H134R)-eYFP virus into the VTA. In these mice, we observed $eYFP^{+}$ fibers in the NAc, but not in the LHb (**Figure 3.2 C**; n = 6 slices from n = 3 mice).

$TH^{VTA\text{-}LHb}$ Neurons Are Distinct from $TH^{VTA\text{-}NAc}$ Neurons

To further confirm that $TH^{VTA\text{-}LHb}$ neurons are anatomically distinct from NAc-projecting VTA dopaminergic neurons ($TH^{VTA\text{-}NAc}$), and to provide an anatomical map of these discrete populations within the VTA, we performed retrograde tracing by injecting red fluorescent beads into the NAc and green fluorescent beads into the LHb of the same C57/BL6J wild-type mice (**Figure 3.3 A**). Three weeks following surgery, VTA sections were collected and immunostained for TH. We found that $TH^{VTA\text{-}LHb}$ neurons were located in anterior and medial regions, congregating mainly in the interfasicular nucleus, whereas $TH^{VTA\text{-}NAc}$ neurons were generally located more posterior and lateral (**Figure 3.3 B**). Additionally, we observed significantly more $TH^{VTA\text{-}NAc}$ neurons than $TH^{VTA\text{-}LHb}$ neurons throughout the VTA (**Figure 3.3 B**). Supporting our viral tracing data, we detected no TH^{+} neurons that expressed both red and green retrobeads in the VTA. Collectively, these data demonstrate that $TH^{VTA\text{-}LHb}$ and $TH^{VTA\text{-}NAc}$ neurons are completely separate neuronal populations.

Because we found that $TH^{VTA\text{-}NAc}$ and $TH^{VTA\text{-}LHb}$ neurons are separate populations of neurons within the VTA, we investigated whether these two

populations display different electrophysiological characteristics. To accomplish this, we injected two groups of TH-GFP mice with red retrobeads either in the NAc or LHb and performed whole-cell recordings from GFP-positive neurons in VTA brain slices containing retrobeads (**Figure 3.4 A**). Unlike $TH^{VTA\text{-}NAc}$ neurons, $TH^{VTA\text{-}LHb}$ neurons did not show a hyperpolarization-activated inward rectifying current (I_h), a traditional (although disputed) marker of midbrain dopaminergic neurons (Margolis et al., 2006; Mercuri et al., 1995) (**Figure 3.4 B**). The lack of I_h, together with increased membrane resistance (**Figure 3.4 C**), suggests that $TH^{VTA\text{-}LHb}$ neurons may be more excitable than $TH^{VTA\text{-}NAc}$ neurons. Supporting this observation, we found that $TH^{VTA\text{-}LHb}$ neurons show enhanced spontaneous activity compared to $TH^{VTA\text{-}NAc}$ neurons (**Figure 3.4 D, E**).

A pharmacological signature of midbrain dopaminergic neurons is their hyperpolarization in response to D2 autoreceptor activation (Beckstead et al., 2004). To determine whether $TH^{VTA\text{-}LHb}$ neurons are sensitive to D2 autoreceptor activation, we performed cell-attached recordings from $TH^{VTA\text{-}LHb}$ and $TH^{VTA\text{-}NAc}$ neurons in the VTA. In line with previous data, we observed a significant decrease in spontaneous firing following a D2 receptor agonist (3 μM quinpirole) bath application in $TH^{VTA\text{-}NAc}$ neurons (**Figure 3.4 D-F**) (Beckstead et al., 2004; Lammel et al., 2008). However, quinpirole did not significantly change the spontaneous firing rate of $TH^{VTA\text{-}LHb}$ neurons (**Figure 3.4 D,F**), demonstrating that $TH^{VTA\text{-}LHb}$ neurons lack functional somatodendritic D2 autoreceptors.

Because $TH^{VTA\text{-}LHb}$ and $TH^{VTA\text{-}NAc}$ neurons are anatomically and electrophysiologically distinct, we quantified the gene expression profiles of these

two populations. To characterize the molecular phenotype of $TH^{VTA\text{-}LHb}$ and $TH^{VTA\text{-}NAc}$ neurons, we injected two groups of TH-GFP mice with red retrobeads either in the NAc or LHb and 7 days later extracted the intracellular contents from individual GFP-positive neurons in VTA brain slices containing retrobeads (**Figure 3.5 A**). The intracellular content was then processed by reverse transcription quantitative PCR assaying the following genes: vesicular glutamate transporter-2 (Vglut2), vesicular GABA transporter (Vgat), glutamate decarboxylase 1 and 2 (GAD1/GAD2), vesicular monoamine transporter-2 (Vmat2), dopamine receptor D2 (DRD2), dopamine transporter (DAT1), and tyrosine hydroxylase (TH). We found that both $TH^{VTA\text{-}LHb}$ and $TH^{VTA\text{-}NAc}$ neurons expressed all tested genes classically associated with dopamine synthesis, release, and uptake (Vmat2, DRD2, DAT1, and TH; **Figure 3.5 B**). However, $TH^{VTA\text{-}LHb}$ neurons expressed significantly lower amounts of Vmat2, DRD2, and DAT1 compared to $TH^{VTA\text{-}NAc}$ neurons (**Figure 3.5 C**). Importantly, none of these dopaminergic markers were detected in GFP-negative neurons (n = 7 neurons). Taken together, these data suggest that $TH^{VTA\text{-}LHb}$ neurons are anatomically, electrophysiologically, and genetically distinct from $TH^{VTA\text{-}NAc}$ neurons.

Characterization of Neurotransmitter Release from $TH^{VTA\text{-}LHb}$ Fibers

To characterize the dynamics of dopamine release from synaptic fibers that innervate the LHb, we performed fast-scan cyclic voltammetry in LHb brain slices obtained from TH^{VTA}::ChR2 mice. Carbon-fiber microelectrodes were placed in areas within the LHb that displayed the highest ChR2-eYFP expression to ensure the

voltammetry electrodes were near presynaptic fibers and synapses that could be optically stimulated. We observed no detectable optically evoked dopamine release within the LHb, even after sustained high-frequency optical stimulation (**Figure 3.6 A-C**). As positive controls, we recorded light-evoked dopamine release in NAc and BNST brain slices obtained from the same TH^{VTA}::ChR2 mouse. We observed robust light-evoked dopamine release that increased as a function of either frequency or pulse number in both the NAc and BNST (**Figure 3.6 A-C**), consistent with previous studies in the NAc and dorsal striatum of rats (Bass et al., 2013; Witten et al., 2011). We were unable to detect dopamine release in the LHb even after altering the parameters of the voltammetry experiments to increase the sensitivity of dopamine detection (data not shown; see **METHODS** for additional details). Fluorescence quantification analysis of TH^{VTA}::ChR2 fibers in the NAc, BNST, and LHb revealed that although the NAc had significantly higher eYFP fluorescence, there was no difference in eYFP intensity between the LHb and BNST (**Figure 3.6 D,E**). These data suggest that the lack of detectable dopamine release in LHb brain slices is not likely due to weaker innervation, as we observed optically-evoked dopamine release in BNST slices that show comparable innervation.

In the NAc and BNST, we also observed intense TH immunofluorescence and a high degree of colocalization between $eYFP^+$ fibers and TH immunostaining (**Figure 3.6 D,F**) in brain slices obtained from TH^{VTA}::ChR2 mice. In contrast, the LHb from the same mice exhibited strong eYFP fluorescence, but almost no TH immunoreactivity (**Figure 3.6 D,F**). Quantitative analysis confirmed that colocalization (as assessed by Pearson's correlation coefficient) between eYFP and

TH was 0.52 ± 0.05 for NAc and 0.50 ± 0.04 for the BNST, but only 0.010 ± 0.004 for the LHb. Together, these data suggest that fibers arising from VTA TH^+ neurons express little or no TH in the fibers that innervate the LHb.

Because we did not observe dopamine release in the LHb, we sought to determine whether this projection might release other neurotransmitters in the LHb. In light of recent studies demonstrating that dopaminergic fibers can corelease glutamate and GABA in the striatum (Stuber et al., 2010; Tecuapetla et al., 2010; Tritsch et al., 2012), we asked whether fibers and synapses originating from TH^{VTA} neurons were capable of releasing either of these neurotransmitters in the LHb. Accordingly, we performed whole-cell voltage-clamped recordings from postsynaptic LHb neurons in brain slices obtained from TH^{VTA}::ChR2 mice. To ensure we were only recording monosynaptic currents from TH^{VTA}::ChR2 fibers, we added a Na^+-channel blocker (1 μM TTX) and a K^+-channel blocker (1 mM 4-AP) to the bath as previously described (Cruikshank et al., 2010). Voltage-clamp recordings from LHb neurons revealed that light pulses that selectively stimulated TH^{VTA}::ChR2 fibers in the LHb ($TH^{VTA\text{-}LHb}$::ChR2), produced light-evoked currents that were blocked by 10 μM of the $GABA_A$ receptor antagonist gabazine (**Figure 3.7 A-C**). Of the neurons we recorded from in the LHb, 82% (45/55) received a direct monosynaptic inhibitory input from TH^{VTA} neurons. Dopaminergic terminals in the dorsal striatum release GABA that is dependent on Vmat2 activity (Tritsch et al., 2012). However, we observed no changes in inhibitory currents in LHb slices from TH^{VTA}::ChR2 mice treated with the Vmat2 inhibitor reserpine, compared to untreated slices (**Figure 3.7 D**). This same reserpine protocol was sufficient to inhibit electrically-evoked

dopamine release in the NAc (data not shown), demonstrating that this treatment was capable of inhibiting Vmat2 and depleting evoked dopamine. These data demonstrate that $TH^{VTA\text{-}LHb}$ neurons do not require Vmat2 function to release GABA in the LHb. Additionally, we observed a small (−7.2 ± 2.2 pA) excitatory current in some of the recorded neurons (5/10), consistent with a previous study demonstrating that Vglut2-expressing VTA neurons (some of which could be dopaminergic) innervate the LHb (Hnasko et al., 2012).

To determine whether activating $TH^{VTA\text{-}LHb}$::ChR2 terminals would affect the spontaneous firing rate of postsynaptic LHb neurons, we performed cell-attached recordings from LHb neurons and found that the average spontaneous firing rate of these neurons was 8.0 ± 2.2 Hz. When we delivered a 1 s 20 Hz optical pulse-train to optically stimulate $TH^{VTA\text{-}LHb}$::ChR2 terminals, we observed that the firing rate of LHb neurons significantly decreased (**Figure 3.7 E-G**), demonstrating that the net effect of $TH^{VTA\text{-}LHb}$::ChR2 terminal stimulation was to suppress the firing of LHb neurons. To determine whether this suppression of firing was due to GABA or dopamine release, we added a D1/D2 receptor antagonist cocktail (10 μM SCH23390 and 10 μM raclopride) to the bath, followed by a $GABA_A$ receptor antagonist (10 μM gabazine). The D1/D2 receptor antagonist did not modify the decrease in firing in response to optical stimulation, but the $GABA_A$ receptor antagonist blocked this decrease (**Figure 3.7 G**), leading us to conclude that the inhibition of spontaneous firing following activation of $TH^{VTA\text{-}LHb}$::ChR2 terminals is due to activation of $GABA_A$ receptors.

We performed electron microscopy to provide anatomical support for the electrophysiological findings. Accordingly, we collected images of $TH^{VTA\text{-}LHb}$::ChR2 synapses (as defined by electron-dense DAB reaction product or silver-enhanced nanogold after pre-embedding immunostaining for eYFP). Postembedding immunogold staining performed on this material showed that many of these presynaptic terminals contained high levels of GABA (**Figure 3.7 H**). In some cases we also saw terminals containing little or no GABA that made asymmetric synaptic contacts (**Figure 3.8 A**); these were likely to be glutamatergic. Collectively, these congruous findings demonstrate that $TH^{VTA\text{-}LHb}$::ChR2 terminals do not release detectable amounts of dopamine in the LHb in an impulse-dependent fashion. Instead, $TH^{VTA\text{-}LHb}$::ChR2 projections contain and release GABA, which functions to suppress the activity of postsynaptic LHb neurons.

The Functional Significance of the $TH^{VTA\text{-}LHb}$ Circuit in Regulating Midbrain Activity

Because the inhibitory $TH^{VTA\text{-}LHb}$ pathway suppresses the activity of postsynaptic LHb neurons (**Figure 3.7 E-G**), we next addressed whether activation of this inhibitory circuit has downstream effects on midbrain activity *in vivo*. Given that the LHb sends a strong glutamatergic projection to the RMTg (Stamatakis and Stuber, 2012), we assessed the functional consequences of $TH^{VTA\text{-}LHb}$ activation on RMTg neuronal activity by recording extracellularly from RMTg neurons in anesthetized mice while stimulating $TH^{VTA\text{-}LHb}$ terminals (**Figure 3.9 A**). Optical stimulation of the $TH^{VTA\text{-}LHb}$ pathway suppressed the spontaneous firing of RMTg neurons (**Figure 3.9 B,C**). Further, these recorded RMTg units did not respond to

optical stimulation within the RMTg (**Figure 3.9 D-G**), confirming that the recorded neurons did not express ChR2-eYFP. In agreement with this, we observed minimal ChR2-eYFP and TH^{+} immunolabeling in RMTg brain slices (**Figure 3.9 D**). Therefore, we considered these neurons to be TH-negative neurons, consistent with previous data (Barrot et al., 2012).

Because RMTg neurons directly inhibit VTA dopaminergic (TH^{VTA}) neurons (Matsui and Williams, 2011), we next determined if optical stimulation of $TH^{VTA\text{-}LHb}$ terminals would enhance TH^{VTA} neuronal activity via disinhibition. First, to optically classify recorded units as TH^{VTA} neurons, we recorded the firing responses of VTA neurons to the delivery of 2 ms light pulses within the VTA (**Figure 3.10 A,B**). Optically identified TH^{VTA} neurons displayed time-locked activation to VTA optical stimulation (**Figure 3.10 B,C**).

Following identification of TH^{VTA} neurons, we determined whether optical stimulation of the $TH^{VTA\text{-}LHb}$ inhibitory pathway (by delivering 473 nm light directly into the LHb) could alter the spontaneous activity of TH^{VTA} neurons. Optical stimulation of $TH^{VTA\text{-}LHb}$ terminals led to enhanced spontaneous activity in optically identified TH^{VTA} neurons (**Figure 3.10 D,E**). Importantly, we determined that these light-evoked responses were unlikely to arise from antidromic activation of $TH^{VTA\text{-}LHb}$ terminals, as $TH^{VTA\text{-}LHb}$ initiated spikes had significantly longer spike latencies and greater spike jitter compared to the light-evoked spikes of TH^{VTA} neurons with direct optical stimulation in the VTA (**Figure 3.10 F**). Furthermore, TH^{VTA} neurons did not respond reliably to 20 Hz optical stimulation of $TH^{VTA\text{-}LHb}$ terminals (**Figure 3.10 G**). Collectively, these data suggest that the increases in firing of TH^{VTA} neurons initiated

by $TH^{VTA\text{-}LHb}$ terminal activation are mediated through synaptic transmission within a polysynaptic circuit. Taken together, these circuit-activity mapping experiments reveal the functional significance of the inhibitory $TH^{VTA\text{-}LHb}$ pathway in regulating midbrain activity.

Optogenetic Activation of the $TH^{VTA\text{-}LHb}$ Pathway Produces Reward-Related Behavioral Phenotypes that Require $GABA_A$ Signaling

In vivo, pharmacological inhibition of the LHb increases dopamine in forebrain regions such as the striatum (Lecourtier et al., 2008). Likewise, we observed that in vivo activation of the $TH^{VTA\text{-}LHb}$ pathway increased the firing rate of midbrain dopaminergic neurons (**Figure 3.10**). Therefore, we hypothesized that *in vivo* activation of the $TH^{VTA\text{-}LHb}$::ChR2 pathway would result in a reward-related phenotype. To test this hypothesis, we implanted bilateral optical fibers (Sparta et al., 2012) aimed directly above the LHb in $TH^{VTA\text{-}LHb}$::ChR2 mice and determined the behavioral ramifications of selectively activating the $TH^{VTA\text{-}LHb}$::ChR2 pathway. Using a real-time place preference assay, as previously described (Stamatakis and Stuber, 2012), $TH^{VTA\text{-}LHb}$::ChR2 mice exhibited a significant preference for the side of the chamber that was paired with optical stimulation. In contrast, littermate controls ($TH^{VTA\text{-}LHb}$::Control) displayed no preference, demonstrating that activation of the $TH^{VTA\text{-}LHb}$::ChR2 pathway produces reward-related behaviors (**Figure 3.11 A-C**). This preference was dependent on $GABA_A$ signaling within the LHb, as intra-LHb microinjections of a $GABA_A$ receptor antagonist (gabazine) through guide cannulas interfaced with the optical fibers (Jennings et al., 2013a) blocked the preference for the stimulation-paired side (**Figure 3.11 D**). Following intra-LHb $GABA_A$ agonist

(gabazine) we observed no significant difference in velocity compared to vehicle (t_{16} = 0.4, p = 0.72). In contrast, intra-LHb microinjection of a dopamine receptor antagonist (D1 and D2) cocktail did not block the rewarding phenotype (**Figure 3.11 D),** whereas a systemic injection of the dopamine antagonist cocktail did disrupt the preference (**Figure 3.11 E**). Velocity was significantly decreased following intra-LHb dopamine antagonist (D1/D2) compared to vehicle (t_{14} = 2.3, p = 0.04), however velocity was not significantly different following systemic dopamine antagonist compared to *TH*$^{VTA\text{-}LHb}$::Control mice (t_{13} = 0.77, p = 0.45). These data suggest that the observed reward-related phenotype induced by optical stimulation of the TH$^{VTA\text{-}LHb}$::ChR2 pathway does not depend on dopamine signaling within the LHb, but rather on downstream dopamine signaling in brain regions such as the NAc. Finally, to determine if activation of the TH$^{VTA\text{-}LHb}$::ChR2 pathway is reinforcing, we trained mice to nose-poke for optical stimulation of the TH$^{VTA\text{-}LHb}$::ChR2 pathway (**Figure 3.11 F,G**). TH$^{VTA\text{-}LHb}$::ChR2 mice made significantly more nose-pokes to receive optical stimulation than TH$^{VTA\text{-}LHb}$::control mice (**Figure 3.11 H**).

Taken together, these data demonstrate that although activation of TH$^{VTA\text{-}LHb}$::ChR2 terminals does not result in detectable dopamine release in the LHb, selective activation of this pathway promotes reward-related behavior by suppressing LHb activity through the release of GABA, leading to disinhibition of VTA dopaminergic neurons.

DISCUSSION

Aberrant mesolimbic and mesocortical dopaminergic signaling has been

implicated in a range of neuropsychiatric diseases, including schizophrenia, addiction, and depression (Chaudhury et al., 2013; Knable and Weinberger, 1997; Lüscher and Malenka, 2011; Phillips et al., 2003b; Tye et al., 2013), motivating extensive studies of VTA dopaminergic projections to the striatum and prefrontal cortex. In contrast, little is known about the VTA's projection to the LHb. Using optogenetics in combination with electrophysiology, genetically targeted neuronal tracing techniques, and behavior, we investigated the functional and behavioral significance of this mesohabenular pathway.

Previous studies have demonstrated that separate populations of VTA dopaminergic neurons project to nonoverlapping target structures such as the NAc, BLA, and mPFC (Ford et al., 2006; Lammel et al., 2008; Swanson, 1982). Our data are consistent with these findings, demonstrating that $TH^{VTA\text{-}LHb}$ neurons do not collateralize to the NAc, BLA, PFC, or BNST. We also found that $TH^{VTA\text{-}LHb}$ neurons display electrophysiological characteristics distinct from $TH^{VTA\text{-}NAc}$ neurons. Notably, we found that $TH^{VTA\text{-}LHb}$ neurons are more excitable than $TH^{VTA\text{-}NAc}$ neurons, are insensitive to D2 autoreceptor activation, and do not display an I_h current, an electrophysiological characteristic often used to identify a neuron as dopaminergic in slice electrophysiological experiments (Mercuri et al., 1995). Recent studies have demonstrated that although NAc-projecting and BLA-projecting VTA dopaminergic neurons typically have robust I_h currents, dopaminergic neurons that project to the mPFC lack I_h currents and functional somatodendritic D2 autoreceptors (Ford et al., 2006; Lammel et al., 2008, 2011). Collectively, these data support the idea that VTA dopaminergic neurons are not a homogenous population, as they can vary greatly

depending on their electrophysiological markers and their projection targets.

Although $TH^{VTA\text{-}LHb}$ neurons express TH mRNA and show TH immunostaining in the soma (**Figure 3.3 and Figure 3.5**), we observed only very weak TH expression in $TH^{VTA\text{-}LHb}$::ChR2 fibers and terminals (**Figure 3.6**). Consistent with this, voltammetric methods failed to detect released dopamine in the LHb following optical stimulation of $TH^{VTA\text{-}LHb}$::ChR2 fibers. It is worth noting that we observed dense core vesicles in presynaptic terminals originating from $TH^{VTA\text{-}LHb}$ neurons (**Figure 3.7 H**) Previous work has demonstrated that the vesicular monoamine transporter can be associated with dense core vesicles in VTA neurons, suggesting that dopamine may be contained in both clear synaptic vesicles and dense core vesicles (Nirenberg et al., 1996). It is possible that a low content of dopamine within the dense core vesicles in the LHb could be released following specific stimulation patterns, leading to concentrations of dopamine in the LHb too low to detect with voltammetric methods. Additionally, because TH is produced in the soma, $TH^{VTA\text{-}LHb}$ neurons may be releasing dopamine locally from the somatodendritic compartment, which could then activate D2 autoreceptors to modulate the firing rate of neighboring VTA neurons (Adell and Artigas, 2004).

Previous studies have found that systemic injections of dopaminergic agonists and bath-application of high concentrations of dopamine result in changes in the firing patterns and glucose utilization of LHb neurons (Jhou et al., 2013; Kowski et al., 2009; McCulloch et al., 1980). However, as dopaminergic agonists often have affinities for serotonin receptors (Newman-Tancredi et al., 2002), which are thought to reside on presynaptic terminals in the LHb (Shabel et al., 2012), it is

unclear whether the effects of these agonists on LHb activity arise from direct activation of dopamine receptors in the LHb.

LHb neurons exhibit a high basal firing rate both in slices (**Figure 3.7**) (Jhou et al., 2013) and in vivo (Bromberg-Martin et al., 2010b; Meier and Herrling, 1993), which likely exerts a tonic inhibitory influence on dopaminergic neurons by activating RMTg GABAergic neurons that directly inhibit VTA dopaminergic neurons. Supporting this hypothesis, we found that inhibition of LHb neurons through activation of $TH^{VTA\text{-}LHb}$::ChR2 terminals decreased RMTg firing and increased the spontaneous firing rate of VTA dopaminergic neurons (**Figure 3.9 and 3.10**), consistent with previous data demonstrating that pharmacological inhibition of the LHb increases dopamine release in the forebrain (Lecourtier et al., 2008). LHb neurons show a decrease in firing in response to cues that predict reward (Matsumoto and Hikosaka, 2007). Thus, we suggest that the phasic dopamine release seen in the NAc in response to motivationally relevant stimuli, at least in part, could require activation of inhibitory afferents to LHb, thus disinhibiting midbrain dopaminergic neurons. Data presented here demonstrate that a hybrid population of VTA neurons expressing dopaminergic and GABAergic markers send an inhibitory projection to the LHb and thus are able to directly inhibit LHb neurons, resulting in profound downstream effects on midbrain circuitry. This provides a circuit mechanism by which activation of the VTA-to-LHb pathway could promote reward.

Along with a robust excitatory projection to GABAergic neurons in the RMTg and posterior VTA, the LHb also sends a modest direct glutamatergic projection to VTA dopaminergic neurons (Balcita-Pedicino et al., 2011; Stamatakis and Stuber,

2012). If the VTA dopaminergic neurons that receive a direct connection from the LHb also project back to the LHb, this could provide an elegant negative feedback mechanism, whereby activation of the LHb would result in activation of $TH^{VTA\text{-}LHb}$ neurons, which in turn would shut down LHb activity.

Although the presence of a mesohabenular pathway has been recognized for many years (Phillipson and Griffith, 1980; Swanson, 1982), the present study characterizes the behavioral and functional relevance of this pathway. Our data add to the mounting evidence that dopaminergic neurons within the VTA are heterogeneous with respect to their electrophysiological and molecular profiles, their projection targets, and neurotransmitter signaling modalities. Further, our data demonstrate that the LHb and midbrain interact in a reciprocal manner and implicate the VTA's projection to the LHb as a key node in the classical midbrain reward circuit. This mechanistic framework underscores the flexibility and complexity of the circuitry that impinges upon VTA dopaminergic neurons to promote motivated behavior.

FIGURES

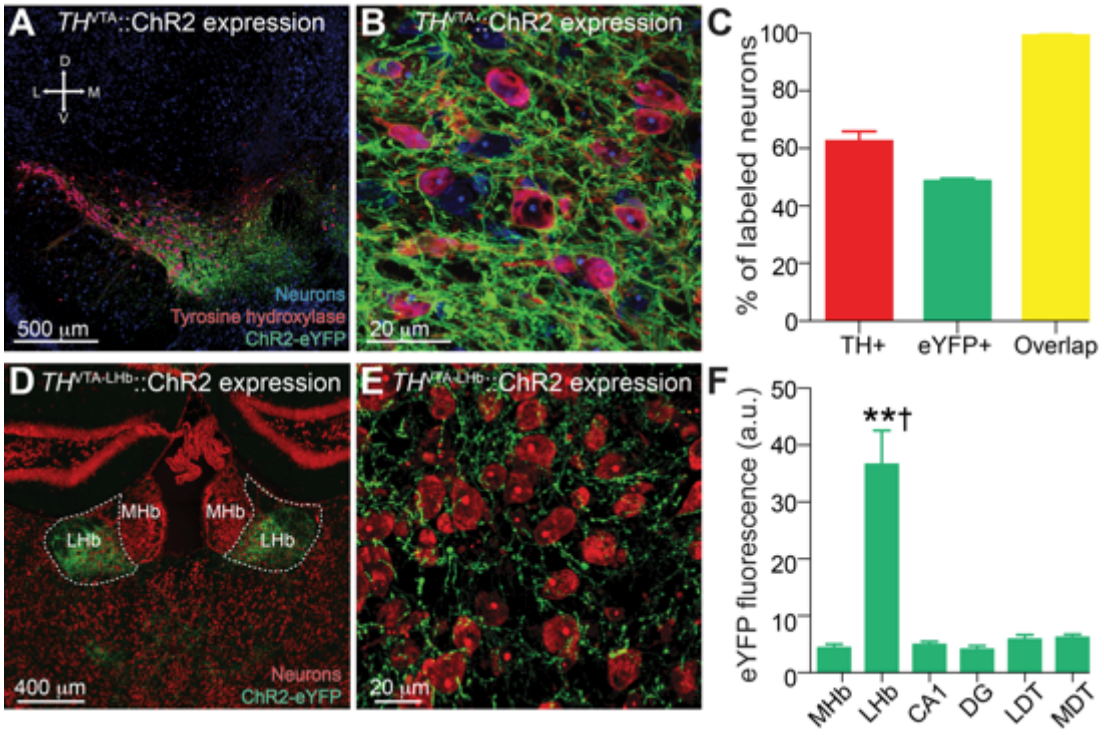

Figure 3.1: *TH*^{VTA} neurons project to the LHb. (**A,B**) Confocal images of coronal sections showing expression of ChR2-eYFP in the VTA following injection of Cre-inducible virus into the VTA of a TH-IRES-Cre (TH^{VTA}::ChR2) mouse. (**C**) Quantification of TH^{+}, eYFP^{+}, and eYFP^{+} neurons that are also TH^{+} (n = 4 sections from n = 3 mice). (**D,E**) Confocal images of coronal sections showing expression of ChR2-eYFP fibers in the LHb of a TH^{VTA}::ChR2 mouse. (**F**) eYFP fluorescence intensity is significantly higher in the LHb than in surrounding regions ($F_{5,30}$ = 5.718, $p < 0.0001$; n = 6 sections from n = 3 mice). MHb, medial habenula; LHb, lateral habenula; DG, dentate gyrus; LDT, lateral dorsal thalamus; MDT, medial dorsal thalamus. Dagger symbol denotes significance compared to all manipulations. All error bars for all figures correspond to the s.e.m. *indicates $p < 0.05$ and ** indicates $p < 0.01$ for all figures.

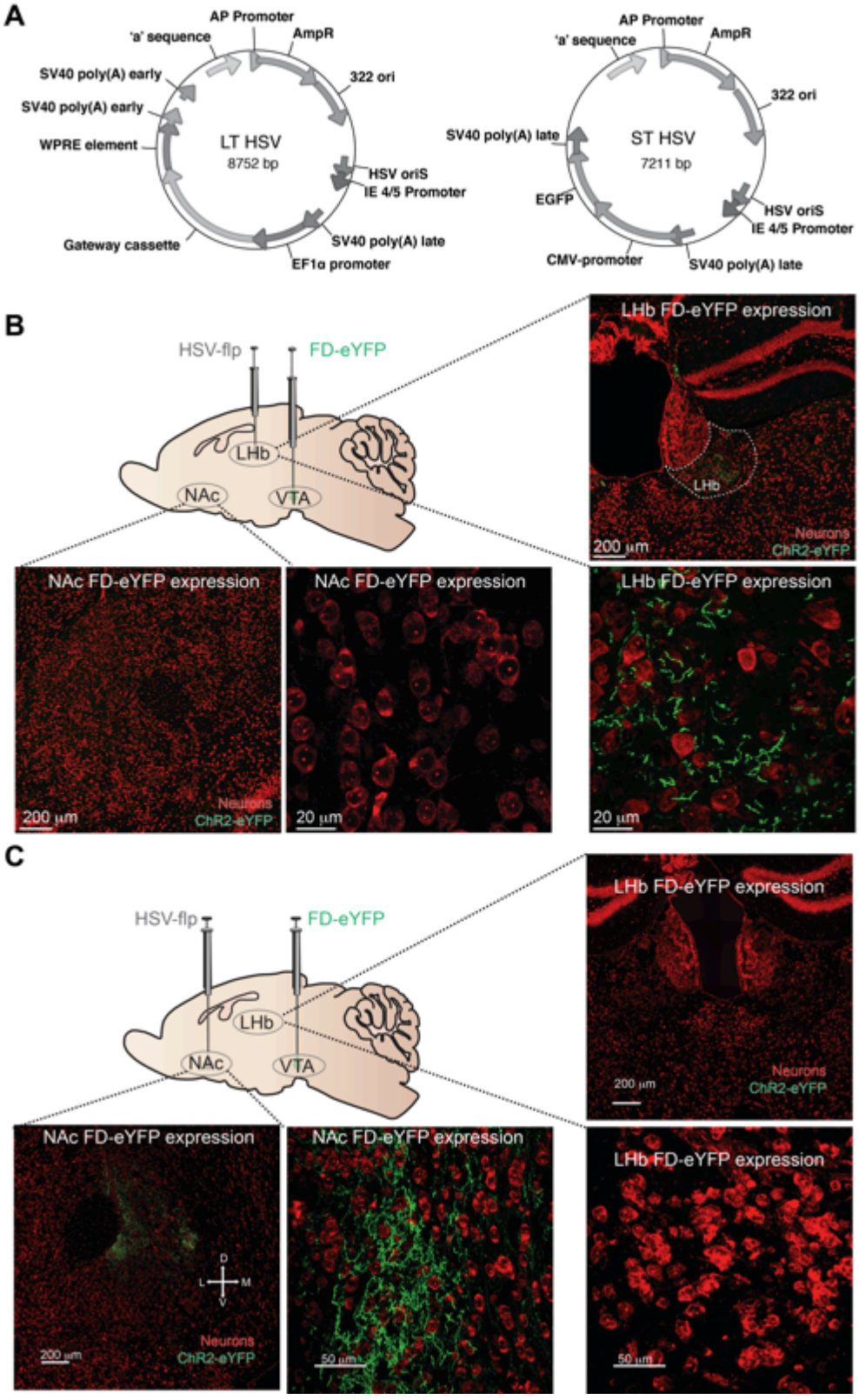

Figure 3.2: *TH*$^{VTA\text{-}LHb}$ neurons are a distinct population of neurons. (**A**) HSV

vector maps. LT HSV virus encoding a cre inducible flp recombinase was modified from previously published ST HSV vectors. LT HSV results in longer term expression of introduced transgenes into neurons compared to standard (ST) HSV vectors. (**B**) Diagram illustrates HSV-EF1α-LS1L-flp (HSV-flp) and AAV5-EF1α-fdhChR2(H134R)-eYFP (FD-eYFP) viral injections. Confocal images show eYFP expression in the NAc (below) and LHb (right) following injection of HSV-flp into the LHb and FD-eYFP into the VTA of TH:IRES:Cre mice. (**C**) Schematic of HSV-flp and FD-eYFP viral injections. Confocal images show eYFP expression in the NAc (below) and LHb (right) following HSV-flp into the NAc and FD-eYFP into the VTA of TH:IRES:Cre mice.

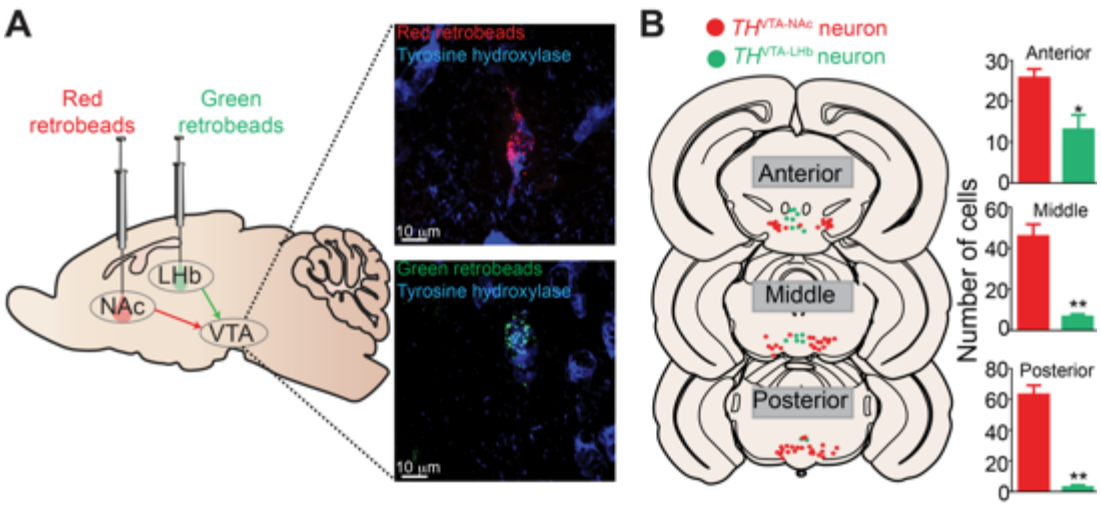

Figure 3.3: *TH*$^{VTA-LHb}$ neurons are located in the medial-anterior portion of the VTA. (**A**) Left: schematic of retrobead injections. Right: confocal images of separate TH^+ neurons containing NAc-injected beads (top) and LHb-injected beads (bottom). (**B**) Left: location of $TH^{VTA-NAc}$ neurons (red) and $TH^{VTA-LHb}$ neurons (green) from a representative animal. Right: more TH^+ neurons in the VTA contained red retrobeads ($TH^{VTA-NAc}$ neurons) than green retrobeads ($TH^{VTA-LHb}$ neurons) (anterior: $t_8 = 3.01$, $p = 0.02$; n = 5 sections from n = 4 mice; middle: $t_8 = 6.51$, $p = 0.0002$; n = 5 sections from n = 4 mice; posterior: $t_6 = 9.58$, $p < 0.0001$; n = 4 sections from n = 4 mice). Error bars represent SEM. $^{**}p < 0.01$ (Student's t test and ANOVA followed by Bonferroni post hoc comparisons, where applicable).

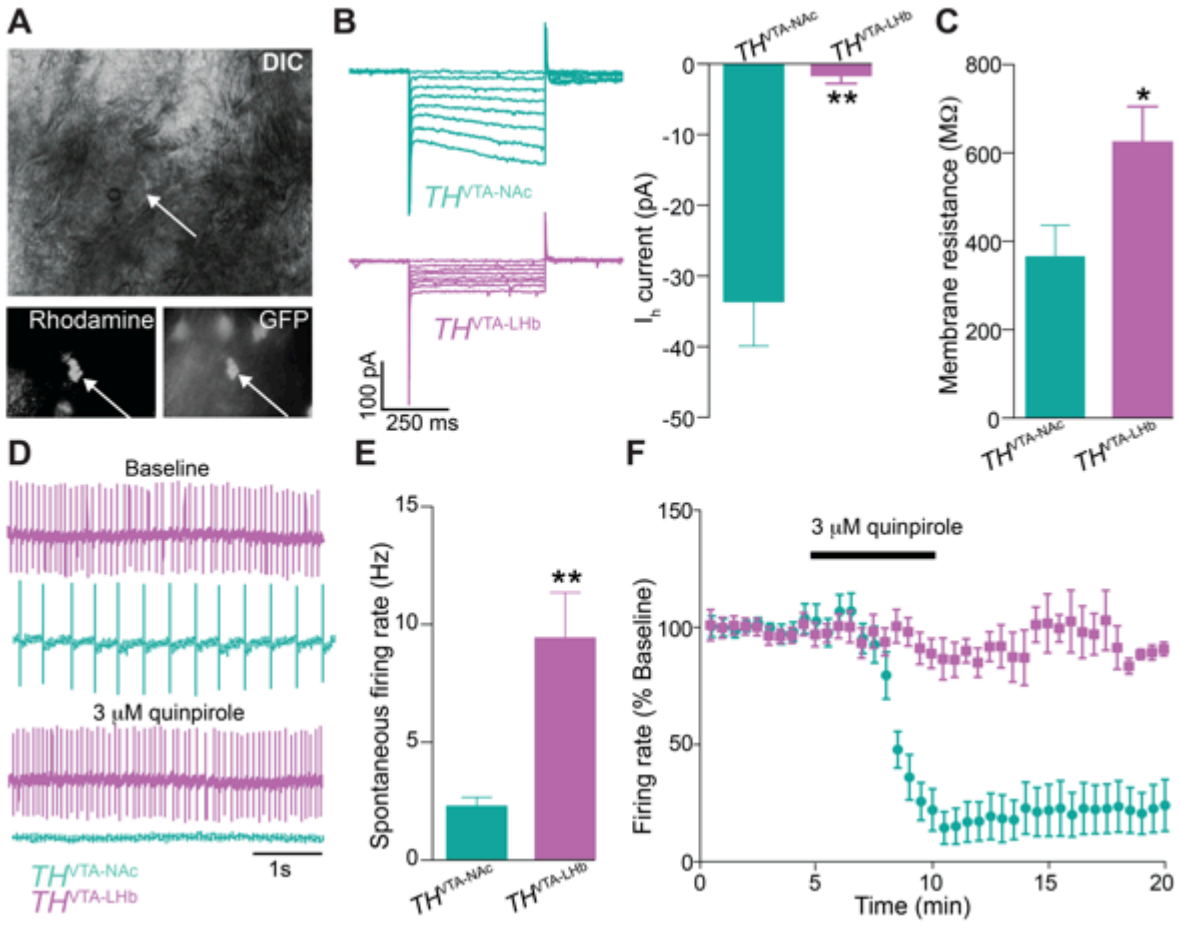

Figure 3.4: *TH*$^{VTA-LHb}$ neurons exhibit distinct electrophysiological characteristics. (**A**) Top: VTA neuron (indicated by arrow) visualized with a DIC microscope. Bottom left: same neuron visualized under epifluorescent illumination with rhodamine filter. Bottom right: same neuron visualized under epifluorescent illumination with GFP filter. (**B**) Left: representative traces showing I_h current in a TH$^{VTA-NAc}$ neuron (top) and TH$^{VTA-LHb}$ neuron (bottom) in response to voltage steps. Right: TH$^{VTA-LHb}$ neurons show significantly less I_h current than TH$^{VTA-NAc}$ neurons (t_{16} = 4.5, p = 0.0004; n = 10 TH$^{VTA-NAc}$ neurons and 8 TH$^{VTA-LHb}$ neurons). (**C**) TH$^{VTA-LHb}$ neurons have a higher membrane resistance than TH$^{VTA-NAc}$ neurons (t_{16} = 2.4, p = 0.03; n = 10 TH$^{VTA-NAc}$ neurons and 8 TH$^{VTA-LHb}$ neurons). (**D**)

Representative traces showing spontaneous firing of $TH^{VTA\text{-}LHb}$ neuron (purple) and $TH^{VTA\text{-}NAc}$ neuron (green) during a baseline period (top) and following a bath application of a D2 agonist (3 μM quinpirole, bottom). (**E**) Spontaneous firing is significantly higher in $TH^{VTA\text{-}LHb}$ neurons than in $TH^{VTA\text{-}NAc}$ neurons ($t_{17} = 3.78$, $p = 0.0015$; n = 10 $TH^{VTA\text{-}NAc}$ neurons and 9 $TH^{VTA\text{-}LHb}$ neurons). (**F**) Bath application (3 μM) of quinpirole decreases the spontaneous firing rate significantly more for $TH^{VTA\text{-}NAc}$ neurons compared to $TH^{VTA\text{-}LHb}$ neurons ($F_{34,490} = 10.58$, $p = < 0.0001$; n = 9 $TH^{VTA\text{-}NAc}$ neurons and 7 $TH^{VTA\text{-}LHb}$ neurons. Error bars represent s.e.m. $^{*}p < 0.05$ $^{**}p < 0.01$ (Student's t test and ANOVA followed by Bonferroni post hoc comparisons, where applicable).

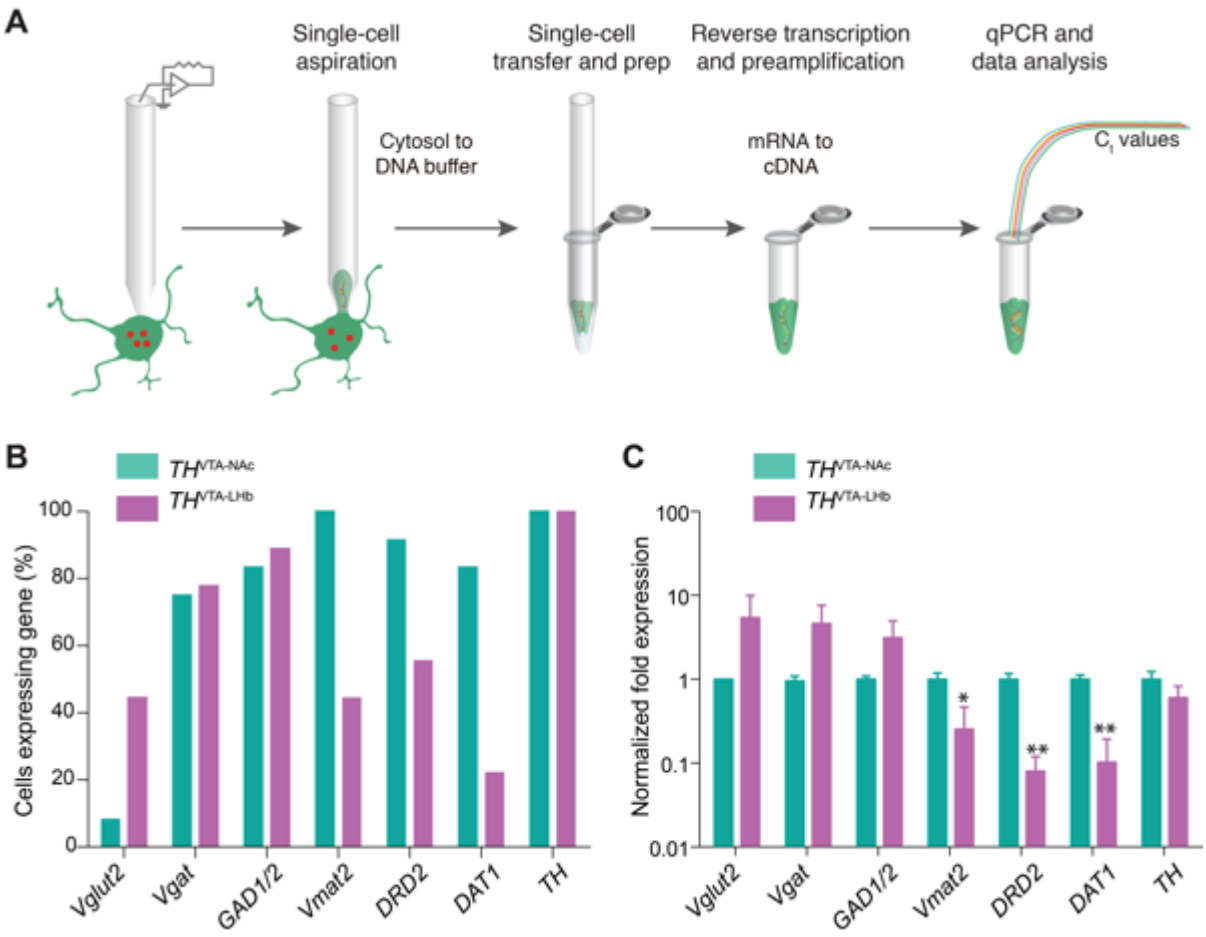

Figure 3.5: *TH*$^{VTA-LHb}$ neurons express lower amounts of mRNA for dopaminergic markers than *TH*$^{VTA-NAc}$ neurons. (**A**) Schematic of single-cell RT-PCR analysis. (**B**) Percentage of TH$^{VTA-LHb}$ and TH$^{VTA-NAc}$ neurons expressing each gene (Vglut2, vesicular glutamate transporter-2; Vgat, vesicular GABA transporter; GAD1/GAD2, glutamate decarboxylase 1 and 2; Vmat2, vesicular monoamine transporter-2; DRD2, dopamine receptor D2; DAT1, dopamine transporter; and TH, tyrosine hydroxylase). (**C**) C_t values for each target gene were normalized to the control gene expressed in all neurons, Rn18s, and log transformed fold expression values represent single cell expression relative to TH$^{VTA-NAc}$ expression. The average

fold expression for Vmat2, DRD2, and DAT1 is significantly lower in $TH^{VTA\text{-}LHb}$ neurons compared $TH^{VTA\text{-}NAc}$ neurons (Vmat2: U = 19, p = 0.0136; DRD2: U = 10, p = 0.0053; DAT1: U = 17.00, p = 0.0069; n = 9 $TH^{VTA\text{-}LHb}$ neurons from n = 4 mice and n = 12 $TH^{VTA\text{-}NAc}$ neurons from n = 3 mice). Error bars represent SEM. $^{*}p < 0.05$ $^{**}p < 0.01$ (Mann-Whitney).

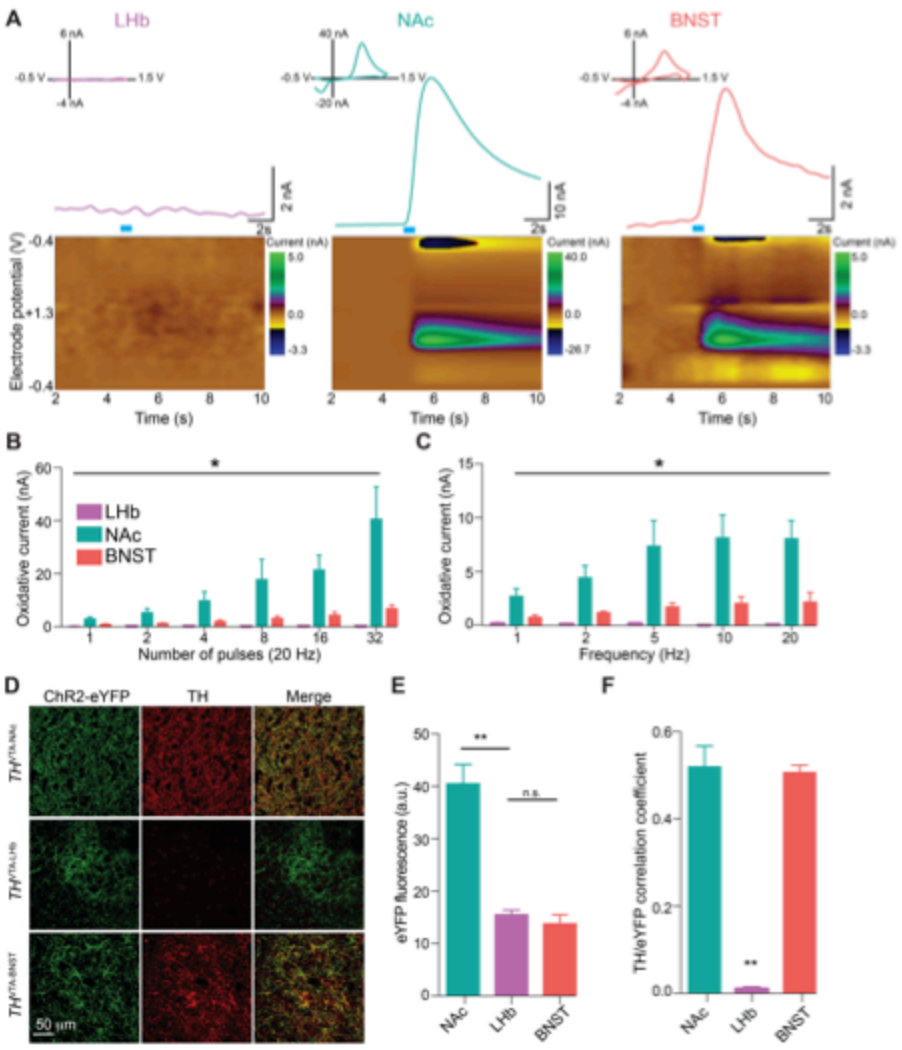

Figure 3.6: *TH*$^{VTA\text{-}LHb}$ neurons do not release detectable levels of dopamine in the LHb (**A**) Fast-scan cyclic voltammetric recordings of optically-evoked dopamine release in LHb (left), NAc (middle), and BNST (right) brain slices from TH^{VTA}::ChR2 mice. Top: example traces of voltammetric recordings from LHb (left), NAc (middle), and BNST (right) brain slices. Insets: background-subtracted cyclic voltammograms showing an electrochemical signal indicative of oxidized dopamine in the NAc and BNST, but not in the LHb. Bottom: consecutive background-subtracted voltammograms recorded over the 8 s interval. Applied potential (E_{apps} versus

Ag/AgCl reference electrode) is shown on y axis. Time at which each voltammogram was recorded is shown on x axis. Current changes are color-coded. (**B**) Light-evoked current is significantly higher in the NAc than LHb at 20 Hz for all measured number of pulses ($F_{5,1}$ = 19.1, $p < 0.0001$). Light-evoked current is significantly higher in the BSNT than LHb at 20 Hz for 8, 16, and 32 pulses ($F_{5,1}$ = 72.59, $p < 0.0001$). (**C**) Light-evoked current is significantly higher in the NAc than LHb for all measured frequencies ($F_{4,1}$ = 29.11, $p < 0.001$). Light-evoked current is significantly higher in the BNST than LHb for 10 and 20 Hz ($F_{4,1}$= 25.43, $p < 0.001$). (**D**) Confocal images showing eYFP- and TH-expression in the NAc (top), LHb (middle), and BNST (bottom) from TH^{VTA}::ChR2 coronal sections. (**E**) eYFP fluorescence intensity is significantly higher in the NAc than in the LHb (t_{10} = 6.58, $p < 0.0001$). eYFP fluorescence intensity is not significantly different between the LHb and BNST (t_{10} = 0.9002, $p = 0.389$). n = 6 slices/region from n = 3 mice. (**F**) ChR2-eYFP and TH colocalize significantly less in the LHb than in the BNST and NAc (Pearson's correlation coefficient, $F_{2,12}$ = 76.49, $p < 0.0001$; n = 5 slices/region from n = 3 mice). Error bars represent s.e.m.. $^{**}p < 0.01$ (Student's t test and ANOVA followed by Bonferroni post hoc comparisons, where applicable).

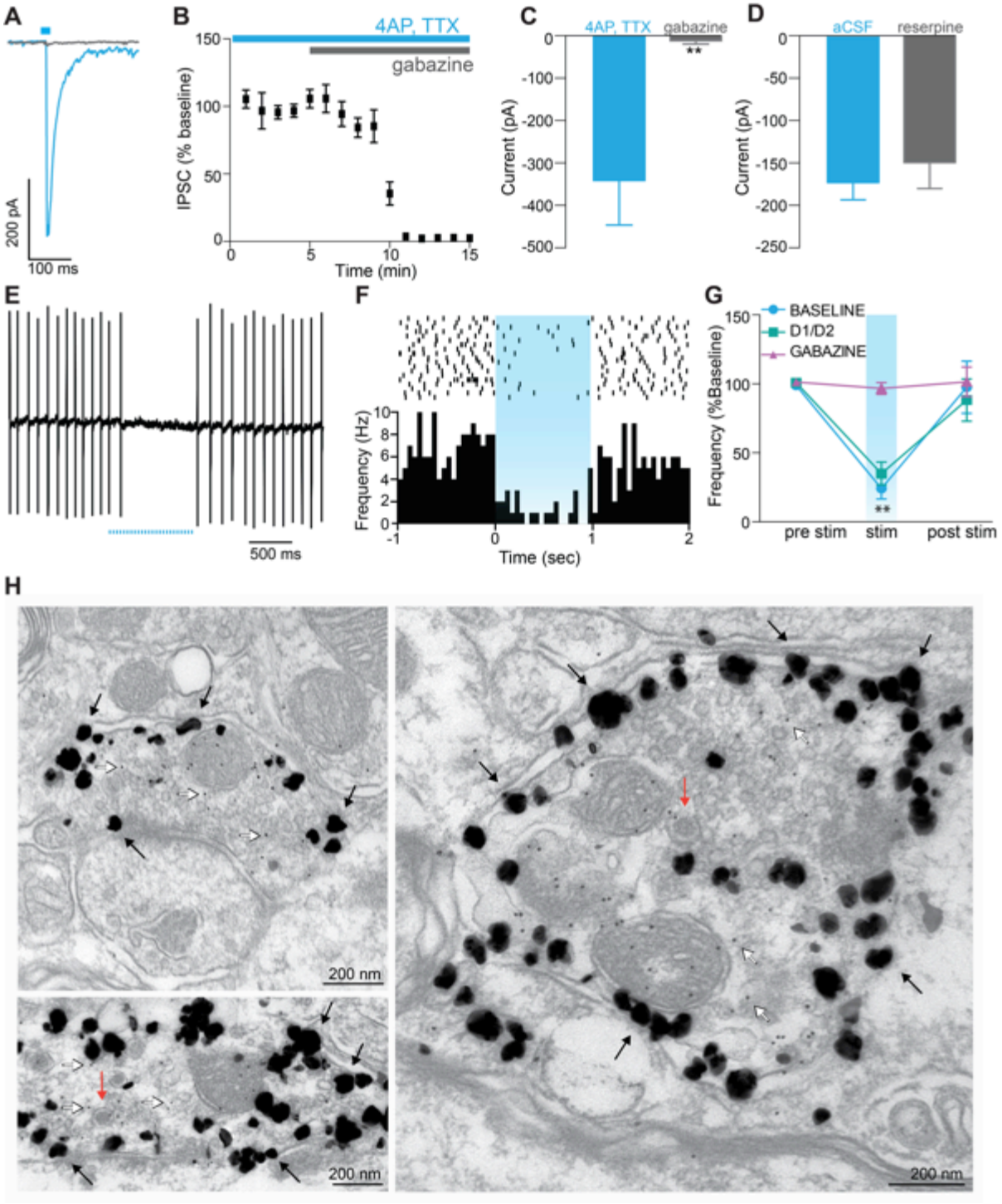

Figure 3.7: *TH*$^{VTA\text{-}LHb}$ neurons release GABA in the LHb. (**A–C**) Light-evoked IPSCs recorded from LHb neurons in the presence of 1 mM 4-AP and 1 μM TTX are blocked by bath-application of 10 μM gabazine (t_{12} = 3.12, p = 0.009; n = 7 neurons).

(**D**) Light-evoked IPSCs recorded from LHb neurons in normal aCSF and from reserpine-treated mice (t_{18} = 0.60; p = 0.56; n = 10 neurons each). (**E–G**) Cell-attached recordings demonstrating a significant decrease in the spontaneous firing rate of LHb neurons in response to a 1 s 20 Hz optical stimulation of $TH^{VTA-LHb}$::ChR2 terminals in the LHb in normal aCSF (baseline: t_{14} = 9.57, p < 0.0001) and after application of a D1/D2 antagonist (D1/D2: t_{14} = 7.76, p < 0.0001), but not after application of a $GABA_A$ receptor antagonist (gabazine: t_{14} = 1.05, p = 0.31) n = 10 neurons. (**H**) Electron micrographs showing $TH^{VTA-LHb}$::ChR2 fibers, as defined by large silver-enhanced nanogold particles (black arrows) containing GABA (detected with 10 nm gold particles, white arrows). $TH^{VTA-LHb}$::ChR2 fibers also contain dense-core vesicles (red arrows). See also Figure S4. Error bars represent s.e.m. **p < 0.01 (Student's t test and ANOVA followed by Bonferroni post hoc comparisons, where applicable).

A

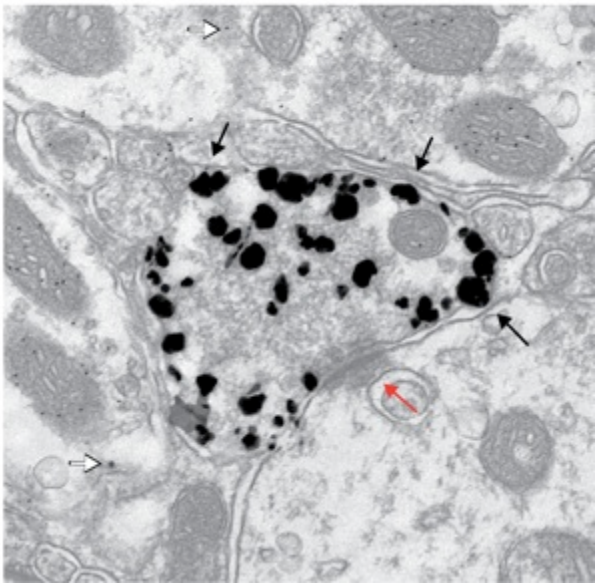

Figure 3.8: GABA-negative asymmetric *TH*$^{VTA\text{-}LHb}$::ChR2 synapse. (**A**) Electron micrograph showing *TH*$^{VTA\text{-}LHb}$::ChR2 presynaptic terminal, as defined by large silver-enhanced particles (black arrows) making an asymmetric synapse (red arrow pointing to postsynaptic density). GABA (white arrow) is located in neighboring synapses, but not in *TH*$^{VTA\text{-}LHb}$::ChR2 presynaptic terminal.

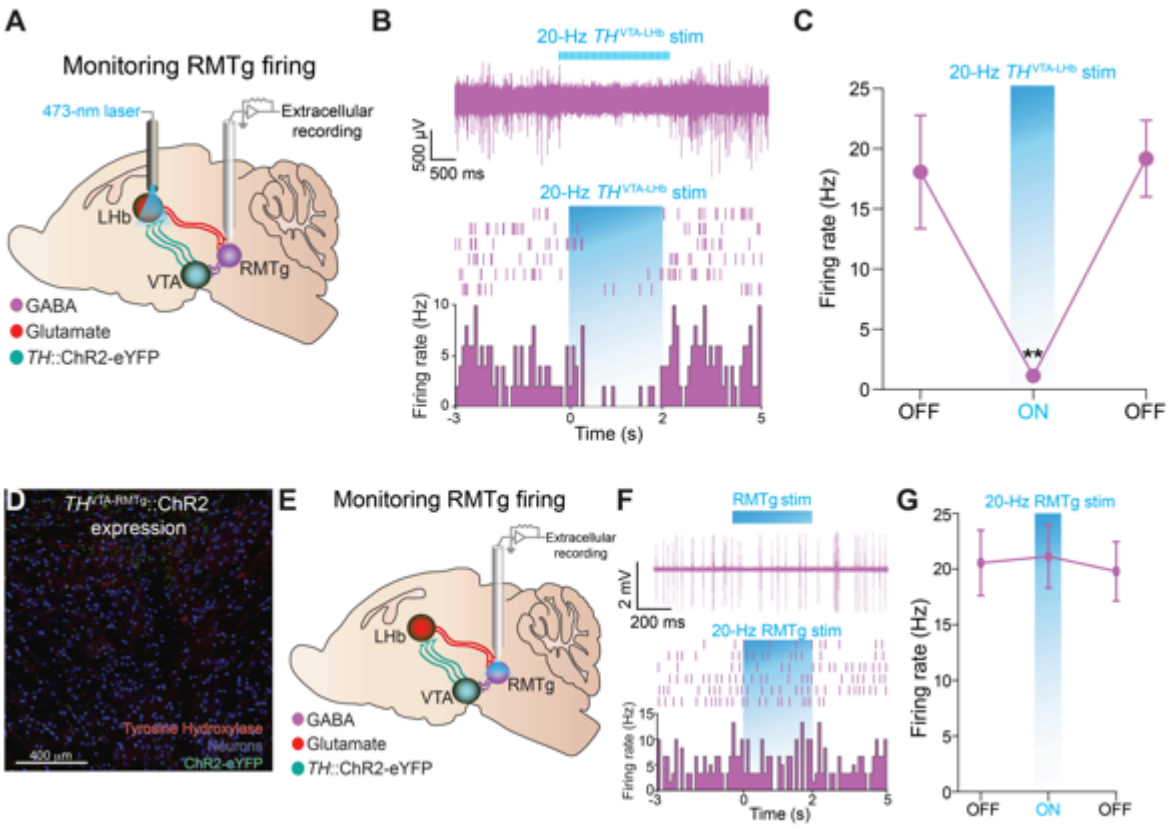

Figure 3.9: In vivo optical stimulation of *TH*$^{VTA-LHb}$ terminals suppresses RMTg activity. (**A**) A schematic depicting anesthetized in vivo electrophysiological recordings from RMTg neurons during TH$^{VTA-LHb}$ terminal optical stimulation. (**B**) Example trace from a single RMTg unit (top) and its representative peri-event histogram and raster (bottom) demonstrating repeated attenuation of firing to 20 Hz optical stimulation of the TH$^{VTA-LHb}$ pathway. (**C**) Off, On, Off: before, during, after 20 Hz photostimulation (3 s each; 20 trials). The average firing rate of RMTg units significantly decreased during the 3 s 20 Hz optical stimulation trials ($F_{2,15}$ = 4.33, p = 0.03, n = 3 mice, n = 6 units). (**D**) Confocal image of coronal section showing expression of ChR2-eYFP in the RMTg following injection of Cre-inducible virus into

the VTA of a TH-IRES-Cre (*TH*^{VTA}::ChR2) mouse. We found that 3.02 ± 0.422% of neurons were TH+. We observed very minimal ChR2-eYFP expression in RMTg brain slices (less than 3 neurons per slice). n = 4 slices from n = 4 mice. (**E**) Schematic detailing RMTg in vivo recordings paired with optical stimulation of the recording region. (**F**) Representative trace from a single non-optically excitable RMTg unit (top) and its representative peri-event histogram and raster (bottom) showing no response to optical stimulation of the RMTg. (**G**) The average firing rate of RMTg neurons did not significantly alter during 20-Hz optical stimulation when compared to the time epochs without stimulation ($F_{2,15}$ = 0.057, p = 0.95, n = 3 mice, n = 6 units). Error bars represent s.e.m. (ANOVA followed by Bonferroni post-hoc comparisons).

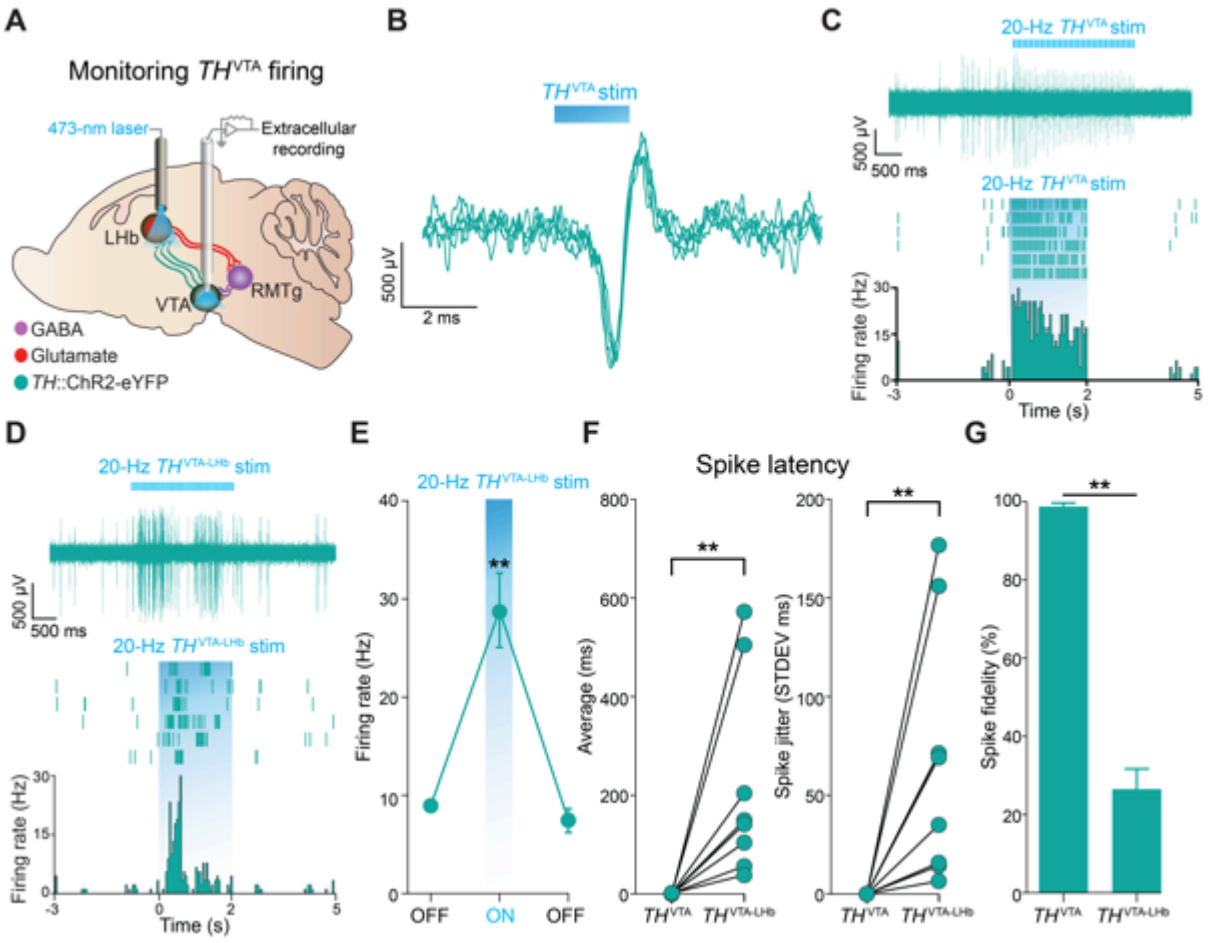

Figure 3.10: In vivo optical stimulation of *TH*$^{VTA-LHb}$ terminals enhances spontaneous firing of *TH*^{VTA} neurons (**A**) Schematic for anesthetized in vivo extracellular recordings in the VTA. (**B**) Example traces from a single optically-tagged TH^{VTA} unit displaying repeated time-locked activation to 2 ms optical stimulation of the VTA. (**C**) Example trace from a single TH^{VTA} unit (top) and its representative peri-event histogram and raster (bottom) displaying repeated time-locked activation to 20 Hz optical stimulation of TH^{VTA} cell bodies. (**D**) Example trace from a single TH^{VTA} unit (top) and its representative peri-event histogram and raster (bottom) displaying enhanced activity in response to 20 Hz optical stimulation of TH$^{VTA-LHb}$ terminals within the LHb. (**E**) The average firing rate of optically-

identified TH^{VTA} units significantly increased during 20 Hz optical stimulation of $TH^{VTA\text{-}LHb}$ terminals within the LHb ($F_{2,12}$ = 10.02, p = 0.0028, n = 3 mice, n = 5 units). (**F**) The average latency of each optical stimulation parameter (soma versus terminal; left) demonstrates that optical stimulation of $TH^{VTA\text{-}LHb}$ terminals resulted in significantly greater spike latencies in optically-identified TH^{VTA} neurons compared to light-evoked spikes from TH^{VTA}-soma optical stimulation (p = 0.0053, n = 3 mice, n = 9 units). The standard deviation (STDEV) of each stimulation type (right) shows that light-evoked spikes from TH^{VTA}-soma optical stimulation displayed significantly greater latency stability compared to $TH^{VTA\text{-}LHb}$-terminal initiated spikes (p = 0.0014, n = 3 mice, n = 9 units). (**G**) TH^{VTA}-soma light-evoked spikes responded more reliably to 20 Hz optical stimulation compared to $TH^{VTA\text{-}LHb}$-terminal light-evoked spikes ($F_{1,18}$ = 11.2, p = 0.0036, n = 3 mice, n = 11 units). Error bars represent s.e.m. **p < 0.01 (Student's t test and ANOVA followed by Bonferroni post hoc comparisons, where applicable).

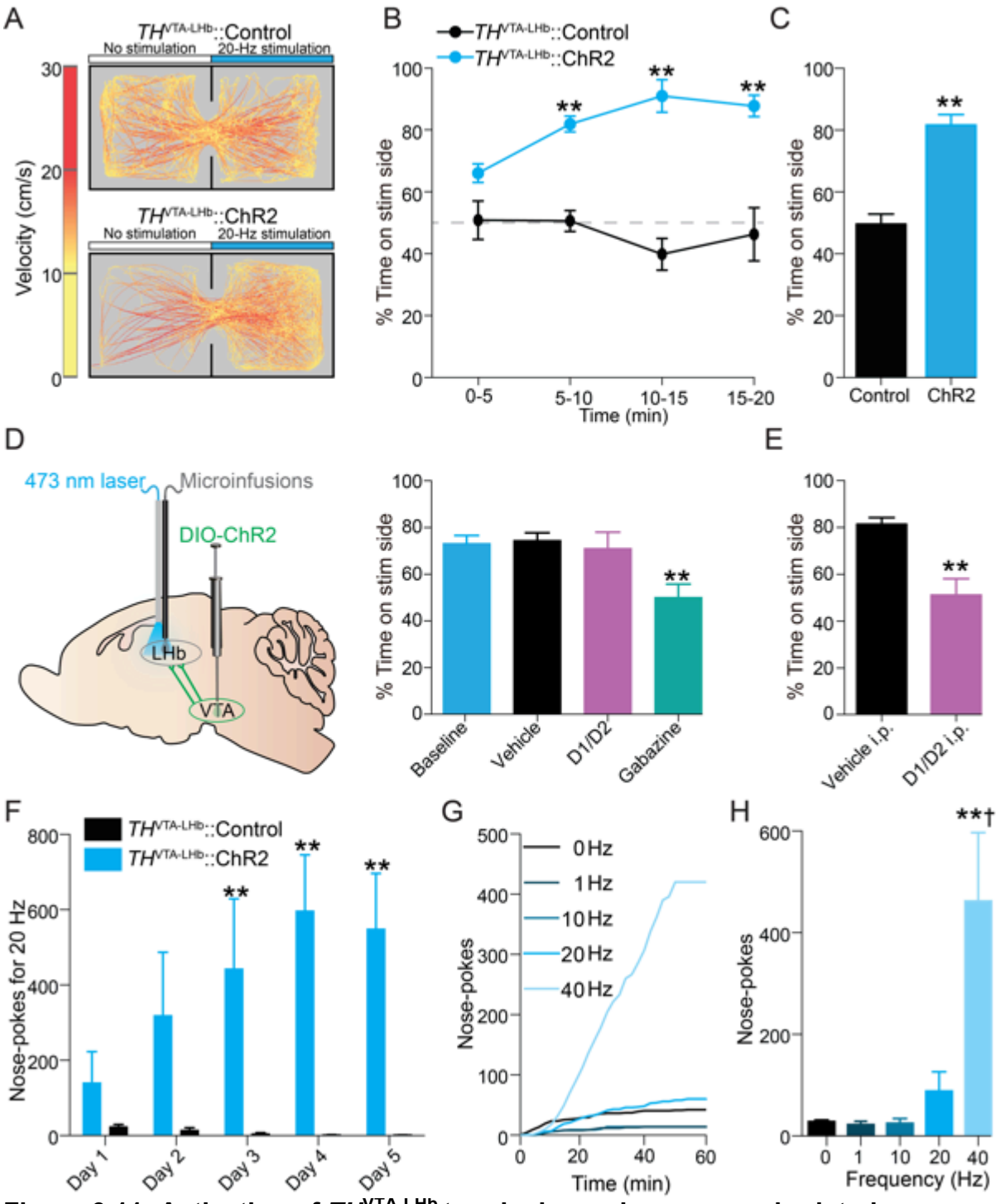

Figure 3.11: Activation of *TH*$^{VTA-LHb}$ terminals produces reward-related behavioral phenotypes . (**A**) Representative tracks from TH$^{VTA-LHb}$::Control (top) and TH$^{VTA-LHb}$::ChR2 (bottom) mice during RTPP task. (**B,C**) TH$^{VTA-LHb}$::ChR2 mice

spent more time on the side of the chamber paired with stimulation than $TH^{VTA-LHb}$::Control mice (5 min time bins: $F_{3,1} = 79.2$, $p < 0.0001$; entire 20 min session: $t_{13} = 8.82$, $p < 0.0001$; n = 8 $TH^{VTA-LHb}$::Control and 7 $TH^{VTA-LHb}$::ChR2). (**D**) Intra-LHb injections of a $GABA_A$ antagonist, but not a dopamine receptor (D1 and D2) antagonist cocktail, followed by $TH^{VTA-LHb}$::ChR2 stimulation blocked the real-time place preference ($F_{3,32} = 5.1$, $p = 0.005$; n = 9 mice). (**E**) Systemic injection of a dopamine receptor (D1 and D2) antagonist cocktail followed by $TH^{VTA-LHb}$::ChR2 stimulation blocked the real-time place preference ($t_{12} = 4.0$, $p = 0.002$; n = 7 mice). (**F**) Active nose-poke responses from $TH^{VTA-LHb}$::ChR2 and $TH^{VTA-LHb}$::Control mice over the first 5 days of training. $TH^{VTA-LHb}$::ChR2 mice made significantly more nose-pokes on Days 3, 4, and 5 than $TH^{VTA-LHb}$::Control mice (Day 3: $t_{12} = 3.78$, $p < 0.01$; Day 4: $t_{12} = 4.45$, $p < 0.001$; Day 5: $t_{12} = 4.22$, $p < 0.001$). (**G**) Example cumulative records of nose-pokes made by a $TH^{VTA-LHb}$::ChR2 mouse for 0, 1, 10, 20, and 40 Hz optical stimulation in the 5-choice nose-poke task. (**H**) $TH^{VTA-LHb}$::ChR2 mice made significantly more nose-pokes for 40 Hz than any other frequency ($F_{4,25} = 9.13$, $p < 0.0001$). n = 6 $TH^{VTA-LHb}$::ChR2 mice. n = 8 $TH^{VTA-LHb}$::Control mice. Dagger symbol denotes significance compared to all manipulations. Error bars represent s.e.m. $^{**}p < 0.01$ (Student's t test and ANOVA followed by Bonferroni post hoc comparisons, where applicable).

CHAPTER 4: A MAJOR GLUTAMATERGIC LATERAL HABENULA AFFERENT FROM THE LATERAL HYPOTHALAMUS NEGATIVELY CONTROLS FEEDING AND REWRAD

INTRODUCTION

The initiation and coordination of complex motivated behaviors, such as the seeking out and consumption of food, is necessary for an organism's survival. Identifying the precise brain regions and neural circuits that direct these behaviors will be necessary to understand neuropsychiatric diseases, such as eating disorders and addiction, that may occur when these circuits become perturbed. The lateral hypothalamus (LH) is a large heterogeneous structure involved in many processes aimed at maintaining homeostasis (Lein et al., 2007; Markakis, 2002; Sternson et al., 2013). Early electrical stimulation studies of the LH revealed that activation produces robust feeding, as well as reward-seeking behavior (DELGADO and ANAND, 1953; Hoebel and Teitelbaum, 1962; Margules and Olds, 1962; Olds and Milner, 1954). However, as the LH is composed of many genetically distinct neuronal subtypes, such as GABAergic, glutamatergic, peptidergic, and monoaminergic neurons, and contains many afferents and fibers of passage, it is unclear which neural substrate is responsible for producing these behaviors.

A recent circuit-based study demonstrated that the extended amygdala sends a robust inhibitory projection to the LH and preferentially synapses onto LH glutamatergic neurons (Jennings et al., 2013b). Activation of this inhibitory input

results in time-locked feeding and reinforcement behaviors. Further, direct optogenetic inhibition of the glutamatergic neurons in the LH promoted feeding and reward, while activation of these neurons suppressed feeding and produced aversion. While it is clear that extended amygdala inputs to LH glutamatergic neurons promotes feeding and reward-seeking, it is unclear whether LH glutamatergic neurons regulate behavior or longer timescales, or if select projections from these cells underlie varying aspects of feeding and reward-seeking. The LH projects to widespread regions of the brain, including the lateral habenula (LHb), midbrain, and hindbrain (Ching Liang Shen, 1983). Here, we focus on the LH's projection to the LHb to determine if this circuit underlies distinct aspects of feeding and reward-seeking.

The LHb encodes aversive events and is involved in negative reward processing. Functionally, LHb neurons show opposite responses to midbrain dopaminergic neurons during aversive and rewarding events. Specifically, midbrain dopaminergic neurons show increases in firing to cues that predict a reward and decreased firing to cues that predict no reward, whereas LHb neurons respond in an opposite manner (Matsumoto and Hikosaka, 2007). Importantly, excitation of LHb neurons precedes the inhibition of dopaminergic neurons. LHb glutamatergic neurons inhibit VTA dopaminergic neurons by activating GABAergic rostromedial tegmental nucleus (RMTg) neurons that synapse onto dopaminergic VTA neurons, and activation of this circuit is aversive and disrupts ongoing positive reinforcement (Matsui and Williams, 2011; Stamatakis and Stuber, 2012). Inputs from the LHb arise from forebrain regions including the LH, entopenduncular nucleus, and

prefrontal cortex (Kim and Lee, 2012; Poller et al., 2013; Shabel et al., 2012; Warden et al., 2012). Because the LH is involved in maintaining homeostasis, and the LHb is a potent modulator of midbrain dopaminergic activity, we sought to determine whether the LH input to the LHb could be driving aspects of reward and feeding.

Here, we report that genetic ablation of LH glutamatergic neurons increases feeding and weight gain on a long-term scale. Additionally, we demonstrate that LH glutamatergic neurons send a functional glutamatergic projection to the LHb, and that this circuit is important for regulating aspects of feeding and motivated behaviors.

METHODS

Subjects

Adult (25 – 30 g) male VGlut2-IRES-Cre or wild-type litter mates and adult (25-30 g) C57BL/6J mice were used. Mice were maintained on a reverse 12-hr light cycle (lights off at 07:00) with *ad libitum* access to food and water unless placed on a food restriction schedule for the free-licking experiment (see below). All food-deprived mice were restricted to 90% of their initial body weight by administering one daily feeding of 2.5 – 3.0 g of standard grain-based chow (immediately following behavioral experiment, if performed). All procedures were conducted in accordance with the Guide for the Care and Use of Laboratory Animals, as adopted by the NIH, and with approval of the Institutional Animal Care and Use Committee at the University of North Carolina at Chapel Hill.

Viral Construct

Purified and concentrated adeno-associated viruses coding for Cre-inducible ChR2-eYFP (AAV5-EF1a-DIO-hChR2(H134R)-eYFP), NpHR3.0-eYFP (AAV5-EF1a-DIO-NpHR3.0-eYFP), and taCasp3 (AAV2-FLEX-taCasp3-TEVp) were all packaged by the UNC Vector Core Facility at titres of ~2 x 10^{12} cfu per mil.

Stereotactic Surgeries

Mice were anesthetized with ketamine (150mg/kg body weight) and xylazine (50mg/kg) solution and placed in a stereotactic frame (Kopf instruments). For the genetic ablation and optogenetic experiments, adult male *VGlut2-IRES-Cre* positive and negative littermates (Controls) were bilaterally microinjected with 0.3 μl of virus into the LH using the following coordinates: -1.0 mm posterior to bregma, ±0.9 mm lateral to midline, and -6.0 mm ventral to skull surface. For the optogenetic experiments, mice were bilaterally implanted with optical fibers aimed directly above the LHb at -1.7 mm posterior to bregma, ±-1.25 lateral to midline, and -3.24 ventral to the skull surface at a 15° angle. For the retrobead mapping and quantification experiments, male C57Bl/6J mice (Jackson Laboratory) received quadrouple injections (Nanoinject) with 70nL of red retrobeads (Lumafluor) in the LHb using the following coordinates: -1.4 mm and -1.8 mm posterior to bregma, ± 0.43 mm lateral to the midline and -3.3 ventral to the skull surface.

Fluorescence in Situ Hybridization

Mice were rapidly decapitated, and brains were snap frozen with dry ice in an

embedding mold of O.C.T Compound (Fisher Scientific, Pitssburgh, PA). Fresh, frozen brains were sectioned at 20 μm on a cryostat (CM3050; Leica Biosystems, Richmond, VA) onto charged slides (Leica Biosystems, Richmond, VA). A given set was hybridized to *VGlut2* antisense and sense riboprobes. A 1749-bp riboprobe complementary to VGlut2-sense cDNA that was inserted into the pGEM-4Z vector (Promega, Madison, WI). Plasmid DNA was cut with either EcoRI or SalI in order to create a template for *in vitro* transcription. All probes were created using digoxigenin (DIG)-labeled nucleotides for detection. The SalI template was transcribed with Sp6 RNA Polymerase to generate the sense riboprobe, and the EcoRI template was transcribed with T7 RNA polymerase to generate the antisense riboprobe. Fluorescence in situ hybridization (FISH) was performed at room temperature unless otherwise indicated. Tissue was dried at 50 °C, fixed in 4% DEPC-PFA for 15 min, and washed in DEPC-PBS 3 x 5 min. The tissue was then acetylated in 1x triethanolamine-HCl with 0.25% acetic anhydride for 10 min and subsequently washed in DEPC-PBS 3 x 5 min each. Next, the tissue was prehybridized for 3 hr at 65 °C in hybridization buffer containing 5X saline sodium citrate (SSC), 50% formamide, 1-mg/mL yeast tRNA, 0.1-mg/mL heparin, 0.1% tween-20, 0.005-M EDTA (pH 8.0), and 0.1% CHAPS. Following prehybridization, the tissue was hybridized by incubating in hybridization buffer containing a probe for *VGlut2* (DIG-labeled). Post-hybridization stringency washes were performed sequentially at 65 °C in pre-warmed buffers: 1 x 15 min in 2X SSC, 3 x 20 min in 0.2X SSC buffer. Following stringency washes, tissue was further washed at room temperature 2 x 10 min in Ts7.5 (0.1-M TRIS-HCl, pH 7.5, 0.15-M NaCl). Tissue was then incubated in

3% H_2O_2 in methanol and washed 3 x 5 in TS7.5 to eliminate endogenous hydrogen peroxidase activity. Sections were then incubated for 1 hr in 1% blocking buffer (Perkin Elmer, Waltham, MA), followed by incubation for 24 hr at 4 °C in anti-DIG-POD (1:100 dilution in 1% blocking buffer). The following day, after washing 3 x 10 min in TNT wash buffer (0.1-M TRIS-HCl, pH 7.5. 0.15-M NaCl, 0.05% Tween-20), sections underwent a tyramide signal amplification with TSA plus DNP 1:50 in amplification diluent. Following a 4-min incubation, sections were vigorously washed with TNT wash buffer 4 x 10 min and incubated in a DNP primary antibody conjugated with Alexa Fluor 488 (1:500 dilution in TNT; Molecular Probes, Eugene, Oregon) at 4 °C overnight. Sections were then washed 3 x 10 min with TNT wash buffer and coverslipped with a mounting media containing DAPI as a counterstain (Life Technologies, Carlsbad, CA).

Histology, immunohistochemistry, and confocal microscopy

Mice were anesthetized with pentobarbital, and transcardially perfused with PBS followed by 4% (w/v) paraformaldehyde in PBS. Brains were then removed and submerged in 4% paraformaldehyde for 24 hr and transferred to 30% sucrose in ddH2O for 48 hr. 40 mm brain sections were obtained and subjected to immunohistochemical staining for neuronal cell bodies (NeuroTrace Invitrogen; 640-nm excitation/660-nm emission or 435-nm excitation/455-nm emission). Brain sections were mounted, and z-stack and tiled images were captured on a Zeiss LSM 710 confocal microscope using a 20x, 40x, or 63x objective and analyzed using ZEN 2009 and ImageJ software. To determine optical fiber placement, tissue was

imaged at 10X and 20X on an upright conventional fluorescent microscope.

Free Feeding Following LH Glutamatergic Genetic Ablation

Following surgery, *VGlut2*^{LH}::taCasp3 and *VGlut2*^{LH}::Control mice were weighed daily. For 4 weeks, mice were given *ad libitum* access to standard grain-based chow (Harlan, 3.5 calories/gram). Chow was weighed daily immediately following weighing of mice. After 4 weeks of access to grain-based chow, mice were given *ad libitum* access to both standard grain-based chow and a calorie-dense chow (Bioserv, High Fat diet, Gat Calories = 60%, 5.49 calories/gram). Body weight, grain-based chow, and calorie-dense chow were weighed daily. Calories consumed were calculated by grams of grain-based chow (3.5 calories/gram) plus grams of calorie-dense chow (5.49 calories/gram).

Open Field Testing

4 weeks following surgery, *VGlut2*^{LH}::taCasp3 and *VGlut2*^{LH}::Control mice were examined in a custom made open field arena (25 x 25 x 25 cm white plexiglass arena) for 35 min. Center zone was defined as the center 156 cm^2 (25% of the entire arena). Corner zones were defined as the 39 cm^2 in each corner. The 35 min session was recorded with a CCD camera that was interfaced with Ethovision software (Noldus Information Technologies). Time spent in the corner and the center of the open-field apparatus was recorded.

Patch-Clamp Electrophysiology

Mice were anesthetized with pentobarbital and perfused transcardially with

modified artificial cerebrospinal fluid containing (in mM): 225 sucrose, 119 NaCl, 1.0 NaH2PO4, 4.9 MgCl2, 0.1 CaCl2, 26.2 NaHCo3, 1.25 glucose. Brains were then rapidly removed and placed in the same solution that was used for perfusion at ~0 °C. Coronal slices containing the LHb (200 μm) were cut on a Vibratome (VT-1200, Leica Microsystems). Following slicing, brain slices were placed in a holding chamber and were allowed to recover for at least 30 minutes before being placed in the recording chamber and superfused with bicarbonate-buffered solution saturated with 95% O_2 and 5% CO_2 containing (in mM): 119 NaCl, 2.5 KCl, 1.0 NaH2PO4, 1.3 MgCl2, 2.5 CaCl2, 26.2 NaHCO3, and 11 glucose (at 32-34°C). Cells were visualized using infrared differential contrast and fluorescence microscopy. For voltage-clamp recordings, patch electrodes (3-5 MΩ) were back-filled with a cesium methanesulfonic acid internal solution containing (in mM): 117 Cs methanesulfonic acid, 20 HEPES, 0.4 EGTA, 2.8 NaCl, 5 TEA, 2 ATP, 0.2 GTP. For cell-attached recordings, patch electrodes (2-4 MΩ) were back-filled with a potassium gluconate internal solution containing (in mM): 130 K-gluconate, 10KCl, 10 HEPES, 10 EGTA, 2 MgCl2, 2ATP, 0.2 GTP. pH = 7.35, 270-285 mOsm for all internal solutions. Whole-cell voltage-clamp, and cell-attached recordings of LHb neurons were made using an Axopatch 700B amplifier (Molecular Devices). For all optical stimulations, blue light (1 mW, 473 nm) was delivered through a 40X objective via a LED. Series resistance (15-25 MΩ) and/or input resistance were monitored online with a 5-mV hyperpolarizing step delivered between stimulation sweeps. All data were filtered at 2kHz, digitized at 5-10kHz, and collected using pClamp10 software (Molecular Devices). For the voltage-clamp recordings in LHb neurons, membrane potentials

were maintained at -70mV, and then at +10mV, and light pulses were delivered every 20 s to evoke neuronal firing. For EPSCs, following 5-10 min of baseline recording, 10 μM of the glutamate antagonist DNQX was bath-applied for 10 min. For IPSCs, following 5-10 min of baseline recording, 10μM of the $GABA_A$ receptor antagonist, SR-95531 (gabazine) was bath-applied for 10 min. IPSC and EPSC amplitudes were calculated by measuring the peak current from the average response from 6 sweeps during baseline and during each drug application. Cells that showed a > 20% change in the holding current or access resistance were excluded from analysis. For cell-attached recordings, a 20-Hz optical stimulation was delivered for 1 s every 20 s for 20 sweeps. Firing rate was averaged across all 20 sweeps.

Real-time place preference

VGlut2$^{LH\text{-}LHb}$::ChR2, *VGlut2*$^{LH\text{-}LHb}$::NpHR3.0, and *VGlut2*$^{LH\text{-}LHb}$::Control mice bilaterally implanted with optical fibers aimed at the LHb were placed in a custom-made behavioral arena (50 × 50 × 25 cm black plexiglass) for 20 min. One counterbalanced side of the chamber was assigned as the stimulation side. At the start of the session, the mouse was placed in the non-stimulated side of the chamber. Every time the mouse crossed to the stimulation side of the chamber, a 20-Hz constant laser stimulation (472 nm for *VGlut2*$^{LH\text{-}LHb}$::ChR2 mice) or a constant 532 nm laser stimulation (for *VGlut2*$^{LH\text{-}LHb}$::NpHR3.0) was delivered until the mouse crossed back into the non-stimulation side. Percent time spent on the stimulation-paired and velocity was recorded via a CCD camera interfaced with Ethovision software (Noldus Information Technologies).

Photoinhibition of *VGlut2*$^{LH \rightarrow LHb}$::NpHR3.0 during consumption behavioral assays

Following the real time place preference experiments, male *VGlut2*$^{LH\text{-}LHb}$::NpHR3.0 and *VGlut2*$^{LH\text{-}LHb}$::Control mice were restricted to 90% of their initial body weight by administering one daily feeding of ~ 2.5 to 3.0 g of standard grain-based chow immediately following each behavioral experiment, if performed. Behavioral training and testing occurred in mouse operant chambers interfaced with optogenetic stimulation equipment as described previously (Stamatakis and Stuber, 2012). Once mice reached 90% of their body weight, they were trained in a standard behavioral box (Med Associates, Vermont, USA) equipped with two bottle lickometers for quantification of consumption of a highly palatable liquid (Ensure). The free-reward consumption task consisted of unlimited access to Ensure during each 20 min session. Lick time stamps were recorded and used for analysis. Mice were trained until the number of licks during each session was stable (<20% change) for three consecutive sessions, which for all mice occurred after 7-15 training sessions. Once the mice stabilized they received constant optical inhibition during a 20 min session (532 nm light from a solid-state laser delivered via custom-made patch cables).

RESULTS

Genetic Ablation of *VGlut2*^{LH} Neurons Increases Caloric Intake and Body Weight

Optogenetic inhibition of glutamatergic neurons in the LH results in time-locked increases in feeding (Jennings et al., 2013b); however, it is unclear if these neurons are important in regulating feeding or body weight over days or weeks.

Therefore, we selectively ablated glutamatergic neurons in the LH by injecting a cre-dependent virus (AAV-FLEX-taCasp3-TEVp) encoding pro-taCaspase-3 and a TEVp enzyme that cleaves pro-taCaspase-3 into the active, proapoptotic signal caspase-3 into Vesicular glutamate transporter-2 (VGlut2)-cre mice (**Figure 4.1A)**. Following virus injections, in situ hybridization revealed a significant reduction in the number of LH neurons that expressed vglut2 (**Figure 4.1 B-E**). We also observed a reduction in the neighboring ventromedial hypothalamus, although to a lesser extent (**Figure 4.1 B-E**). We observed no differences in body weight or caloric intake when mice were had ad libitum access to standard rodent chow (**Figure 4.1 F**). However, when mice were exposed to a calorie-dense diet, *VGlut2*^{LH}:taCasp3 mice showed a significant increase in body weight and caloric intake compared to *VGlut2*^{LH}:Control mice (**Figure 4.1 F,G**).

To determine whether ablation of LH glutamatergic neurons resulted in changes in locomotor activity or anxiety-like phenotypes, which could account for a change in feeding, we next tested mice in an open-field assay. Although we observed a slight increase in locomotor activity (**Figure 4.1 H,I**), and a slight decrease in the amount of time spent in the center of the open-field (**Figure 4.1 J,K**), these results did not reach statistical significance.

LHb-projecting LH neurons are glutamatergic and are localized to the anterior LH

The lateral hypothalamus sends widespread projections throughout the brain, including to the LHb, the midbrain and hindbrain (Ching Liang Shen, 1983). The projection from the LH to the LHb is almost strictly glutamatergic (Poller et al., 2013),

and thus we focused on this projection, since the LHb is critical for inhibiting and promoting aspects of motivated behaviors (Stamatakis and Stuber, 2012; Stamatakis et al., 2013). To provide an anatomical map of the LHb-projecting LH neurons within the LH, we injected fluorescent retrograde beads into the LHb of wild-type mice (**Figure 4.2 A,B**). Three weeks following surgery, we observed neurons in the LH and entopenduncular nucleus labeled with retrogradely transported beads from the LHb. While LHb-projecting LH neurons spanned the length of the LH, we observed the highest density of LHb-projecting LH neurons in the anterior portion of the LH (**Figure 4.2 C**).

Confocal and electron microscopy studies have revealed that the majority of LH presynaptic terminals in the LHb contain VGlut2, but lack the GABA-synthesizing enzyme glutamate decarboxylase (GAD) (Poller et al., 2013). To selectively target LH glutamatergic neurons and confirm that the LH-to-LHb pathway was glutamatergic, we introduced a cre-inducible viral construct coding for channelrhodopsin-2 conjugated to enhanced yellow fluorescent protein (ChR2-eYFP) bilaterally into the LH of VGlut2-Cre mice (**Figure 4.2 D)**. Six weeks following surgery, we observed robust eYFP expression in the LH as well as in fibers from the LH that innervate the LHb **(Figure 4.2 E,F).** To explore whether there was a GABAergic projection from the LH, we introduced a cre-inducible viral construct coding for ChR2-eYFP bilaterally into the LH of Vgat-Cre adult mice as well (**Figure 4.2 G**). Six weeks following surgery, we observed robust eYFP expression in the LH and in regions surrounding the LHb, such as the thalamus, but only observed very modest eYFP expression in the LHb (**Figure 4.2 G-I**). Collectively, these data

support earlier findings demonstrating a primarily glutamatergic input from the LH to the LHb.

Characterization of neurotransmitter release from *VGlut2*$^{LH\text{-}LHb}$ fibers

We next sought to confirm that LH glutamatergic neurons functionally project to LHb neurons and release glutamate. We performed whole-cell voltage-clamped recordings from postsynaptic LHb neurons in brain slices obtained from *VGlut2*^{LH}::ChR2 mice. Voltage-clamp recordings from LHb neurons revealed that light pulses that selectively stimulated *VGlut2*^{LH}::ChR2 fibers in the LHb, produced light-evoked currents that were blocked by the glutamate receptor antagonist DNQX (n = 25 cells, 76% were light responsive) (**Figure 4.3 A,B**). At the reversal potential for AMPA receptors, we observed a small amplitude light-evoked current that was blocked by the $GABA_A$ receptor antagonist, gabazine (n = 8 cells, 50% were light responsive) (**Figure 4.3 C,D**). Since we observed both excitatory and inhibitory components from *VGlut2*$^{LH\text{-}LHb}$::ChR2 terminals, we next investigated how activating *VGlut2*$^{LH\text{-}LHb}$::ChR2 terminals would affect the spontaneous firing rate of postsynaptic LHb neurons. To accomplish this, we performed cell-attached recordings from LHb neurons and found that when we delivered a 1s 20 Hz optical pulse-train to selectively stimulate *VGlut2*^{LH}::ChR2 terminals, the majority of LHb neurons showed increases in firing (70.6%) (**Figure 4.3 E-G**). We also observed a much smaller population of LHb neurons that demonstrated a decrease in spontaneous firing following optical stimulation (5.9%) (**Figure 4.3 H-J**). These data suggest that while LH glutamatergic neurons might be co-releasing GABA, the net effect of

neurotransmitter release of stimulating *VGlut2*^{LH}::ChR2 terminals is to increase the firing rate of LHb neurons.

Optical stimulation and inhibition of LH-to-LHb pathway bidirectionally modulates reward-seeking behavior

Given that optogenetic activation of LH glutamatergic neurons produces aversive phenotypes (Jennings et al., 2013b), and that the LH sends a dense projection to the LHb (**Figure 4.2 E**), we explored the functional role of the LH-to-LHb circuit in modulating reward-seeking using *in vivo* optogenetics. To selectively control the LH-to-LHb circuit, we injected VGlut2-Cre mice with either cre-inducible ChR2-eYFP (**Figure 4.2D**; *VGlut2*$^{LH\text{-}LHb}$::ChR2), cre-inducible eYFP (*VGlut2*$^{LH\text{-}LHb}$::Control), or cre-inducible halorhodopsin3.0 (*VGlut2*$^{LH\text{-}LHb}$::NpHR3.0), and bilaterally implanted optical fibers aimed above the LHb (**Figure 4.4 A**).

Approximately 6 weeks after surgery, we tested whether direct optical activation or inhibition of *VGlut2*$^{LH\text{-}LHb}$ afferents in the LHb influences feeding and reward-related behavioral phenotypes. Activation of *VGlut2*$^{LH\text{-}LHb}$ terminals decreased time spent in a location paired with optical stimulation, while inhibition of *VGlut2*$^{LH\text{-}LHb}$ terminals increased time spent in a location paired with optical inhibition (**Figure 4.4 C-E**). *VGlut2*$^{LH\text{-}LHb}$::NphR3.0 and *VGlut2*$^{LH\text{-}LHb}$::Control mice were then food restricted to 90% of their free-feeding body weight to assess whether the *VGlut2*$^{LH\text{-}LHb}$ circuit is necessary to promote aspects of feeding. Mice were given free access to a highly palatable calorically dense liquid for 20 minutes. Once mice displayed stable baseline drinking behavior (<20% difference across 3 days), mice were exposed to constant optical inhibition of the *VGlut2*$^{LH\text{-}LHb}$ circuit during the

entire 20-minute session. Optical inhibition of the circuit resulted in a significant increase in drinking in *VGlut2*$^{LH\text{-}LHb}$::NphR3.0 mice, compared to *VGlut2*$^{LH\text{-}LHb}$::Control mice (**Figure 4.4 F-I**). These data suggest the glutamatergic projections from the LH to the LHb may serve as a valence detector, by increasing glutamatergic tone to promote avoidance, or decreasing glutamatergic tone in the LHb to promote ongoing rewarding behavior.

DISCUSSION

The LH has been long recognized as a critical brain region for both feeding and reward-seeking (Hoebel and Teitelbaum, 1962; Margules and Olds, 1962). However, given the rich cellular heterogeneity and distributed afferent and efferent connectivity, it has been difficult to understand the precise LH circuit connectivity that controls distinct aspects of motivated behaviors. Electrical stimulation of the LH causes voracious feeding and reward-seeking behavior (DELGADO and ANAND, 1953; Olds and Milner, 1954), yet activation of glutamatergic neurons in the LH disrupts feeding and causes avoidance behaviors (Jennings et al., 2013b). Interestingly, lesions of the LH can result in weight loss and significant aphagia (Von Der Porten and Davis, 1979; Harrell et al., 1975; Schallert and Whishaw, 1978). However, here we demonstrate that genetic ablation of LH glutamatergic neurons causes increases in caloric intake and increased body weight after weeks of access to a high fat diet, suggesting that LH glutamatergic neurons may be involved in long-term homeostatic feeding mechanisms, such as metabolism regulation. The LH contains GABAergic neurons as well as glutamatergic neurons, and in situ data

suggest that the population of GABAergic LH neurons may be larger than the population of glutamatergic neurons (Meister, 2007; Rosin et al., 2003). These data underscore the heterogeneity of the LH and demonstrate that different genetically distinct cell groups can have profound differences on feeding behaviors.

Since we observed an effect on feeding and body weight with genetic ablation of LH glutamatergic neurons, we next sought to investigate an output of the LH, which may be mediating these effects. We found that the LH sends a strong projection to the LHb, an area involved in promoting negative reward behaviors. Optogenetic manipulation of this circuit resulted in a bidirectional effect on motivated behavior. Activation of the LH-to-LHb circuit was aversive, while inhibition of the circuit was rewarding. Previous data has demonstrated a similar aversive phenotype when activating inputs from the entopenduncular nucleus, an output of the basal ganglia (Shabel et al., 2012). It is important to note that the entopenduncular nucleus and lateral hypothalamus are neighboring structures and it is possible that viral targeting of one region could result in viral transduction of the neighboring region. Following retrobead injections into the LHb, we observed LHb-projecting neurons in both the entopenduncular nucleus and the LH. However, the entopenduncular nucleus, and the globus pallidus internus (the primate homolog) contains mainly GABAergic neurons (Oertel et al., 1984; Stephenson et al., 2005). In addition, our method for targeting the LH glutamatergic neurons, using cre-inducible ChR2, did not result in significant infection of entopenduncular neurons (**Figure 4.2 E**), supporting our conclusions that our behavioral phenotypes are the

result of the modulation of LH afferents, rather than entopenduncular nucleus afferents.

We observed both excitatory and inhibitory responses in LHb neurons following optical stimulation of *VGlut2*$^{LH\text{-}LHb}$ fibers (**Figure 4.3**). This could be due to co-release of GABA and glutamate from the same LH neuron, or due to ectopic cre expression in non-glutamatergic LH neurons. Previous studies have demonstrated specificity for cre-inducible viruses to target glutamate neurons in other brain regions in the VGlut2-Cre mouse, such as the bed nucleus of the stria terminalis (Jennings et al., 2013b). However, it is unclear if this is the case in the LH, and thus further studies should be conducted to determine if LH neurons are capable of co-releasing both glutamate and GABA.

Regulating homeostatic processes likely requires strong recruitment from the reward system. Here, we demonstrate a robust, and behaviorally relevant, projection from the LH to the LHb. Previous studies have demonstrated a prominent role for the LHb in regulating midbrain reward circuits. Combined, these data suggest that the LHb may recruit reward circuits to drive motivated behaviors towards maintaining homeostasis.

FIGURES

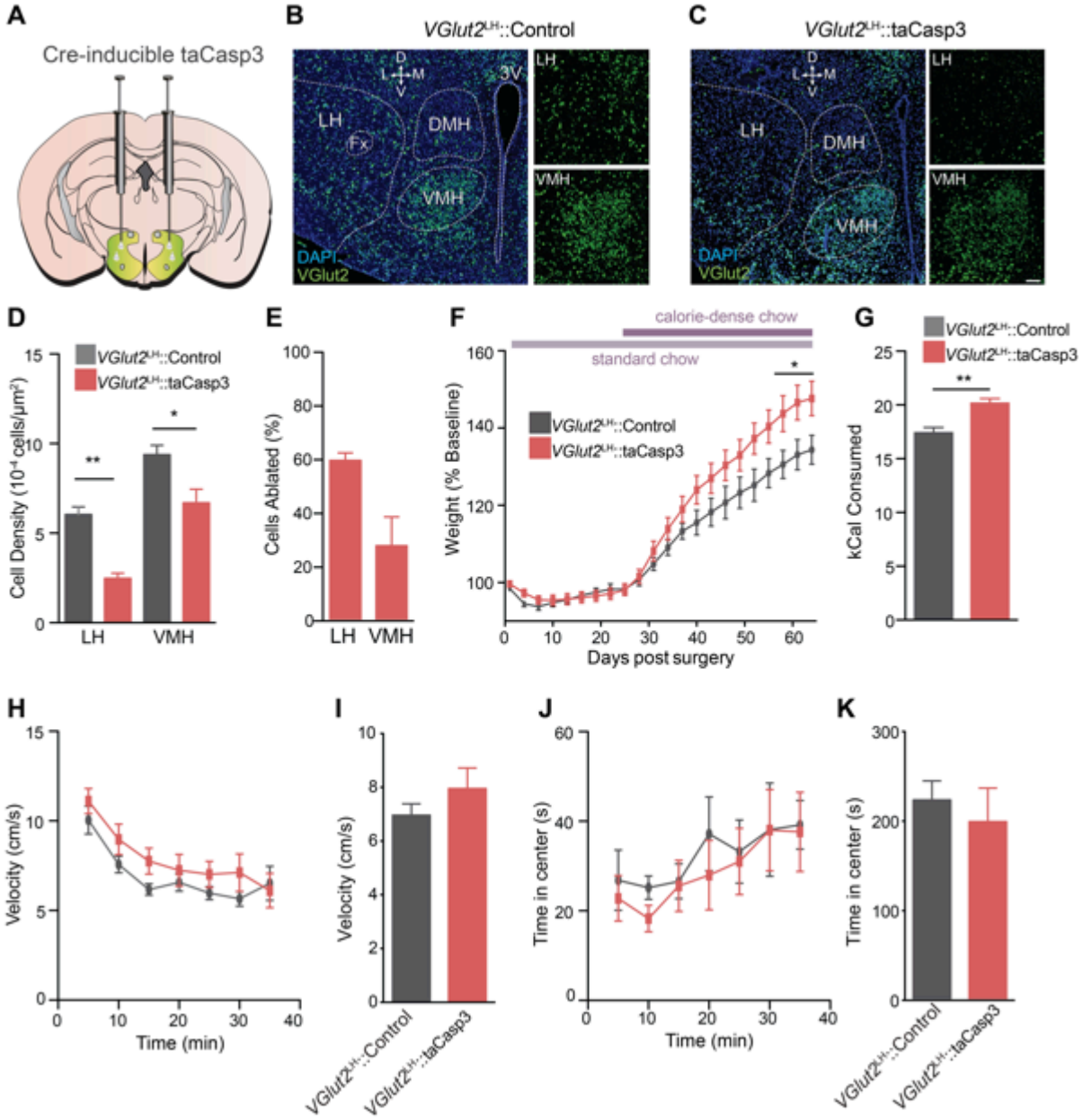

Figure 4.1: Genetic Ablation of LH Glutamatergic Neurons Increases Caloric Intake and Weight Gain. (A) Schematic for viral injection of AAV2-FLEX-taCasp3-TEVp into the LH of *VGlut2-IRES-Cre* mice. (**B** and **C**) 20x confocal images demonstrating decreased VGlut2 expression in *VGlut2*^{LH}::taCasp3 (**B**) compared to *VGlut2*^{LH}::Control (**C**) mice. LH: lateral hypothalamus, Fx: fornix, DMH: dorsomedial

hypothalamic nucleus, VMH: ventromedial hypothalamic nucleus, 3V: third ventricle, D: dorsal, L: lateral, M: medial, V: ventral. Scale bars, 200 μm. (**D**) VGlut2 expression is significantly decreased in the LH (n = 5 slices per group, $t_8 = 7.054$, $p < 0.0001$) and VMH (n = 5 slices per group, $t_8 = 2.88$, $p = 0.02$) of *VGlut2*^{LH}::taCasp3 mice compared to *VGlut2*^{LH}::Controls. (**E**) Injection of AAV2-FLEX-taCasp-TEVp into the LH of *VGlut2-IRES-Cre* mice resulted in a 59.23± 2.8% decrease in glutamate cells in the LH and a 27.47± 10.8% decrease in glutamatergic neurons in the VMH in *VGlut2*^{LH}::taCasp3 mice. (**F**) Ablation of LH glutamatergic neurons significantly potentiated weight gain induced from a calorie-dense diet (n=8 per group, $F_{1,21} = 39.27$, $p < 0.001$). (**G**) Ablation of LH glutamatergic neurons significantly increased caloric intake as measured by the average daily calories consumed over the last 7 days of exposure to the calorie-dense diet (n = 8 per group, $t_{14} = 4.50$, $p < 0.001$). (**H,I**) Open-field velocity was not significantly different between *VGlut2*^{LH}::taCasp3 and *VGlut2*^{LH}::Control mice (n = 9 per group, $t_{16} = 0.57$, $p = 0.58$). (**J, K**) Open-field center time was not significantly different between *VGlut2*^{LH}::taCasp3 and *VGlut2*^{LH}::Control mice (n = 9 per group, $t_{16} = 1.13$, $p = 0.27$).

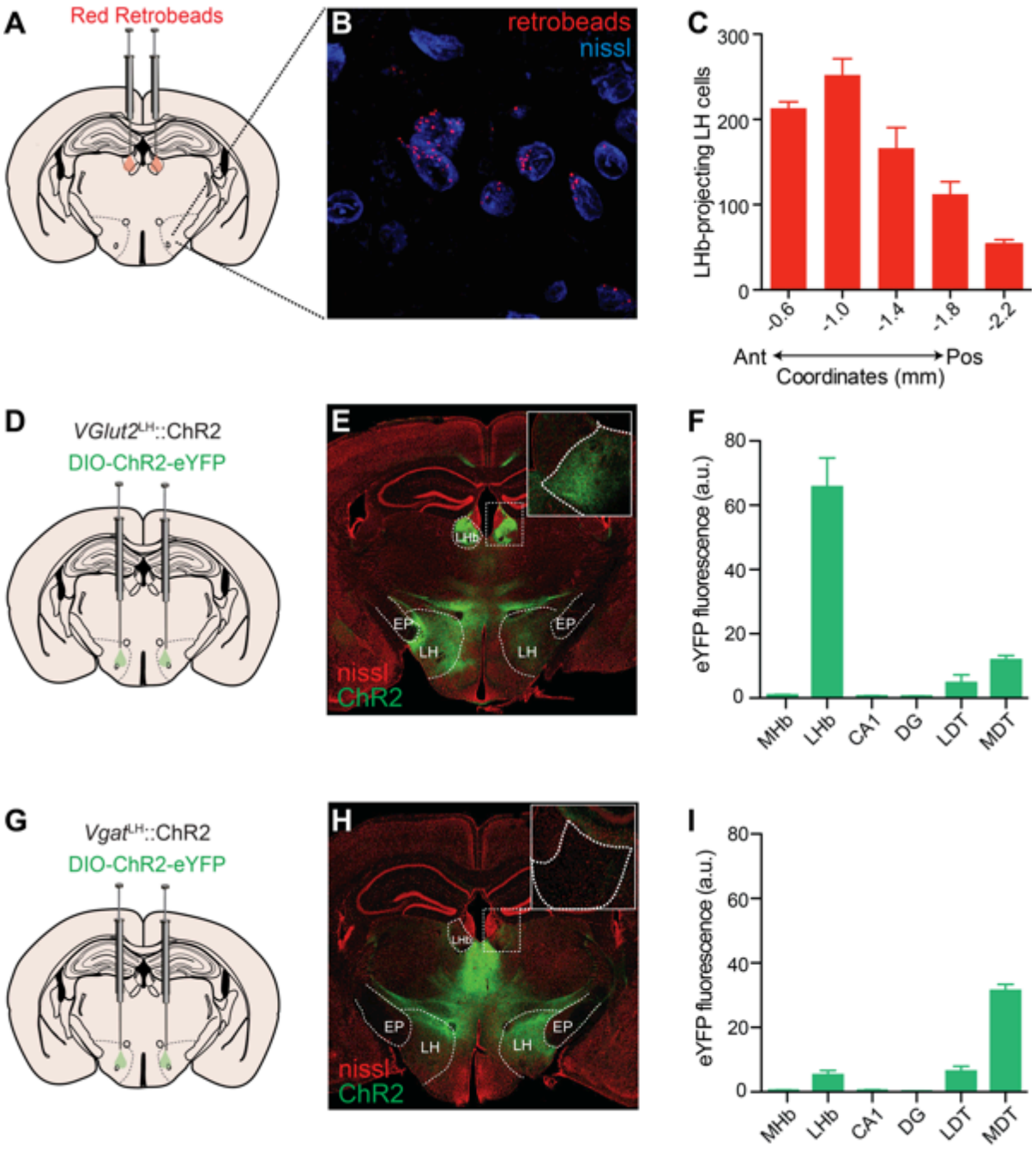

Figure 4.2: The anterior LH sends a glutamatergic projection to the LHb. (**A**) Schematic for injection of red retrobeads into the LHb of a C57BL/6J mouse. (**B**) Confocal image of the LH showing LHb-projecting LH neurons. (**C**) Quantification of LHb-projecting LH neurons along the anterior-posterior axis of the LH. Ant: Anterior, Post: Posterior. (**D**) Schematic for viral injection of AAV5-AAV5-EF1a-DIO-ChR2-

eYFP into the LH of *VGlut2-IRES-Cre* mice (*VGlut2*^{LH}::ChR2). (**E**) Confocal images of coronal sections showing expression of ChR2-eYFP in the LH and LHb (inset) of a *VGlut2*^{LH}::ChR2 mouse. Scale bar, 100 μm. (**F**) *VGlut2*$^{LH\text{-}LHb}$::ChR2 eYFP fluorescence intensity is significantly higher in the LHb than in surrounding regions ($F_{5,41}$ = 43.92, $p < 0.0001$; n = 8 sections from n = 2 mice). MHb, medial habenula; LHb, lateral habenula; DG, dentate gyrus; LDT, lateral dorsal thalamus; MDT, medial dorsal thalamus. (**G**) Schematic for viral injection of AAV5-EF1a-DIO-ChR2-eYFP into the LH of *Vgat-IRES-Cre* mice. (**H**) Confocal images of coronal sections showing expression of ChR2-eYFP in the LH and sparse ChR2-eYFP expression in the LHb (inset) of a *Vgat-IRES-Cre* mouse. Scale bar, 100 μm. (**I**) *VGat*$^{LH\text{-}LHb}$::ChR2 eYFP fluorescence intensity is significantly higher in the MDT than in surrounding regions ($F_{5,42}$ = 115.1, $p < 0.0001$; n = 8 sections from n = 2 mice).

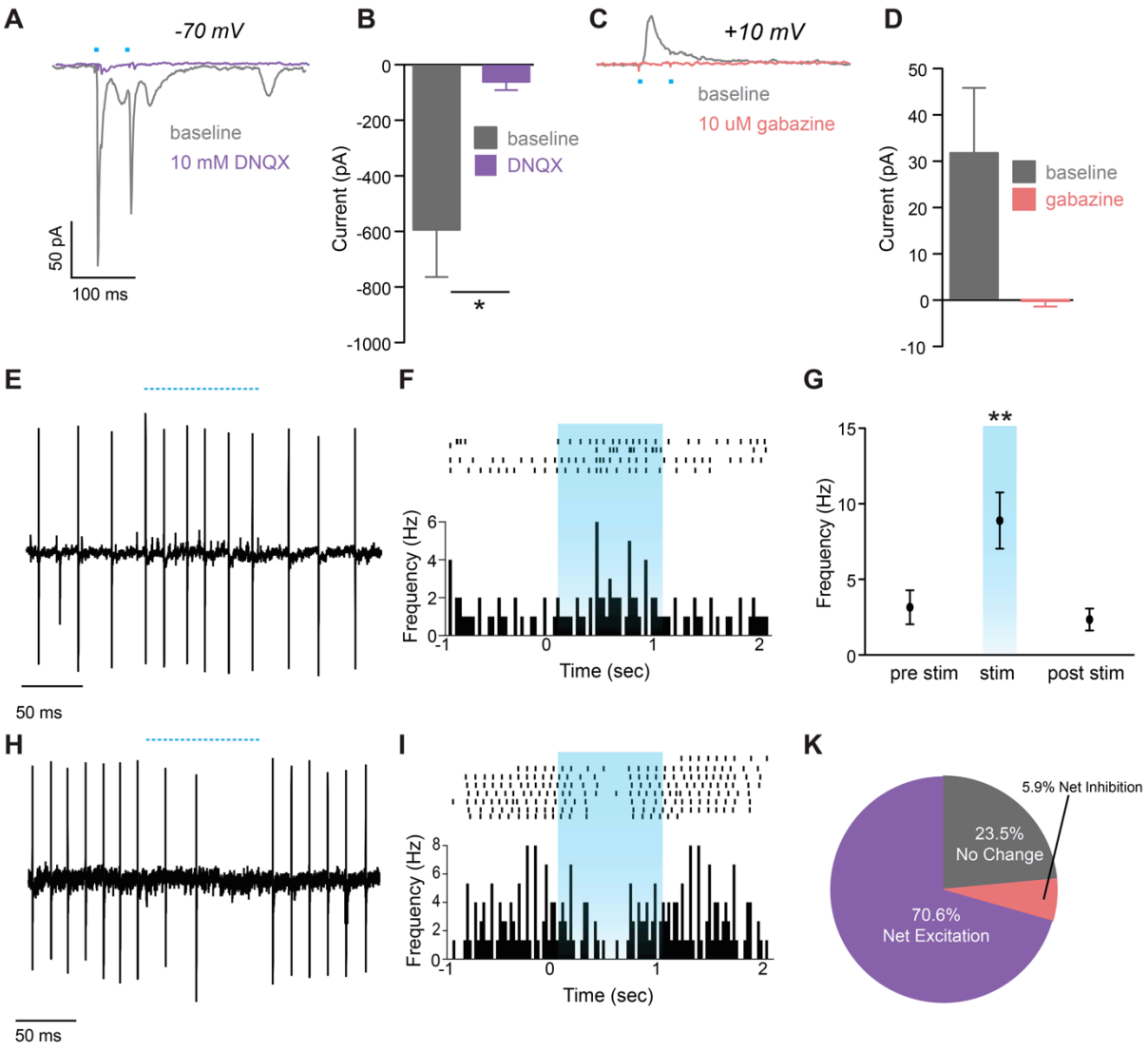

Figure 4.3: Characterization of neurotransmitter release from *VGlut2*$^{LH\text{-}LHb}$::ChR2 terminals (A-B) Postsynaptic light-evoked EPSCs recorded from LHb neurons at -70mV are significantly attenuated following bath-application of 10 μM DNQX (n = 10 cells, t_{10} =2.37, p = 0.039). (**C-D**) Postsynaptic light-evoked IPSCs recorded from LHb neurons at +10mV are attenuated by bath-application of 10 μM gabazine (n = 4 cells, t_6 = 2.28, p = 0.06). (**E-G**) Cell-attached recordings demonstrating a significant increase in the spontaneous firing rate of a subset LHb neurons in response to a 1s 20 Hz optical stimulation of *VGlut2*$^{LH\text{-}LHb}$::ChR2

terminals in the LHb (n = 12 cells, $F_{2,33}$ = 7.27, p = 0.002). (**H,I**) Cell-attached recordings demonstrating a decrease in the spontaneous firing rate from a LHb neurons in response to a 1s 20 Hz optical stimulation of *VGlut2*$^{LH\text{-}LHb}$::ChR2 terminals in the LHb. (**K**) 1s 20 Hz optical stimulation of *VGlut2*$^{LH\text{-}LHb}$::ChR2 terminals in the LHb resulted in 70.6% of LHb neurons showing a net excitation, 23.5% of LHb neurons showing less than a 20% change in firing, and 5.9% of LHb neurons showing a net inhibition (n = 17 neurons total).

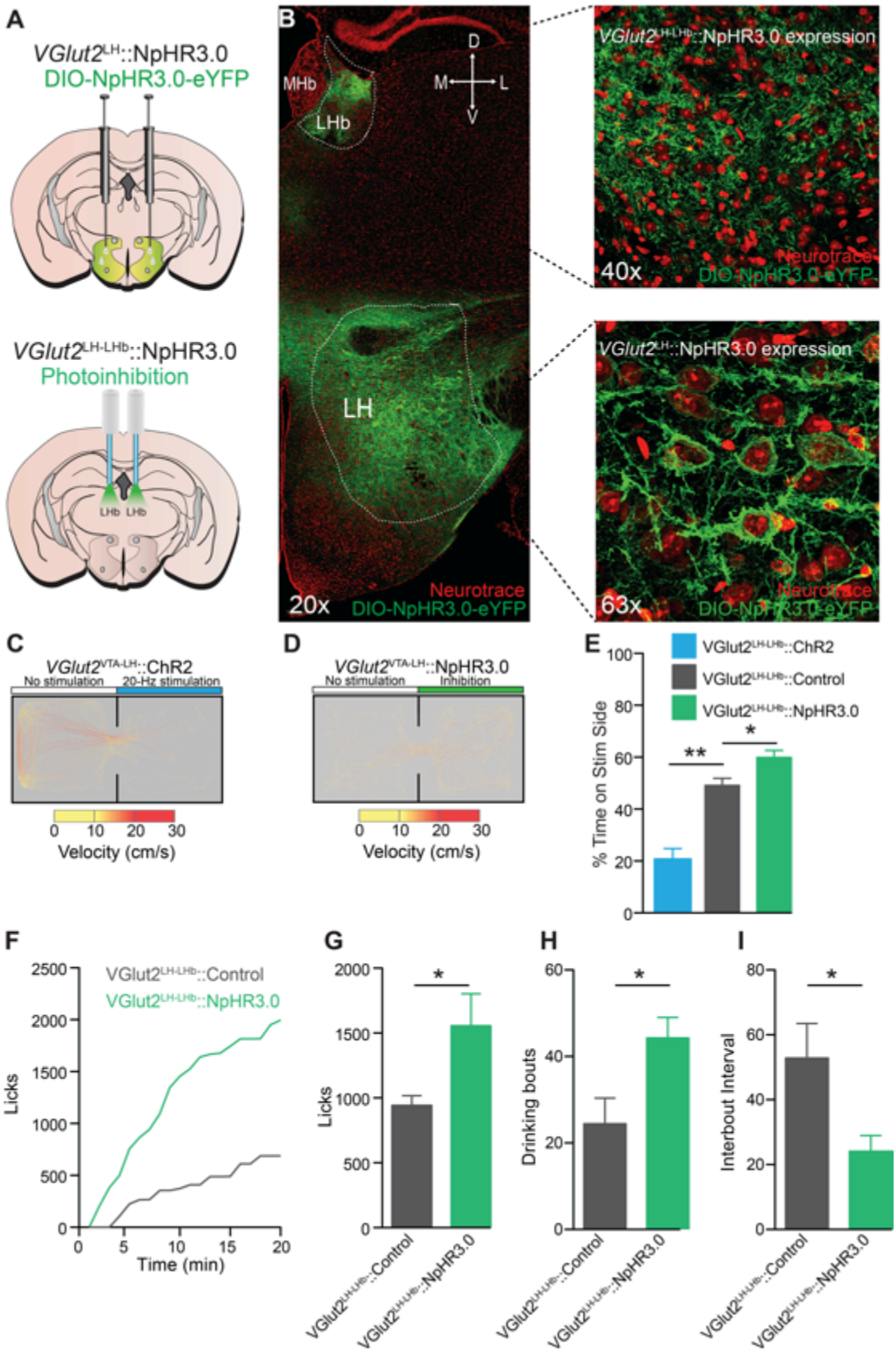

Figure 4.4: Optogenetic modulation of *VGlut2*$^{LH\text{-}LHb}$ circuit bidirectionally

modulates feeding and reward-related behaviors. (**A**) Schematic for viral injection of AAV5-EF1a-DIO-NpHR3.0-eYFP into the LH of *VGlut2-IRES-Cre* mice (*VGlut2*$^{LH\text{-}LHb}$::NpHR3.0). (**B**) Confocal images of coronal sections showing expression of NpHR3.0-eYFP in the LH and LHb of a*VGlut2-IRES-Cre* mouse. (**C,D**) Representative tracks from *VGlut2*$^{LH\text{-}LHb}$::ChR2 (**C**) and *VGlut2*$^{LH\text{-}LHb}$::NpHR3.0 (**D**) during real time place preference task. (**E**) *VGlut2*$^{LH\text{-}LHb}$::ChR2 spent less time on the side of the chamber paired with stimulation than *VGlut2*$^{LH\text{-}LHb}$::Control mice (n = 5 *VGlut2*$^{LH\text{-}LHb}$::ChR2 mice and n = 7 *VGlut2*$^{LH\text{-}LHb}$::Control mice, $t_{10} = 5.9$, $p < 0.001$). *VGlut2*$^{LH\text{-}LHb}$::NpHR3.0 spent more time on the side of the chamber paired with stimulation than *VGlut2*$^{LH\text{-}LHb}$::Control mice (n = 7 per group, $t_{12} = 2.579$, $p = 0.017$). (**F**) Example licks for ensure free-licking experiment for *VGlut2*$^{LH\text{-}LHb}$::NpHR3.0 and *VGlut2*$^{LH\text{-}LHb}$::Control mouse. (**G**) *VGlut2*$^{LH\text{-}LHb}$::NpHR3.0 licked more for a palatable liquid during a free-licking task than *VGlut2*$^{LH\text{-}LHb}$::Control mice (n = 7 per group, $t_{12} = 2.374$, $p = 0.035$). (**H**) *VGlut2*$^{LH\text{-}LHb}$::NpHR3.0 had more licking bouts than *VGlut2*$^{LH\text{-}LHb}$::Control mice (n = 7 per group, $t_{12} = 2.63$, $p = 0.02$) (**I**) *VGlut2*$^{LH\text{-}LHb}$::NpHR3.0 had a significantly lower Interbout Interval than *VGlut2*$^{LH\text{-}LHb}$::Control mice (n = 7 per group, $t_{12} = 2.56$, $p = 0.02$).

CHAPTER 5: DISCUSSION

Determining the causality between neural circuits and motivated behaviors, such as reward seeking and avoidance, are critical first steps in the development of novel treatments for neuropsychiatric diseases that occur when these circuits become perturbed. Abnormalities in the function and connectivity of dopaminergic neurons are thought to underlie many neuropsychiatric diseases such as addiction, depression, anxiety, schizophrenia, ADHD, and autism (Chevallier et al., 2012; Goto and Grace, 2007; Jennings et al., 2013a; Lau et al., 2013; Nestler and Carlezon, 2006; Viggiano et al., 2003; Wise and Koob, 2014; Zahm, 2010). Thus, the main goal of this dissertation was to use innovative and novel techniques to determine how the functional connectivity between the VTA and LHb promote various aspects of motivated behaviors and to determine the functional and behavioral significance of this reciprocal connection.

I found that the LHb sends a robust glutamatergic projection to GABAergic neurons in the RMTg and VTA. Previous studies have demonstrated that LHb neurons and midbrain dopaminergic neurons show opposite responses to motivationally relevant stimuli (Matsumoto and Hikosaka, 2007). However, the mechanism by which LHb glutamatergic neurons inhibit VTA dopaminergic neurons was unclear. Our data, along with other recently published studies, demonstrates that the LHb negatively modulates VTA dopaminergic neurons via the RMTg, a

recently characterized GABAergic midbrain structure (Barrot et al., 2012; Jhou et al., 2009a, 2009b; Lammel et al., 2011; Matsui and Williams, 2011; Stamatakis and Stuber, 2012). We next demonstrated that exposing an animal to a single aversive event increased excitatory synaptic strength in the LHb-to-RMTg circuit. These data are important because it demonstrates how brief, but salient, negative experiences can have potent long lasting effects on this circuit. I only recorded changes in synaptic strength one hour following the exposure to the aversive event, and thus, future studies could investigate how long this circuit remains potentiated. I then demonstrated that optogenetic activation of this circuit resulted in passive, active, and conditioned behavioral avoidance. Additionally, activation of the LHb-to-RMTg circuit promoted negative reinforcement, and disrupted ongoing positive reinforcement, suggesting that although activation of this circuit is aversive, it promotes motivated behavior to avoid a negative outcome.

The majority of LHb afferents arise from forebrain areas, although the LHb also receives a substantial projection from the VTA (Gruber et al., 2007; Kim and Lee, 2012; Phillipson and Griffith, 1980; Poller et al., 2013; Shabel et al., 2012; Stamatakis et al., 2013; Warden et al., 2012). In this dissertation, I investigated two of these afferents: the lateral hypothalamus and the VTA. I found that a unique population of VTA neurons projects to the LHb and releases GABA, which in turn decreases LHb firing, and increases the spontaneous firing rate of VTA dopaminergic neurons. Additionally, I found that activation of this circuit *in vivo* is rewarding and depends on LHb GABAergic signaling as well as downstream dopaminergic signaling. Although I provided a thorough functional characterization

of the VTA-to-LHb pathway, it still remains unclear how, or when, LHb-projecting VTA dopaminergic neurons are activated. LHb neurons exhibit a high basal firing rate both in slices (**Fig. 3.4**) and *in vivo* (Bromberg-Martin et al., 2010b; Meier and Herrling, 1993). This high basal firing rate likely exerts a tonic inhibitory influence on dopaminergic neurons by activating RMTg GABAergic neurons that directly inhibit VTA dopaminergic neurons. This circuitry may explain why inhibition of the LHb increases dopamine release in the forebrain (Lecourtier et al., 2008). I hypothesize that the phasic dopamine release seen in the NAc in response to motivationally relevant stimuli, at least in part, could require activation of inhibitory afferents to the LHb, thus disinhibiting midbrain dopaminergic neurons. This hypothesis is supported by the decreased firing rate of LHb neurons in response to cues that predict rewards (Matsumoto and Hikosaka, 2007). Data presented here demonstrate that VTA neurons themselves send an inhibitory projection to the LHb, and thus are able to directly inhibit LHb neurons. However, it remains unclear whether LHb-projecting neurons show changes in firing in response to motivationally relevant stimuli. Future studies could use electrophysiology paired with optogenetics to identify and record from genetically-distinct projection-specific neurons in vivo (Jennings et al., 2013a) to investigate if, and if so when, LHb-projecting VTA dopaminergic neurons become activated in response to motivationally-relevant stimuli. It would also be beneficial for future studies to compare these responses to NAc-projecting dopaminergic neurons in the same animals. I hypothesize that LHb-projecting VTA dopaminergic neurons will become activated in response to cues that predict rewards, which would provide a functional explanation for why activation of

this pathway *in vivo* is rewarding. Further, I predict that NAc-projecting VTA dopaminergic neurons will also become activated by reward-predictive cues, but that the response latency between the two populations of neurons will be different.

A significant outstanding question with regards to VTA circuitry is which VTA afferent is providing dopaminergic neurons with reward-related information? It is clear that dopaminergic neurons show increased activation to reward and reward-predictive cues, and this results in phasic dopamine release in the NAc, but it is unclear which VTA afferent is causing this increase in firing. It is also likely that more than one VTA afferent are relaying various aspects of reward to the VTA. For example, the PPTg preferentially responds to auditory stimuli, and thus may be providing dopaminergic neurons with information about reward-predictive auditory cues (Pan and Hyland, 2005). On the other hand, the superior colliculus appears to relay information about visual cues to dopaminergic neurons (Coizet et al., 2003; Comoli et al., 2003; Dommett et al., 2005). Future studies could inhibit select afferents while recording from VTA dopaminergic neurons during a reward-predictive cue to determine which afferent disrupts the cue-evoked spiking of dopaminergic neurons. While it is still unclear which afferent is providing dopaminergic neurons with positive reward prediction error, recent evidence, including data generated in this dissertation, has suggested that the LHb is relaying negative reward prediction error to the VTA (Hong et al., 2011). The LHb conveys negative reward information to the RMTg, which then robustly inhibits VTA dopaminergic neurons. Here, I have shown that activation of LHb glutamatergic inputs to the RMTg promotes aversive behavioral phenotypes. In addition, activation of LH glutamatergic afferents to the

LHb results in a similar behavioral phenotype. Combined, these data suggest that the LH may be providing the LHb with negative reward prediction error, which in turn provides dopaminergic neurons with negative reward-related information via the RMTg. Future studies could address this hypothesis by recording from dopaminergic neurons during negative reward prediction error tasks while simultaneously inhibiting either LH glutamatergic inputs to the LHb, LHb glutamatergic inputs to the RMTg, or RMTg GABAergic inputs to the VTA.

I characterized a population of VTA dopaminergic neurons that project to the LHb and release GABA, but no detectable amounts of dopamine. I targeted these neurons using a mouse line that expresses cre recombinase under a TH promoter. Indeed, I found that these neurons contain TH mRNA and TH protein in the soma, but little TH protein in the terminals. These neurons also express mRNA for other markers for dopaminergic neurons, such as vesicular monoamine transporter, dopamine transporter, and dopamine D2 receptor, but at much lower levels than NAc-projecting dopaminergic neurons. Thus, a significant outstanding question is whether or not these neurons should be characterized as dopaminergic or GABAergic. One possibility is that the phenotype of these neurons is developmentally regulated. It is possible that these neurons release dopamine during development, but then switch to releasing GABA once connectivity has been established. A recent study has demonstrated strong labeling of tyrosine hydroxylase in dopaminergic afferents in the LHb from mouse embryos (Schmidt et al., 2014), and previous studies have shown that certain populations of neurons are

capable of switching their neuronal phenotype (Dulcis et al., 2013; Gómez-Lira et al., 2005; Guemez-Gamboa et al., 2014; Telese et al., 2013).

While the studies from this dissertation have provided pivotal insight into midbrain reward circuitry, it is important to discuss the limitations associated with these methods. One of the main limitations of optogenetics is that the method typically either uniformly excites or inhibits a global population of genetically-distinct and/or projection-specific population of neurons. While this technique provides a general understanding of the causality of a defined circuit, it may not represent the physiological state of the circuit. For example, global activation of LHb glutamatergic inputs to the RMTg produced a robust aversive phenotype (Stamatakis and Stuber, 2012). However, it is possible that when an animal is exposed to an aversive stimulus, there may be subtle differences in either the timing or percentage of neuronal activation. These subtleties are difficult to recapitulate with optogenetics but may have important differences on behavioral output.

Another important caveat of optogenetic projection targeting techniques is that oftentimes afferent fibers are bundled together, and stimulating terminals in one region may also stimulate fibers of passage that are en route to a more distal target region. For example, dopaminergic afferents from the VTA projecting to the mPFC pass through the NAc (Beckstead et al., 1979; Herbert et al., 1997), and stimulation of dopaminergic terminals in the NAc will also likely stimulate mPFC-projecting fibers. Techniques that allow for retrograde delivery of viruses encoding opsins to specific presynaptic inputs may circumvent some of these limitations (Jennings and Stuber, 2014).

Another limitation of optogenetics is the possibility of back-propagating action potentials. Optical stimulation of terminals in one region may lead to back-propagating action potentials that activate the cell bodies, and can then activate afferents projecting to other regions. However, this limitation can be addressed by injecting lidocaine to prevent back propagating action potentials at the level of the cell bodies of the population of neurons that was transduced (Stuber et al., 2011). Even if the targeted population of neurons do not collateralize, it is still important to determine if that population has local effects on network activity. For example, although VTA dopaminergic neurons do not collateralize for the most part (Ford et al., 2006; Lammel et al., 2008; Stamatakis et al., 2013; Swanson, 1982), they do release dopamine locally (Adell and Artigas, 2004), which could be initiated by terminal optical stimulation.

There are also important considerations that should be discussed when using cre-driver lines. Data from this dissertation, as well as a number of recent studies, demonstrate that neurons can have phenotypes that are not consistent with a single neurotransmitter (Root et al., 2014; Shabel et al., 2014; Stuber et al., 2010; Tecuapetla et al., 2010; Tritsch et al., 2012). Recent developments in cre-driver lines may begin to address this issue by utilizing tools to target neurons based on multiple genetic markers (Fenno et al., 2014). In addition, the expression patterns of particular genes and proteins likely vary widely amongst a population of neurons targeted by cre-driver lines. Differences in gene and protein expression likely have functional and physiological consequences, yet cre-mediated recombination does not reflect the differences in endogenous gene expression (Atasoy et al., 2008;

Sohal et al., 2009). Finally, experiments using cre-driver lines often make the assumption that the neuronal population studied remains fixed throughout life. However, recent studies have demonstrated that the phenotype of certain populations of neurons are developmentally, environmentally, and epigenetically regulated (Andersson et al., 2006; Dulcis et al., 2013; Gómez-Lira et al., 2005; Guemez-Gamboa et al., 2014; Matsushita et al., 2002; Scott et al., 2013; Telese et al., 2013).

Finally, as with all circuit-based experiments, it is important to put the particular circuit studied into a broader context of overall neural function and activity. While the techniques used in this dissertation have provided an elegant way to modulate a particular population of genetically-distinct, projection-specific neurons, isolation of a select circuit does not take into account simultaneous neural processing from other afferents or efferents, which likely act in concert to promote various behaviors.

The inherent complexity and heterogeneity of VTA circuitry makes it a technically challenging, but elegant and prolific system to study. The resurgence of neurobiological techniques used to dissect neural circuits has allowed researchers to make great strides in understanding how precise neural circuit elements of reward circuitry contribute to motivated behavior (Jennings and Stuber, 2014). Data generated from this dissertation has increased our understanding of the neural circuitry involved in processing aversive and rewarding stimuli, and may aid in the identification of novel targets for the treatment of addiction and other neuropsychiatric diseases.

REFERENCES

Abler, B., Grön, G., Hartmann, A., Metzger, C., and Walter, M. (2012). Modulation of frontostriatal interaction aligns with reduced primary reward processing under serotonergic drugs. J. Neurosci. Off. J. Soc. Neurosci. *32*, 1329–1335.

Adamantidis, A.R., Tsai, H.-C., Boutrel, B., Zhang, F., Stuber, G.D., Budygin, E.A., Touriño, C., Bonci, A., Deisseroth, K., and de Lecea, L. (2011). Optogenetic interrogation of dopaminergic modulation of the multiple phases of reward-seeking behavior. J. Neurosci. Off. J. Soc. Neurosci. *31*, 10829–10835.

Adell, A., and Artigas, F. (2004). The somatodendritic release of dopamine in the ventral tegmental area and its regulation by afferent transmitter systems. Neurosci. Biobehav. Rev. *28*, 415–431.

Adesnik, H., and Scanziani, M. (2010). Lateral competition for cortical space by layer-specific horizontal circuits. Nature *464*, 1155–1160.

Andersson, E., Tryggvason, U., Deng, Q., Friling, S., Alekseenko, Z., Robert, B., Perlmann, T., and Ericson, J. (2006). Identification of Intrinsic Determinants of Midbrain Dopamine Neurons. Cell *124*, 393–405.

Araki, M., McGeer, P.L., and Kimura, H. (1988). The efferent projections of the rat lateral habenular nucleus revealed by the PHA-L anterograde tracing method. Brain Res. *441*, 319–330.

Aravanis, A.M., Wang, L.-P., Zhang, F., Meltzer, L.A., Mogri, M.Z., Schneider, M.B., and Deisseroth, K. (2007). An optical neural interface: in vivo control of rodent motor cortex with integrated fiberoptic and optogenetic technology. J. Neural Eng. *4*, S143–S156.

Arenkiel, B.R., Peca, J., Davison, I.G., Feliciano, C., Deisseroth, K., Augustine, G.J., Ehlers, M.D., and Feng, G. (2007). In vivo light-induced activation of neural circuitry in transgenic mice expressing channelrhodopsin-2. Neuron *54*, 205–218.

Atasoy, D., Aponte, Y., Su, H.H., and Sternson, S.M. (2008). A FLEX Switch Targets Channelrhodopsin-2 to Multiple Cell Types for Imaging and Long-Range Circuit Mapping. J. Neurosci. *28*, 7025–7030.

Bach, M.E., Barad, M., Son, H., Zhuo, M., Lu, Y.F., Shih, R., Mansuy, I., Hawkins, R.D., and Kandel, E.R. (1999). Age-related defects in spatial memory are correlated with defects in the late phase of hippocampal long-term potentiation in vitro and are attenuated by drugs that enhance the cAMP signaling pathway. Proc. Natl. Acad. Sci. U. S. A. *96*, 5280–5285.

Badrinarayan, A., Wescott, S.A., Vander Weele, C.M., Saunders, B.T., Couturier, B.E., Maren, S., and Aragona, B.J. (2012). Aversive stimuli differentially modulate

real-time dopamine transmission dynamics within the nucleus accumbens core and shell. J. Neurosci. Off. J. Soc. Neurosci. *32*, 15779–15790.

Balcita-Pedicino, J.J., Omelchenko, N., Bell, R., and Sesack, S.R. (2011). The inhibitory influence of the lateral habenula on midbrain dopamine cells: ultrastructural evidence for indirect mediation via the rostromedial mesopontine tegmental nucleus. J. Comp. Neurol. *519*, 1143–1164.

Barrot, M., Sesack, S.R., Georges, F., Pistis, M., Hong, S., and Jhou, T.C. (2012). Braking dopamine systems: a new GABA master structure for mesolimbic and nigrostriatal functions. J. Neurosci. Off. J. Soc. Neurosci. *32*, 14094–14101.

Bass, C.E., Grinevich, V.P., Kulikova, A.D., Bonin, K.D., and Budygin, E.A. (2013). Terminal effects of optogenetic stimulation on dopamine dynamics in rat striatum. J. Neurosci. Methods *214*, 149–155.

Beckstead, M.J., Grandy, D.K., Wickman, K., and Williams, J.T. (2004). Vesicular dopamine release elicits an inhibitory postsynaptic current in midbrain dopamine neurons. Neuron *42*, 939–946.

Beckstead, R.M., Domesick, V.B., and Nauta, W.J. (1979). Efferent connections of the substantia nigra and ventral tegmental area in the rat. Brain Res. *175*, 191–217.

Bernabeu, R., Cammarota, M., Izquierdo, I., and Medina, J.H. (1997). Involvement of hippocampal AMPA glutamate receptor changes and the cAMP/protein kinase A/CREB-P signalling pathway in memory consolidation of an avoidance task in rats. Braz. J. Med. Biol. Res. Rev. Bras. Pesqui. Médicas E Biológicas Soc. Bras. Biofísica Al *30*, 961–965.

Berridge, K.C. (2007). The debate over dopamine's role in reward: the case for incentive salience. Psychopharmacology (Berl.) *191*, 391–431.

Berridge, K.C., and Robinson, T.E. (1998). What is the role of dopamine in reward: hedonic impact, reward learning, or incentive salience? Brain Res. Brain Res. Rev. *28*, 309–369.

Bittencourt, J.C., Presse, F., Arias, C., Peto, C., Vaughan, J., Nahon, J.L., Vale, W., and Sawchenko, P.E. (1992). The melanin-concentrating hormone system of the rat brain: an immuno- and hybridization histochemical characterization. J. Comp. Neurol. *319*, 218–245.

Björklund, A., and Lindvall, O. (1975). Dopamine in dendrites of substantia nigra neurons: suggestions for a role in dendritic terminals. Brain Res. *83*, 531–537.

Bocklisch, C., Pascoli, V., Wong, J.C.Y., House, D.R.C., Yvon, C., de Roo, M., Tan, K.R., and Lüscher, C. (2013). Cocaine disinhibits dopamine neurons by potentiation of GABA transmission in the ventral tegmental area. Science *341*, 1521–1525.

Van Bockstaele, E.J., and Pickel, V.M. (1995). GABA-containing neurons in the ventral tegmental area project to the nucleus accumbens in rat brain. Brain Res. *682*, 215–221.

Bonci, A., Bernardi, G., Grillner, P., and Mercuri, N.B. (2003). The dopamine-containing neuron: maestro or simple musician in the orchestra of addiction? Trends Pharmacol. Sci. *24*, 172–177.

Bourque, M.J., and Trudeau, L.E. (2000). GDNF enhances the synaptic efficacy of dopaminergic neurons in culture. Eur. J. Neurosci. *12*, 3172–3180.

Boyden, E.S., Zhang, F., Bamberg, E., Nagel, G., and Deisseroth, K. (2005). Millisecond-timescale, genetically targeted optical control of neural activity. Nat. Neurosci. *8*, 1263–1268.

Brinschwitz, K., Dittgen, A., Madai, V.I., Lommel, R., Geisler, S., and Veh, R.W. (2010). Glutamatergic axons from the lateral habenula mainly terminate on GABAergic neurons of the ventral midbrain. Neuroscience *168*, 463–476.

Brischoux, F., Chakraborty, S., Brierley, D.I., and Ungless, M.A. (2009). Phasic excitation of dopamine neurons in ventral VTA by noxious stimuli. Proc. Natl. Acad. Sci. U. S. A. *106*, 4894–4899.

Bromberg-Martin, E.S., and Hikosaka, O. (2011). Lateral habenula neurons signal errors in the prediction of reward information. Nat. Neurosci. *14*, 1209–1216.

Bromberg-Martin, E.S., Matsumoto, M., and Hikosaka, O. (2010a). Dopamine in motivational control: rewarding, aversive, and alerting. Neuron *68*, 815–834.

Bromberg-Martin, E.S., Matsumoto, M., and Hikosaka, O. (2010b). Distinct tonic and phasic anticipatory activity in lateral habenula and dopamine neurons. Neuron *67*, 144–155.

Brown, M.T.C., Tan, K.R., O'Connor, E.C., Nikonenko, I., Muller, D., and Lüscher, C. (2012). Ventral tegmental area GABA projections pause accumbal cholinergic interneurons to enhance associative learning. Nature *492*, 452–456.

Caldecott-Hazard, S., Mazziotta, J., and Phelps, M. (1988). Cerebral correlates of depressed behavior in rats, visualized using 14C-2-deoxyglucose autoradiography. J. Neurosci. Off. J. Soc. Neurosci. *8*, 1951–1961.

Cardin, J.A., Carlén, M., Meletis, K., Knoblich, U., Zhang, F., Deisseroth, K., Tsai, L.-H., and Moore, C.I. (2009). Driving fast-spiking cells induces gamma rhythm and controls sensory responses. Nature *459*, 663–667.

Cardin, J.A., Carlén, M., Meletis, K., Knoblich, U., Zhang, F., Deisseroth, K., Tsai, L.-H., and Moore, C.I. (2010). Targeted optogenetic stimulation and recording of

neurons in vivo using cell-type-specific expression of Channelrhodopsin-2. Nat. Protoc. *5*, 247–254.

Carr, D.B., and Sesack, S.R. (2000a). GABA-containing neurons in the rat ventral tegmental area project to the prefrontal cortex. Synap. N. Y. N *38*, 114–123.

Carr, D.B., and Sesack, S.R. (2000b). Projections from the rat prefrontal cortex to the ventral tegmental area: target specificity in the synaptic associations with mesoaccumbens and mesocortical neurons. J. Neurosci. Off. J. Soc. Neurosci. *20*, 3864–3873.

Chaudhury, D., Walsh, J.J., Friedman, A.K., Juarez, B., Ku, S.M., Koo, J.W., Ferguson, D., Tsai, H.-C., Pomeranz, L., Christoffel, D.J., et al. (2013). Rapid regulation of depression-related behaviours by control of midbrain dopamine neurons. Nature *493*, 532–536.

Chevallier, C., Kohls, G., Troiani, V., Brodkin, E.S., and Schultz, R.T. (2012). The social motivation theory of autism. Trends Cogn. Sci. *16*, 231–239.

Di Chiara, G., and Imperato, A. (1988). Drugs abused by humans preferentially increase synaptic dopamine concentrations in the mesolimbic system of freely moving rats. Proc. Natl. Acad. Sci. U. S. A. *85*, 5274–5278.

Ching Liang Shen (1983). Efferent projections from the lateral hypothalamus in the guinea pig: An autoradiographic study. Brain Res. Bull. *11*, 335–347.

Chow, B.Y., Han, X., Dobry, A.S., Qian, X., Chuong, A.S., Li, M., Henninger, M.A., Belfort, G.M., Lin, Y., Monahan, P.E., et al. (2010). High-performance genetically targetable optical neural silencing by light-driven proton pumps. Nature *463*, 98–102.

Christoph, G.R., Leonzio, R.J., and Wilcox, K.S. (1986). Stimulation of the lateral habenula inhibits dopamine-containing neurons in the substantia nigra and ventral tegmental area of the rat. J. Neurosci. *6*, 613–619.

Chuhma, N., Choi, W.Y., Mingote, S., and Rayport, S. (2009). Dopamine neuron glutamate cotransmission: frequency-dependent modulation in the mesoventromedial projection. Neuroscience *164*, 1068–1083.

Chuhma, N., Tanaka, K.F., Hen, R., and Rayport, S. (2011). Functional connectome of the striatal medium spiny neuron. J. Neurosci. Off. J. Soc. Neurosci. *31*, 1183–1192.

Cohen, J.Y., Haesler, S., Vong, L., Lowell, B.B., and Uchida, N. (2012). Neuron-type-specific signals for reward and punishment in the ventral tegmental area. Nature *482*, 85–88.

Coizet, V., Comoli, E., Westby, G.W.M., and Redgrave, P. (2003). Phasic activation of substantia nigra and the ventral tegmental area by chemical stimulation of the

superior colliculus: an electrophysiological investigation in the rat. Eur. J. Neurosci. *17*, 28–40.

Comoli, E., Coizet, V., Boyes, J., Bolam, J.P., Canteras, N.S., Quirk, R.H., Overton, P.G., and Redgrave, P. (2003). A direct projection from superior colliculus to substantia nigra for detecting salient visual events. Nat. Neurosci. *6*, 974–980.

Cruikshank, S.J., Urabe, H., Nurmikko, A.V., and Connors, B.W. (2010). Pathway-specific feedforward circuits between thalamus and neocortex revealed by selective optical stimulation of axons. Neuron *65*, 230–245.

Dahlstroem, A., and Fuxe, K. (1964). EVIDENCE FOR THE EXISTENCE OF MONOAMINE-CONTAINING NEURONS IN THE CENTRAL NERVOUS SYSTEM. I. DEMONSTRATION OF MONOAMINES IN THE CELL BODIES OF BRAIN STEM NEURONS. Acta Physiol. Scand. Suppl. SUPPL 232:1–55.

Dallvechia-Adams, S., Kuhar, M.J., and Smith, Y. (2002). Cocaine- and amphetamine-regulated transcript peptide projections in the ventral midbrain: colocalization with gamma-aminobutyric acid, melanin-concentrating hormone, dynorphin, and synaptic interactions with dopamine neurons. J. Comp. Neurol. *448*, 360–372.

Day, J.J., Roitman, M.F., Wightman, R.M., and Carelli, R.M. (2007). Associative learning mediates dynamic shifts in dopamine signaling in the nucleus accumbens. Nat. Neurosci. *10*, 1020–1028.

DELGADO, J.M.R., and ANAND, B.K. (1953). Increase of food intake induced by electrical stimulation of the lateral hypothalamus. Am. J. Physiol. *172*, 162–168.

Von Der Porten, K., and Davis, J.R. (1979). Weight loss following LH lesions independent of changes in motor activity or metabolic rate. Physiol. Behav. *23*, 813–819.

Dobi, A., Margolis, E.B., Wang, H.-L., Harvey, B.K., and Morales, M. (2010). Glutamatergic and nonglutamatergic neurons of the ventral tegmental area establish local synaptic contacts with dopaminergic and nondopaminergic neurons. J. Neurosci. Off. J. Soc. Neurosci. *30*, 218–229.

Dommett, E., Coizet, V., Blaha, C.D., Martindale, J., Lefebvre, V., Walton, N., Mayhew, J.E.W., Overton, P.G., and Redgrave, P. (2005). How visual stimuli activate dopaminergic neurons at short latency. Science *307*, 1476–1479.

Donello, J.E., Loeb, J.E., and Hope, T.J. (1998). Woodchuck hepatitis virus contains a tripartite posttranscriptional regulatory element. J. Virol. *72*, 5085–5092.

Dulcis, D., Jamshidi, P., Leutgeb, S., and Spitzer, N.C. (2013). Neurotransmitter switching in the adult brain regulates behavior. Science *340*, 449–453.

Edinger, H.M., Kramer, S.Z., and Siegel, A. (1977). Effect of hypothalamic stimulation on mesencephalic neurons. Exp. Neurol. *54*, 91–103.

Fadel, J., and Deutch, A.Y. (2002). Anatomical substrates of orexin-dopamine interactions: lateral hypothalamic projections to the ventral tegmental area. Neuroscience *111*, 379–387.

Fenno, L., Yizhar, O., and Deisseroth, K. (2011). The development and application of optogenetics. Annu. Rev. Neurosci. *34*, 389–412.

Fenno, L.E., Mattis, J., Ramakrishnan, C., Hyun, M., Lee, S.Y., He, M., Tucciarone, J., Selimbeyoglu, A., Berndt, A., Grosenick, L., et al. (2014). Targeting cells with single vectors using multiple-feature Boolean logic. Nat. Methods *11*, 763–772.

Fields, H.L., Hjelmstad, G.O., Margolis, E.B., and Nicola, S.M. (2007). Ventral tegmental area neurons in learned appetitive behavior and positive reinforcement. Annu. Rev. Neurosci. *30*, 289–316.

Floresco, S.B., West, A.R., Ash, B., Moore, H., and Grace, A.A. (2003). Afferent modulation of dopamine neuron firing differentially regulates tonic and phasic dopamine transmission. Nat. Neurosci. *6*, 968–973.

Ford, C.P., Mark, G.P., and Williams, J.T. (2006). Properties and Opioid Inhibition of Mesolimbic Dopamine Neurons Vary according to Target Location. J. Neurosci. *26*, 2788–2797.

Gantz, S.C., Bunzow, J.R., and Williams, J.T. (2013). Spontaneous inhibitory synaptic currents mediated by a G protein-coupled receptor. Neuron *78*, 807–812.

Gasbarri, A., Sulli, A., Innocenzi, R., Pacitti, C., and Brioni, J.D. (1996). Spatial memory impairment induced by lesion of the mesohippocampal dopaminergic system in the rat. Neuroscience *74*, 1037–1044.

Geffen, L.B., Jessell, T.M., Cuello, A.C., and Iversen, L.L. (1976). Release of dopamine from dendrites in rat substantia nigra. Nature *260*, 258–260.

Geisler, S., and Trimble, M. (2008). The lateral habenula: no longer neglected. CNS Spectr. *13*, 484–489.

Geisler, S., and Zahm, D.S. (2005). Afferents of the ventral tegmental area in the rat-anatomical substratum for integrative functions. J. Comp. Neurol. *490*, 270–294.

Geisler, S., Derst, C., Veh, R.W., and Zahm, D.S. (2007). Glutamatergic afferents of the ventral tegmental area in the rat. J. Neurosci. Off. J. Soc. Neurosci. *27*, 5730–5743.

Gómez-Lira, G., Lamas, M., Romo-Parra, H., and Gutiérrez, R. (2005). Programmed and Induced Phenotype of the Hippocampal Granule Cells. J. Neurosci. *25*, 6939–6946.

Gonon, F.G. (1988). Nonlinear relationship between impulse flow and dopamine released by rat midbrain dopaminergic neurons as studied by in vivo electrochemistry. Neuroscience *24*, 19–28.

Goto, Y., and Grace, A.A. (2007). The dopamine system and the pathophysiology of schizophrenia: a basic science perspective. Int. Rev. Neurobiol. *78*, 41–68.

Grace, A.A. (1991). Phasic versus tonic dopamine release and the modulation of dopamine system responsivity: a hypothesis for the etiology of schizophrenia. Neuroscience *41*, 1–24.

Gradinaru, V., Zhang, F., Ramakrishnan, C., Mattis, J., Prakash, R., Diester, I., Goshen, I., Thompson, K.R., and Deisseroth, K. (2010). Molecular and Cellular Approaches for Diversifying and Extending Optogenetics. Cell *141*, 154–165.

Gruber, C., Kahl, A., Lebenheim, L., Kowski, A., Dittgen, A., and Veh, R.W. (2007). Dopaminergic projections from the VTA substantially contribute to the mesohabenular pathway in the rat. Neurosci. Lett. *427*, 165–170.

Guemez-Gamboa, A., Xu, L., Meng, D., and Spitzer, N.C. (2014). Non-cell-autonomous mechanism of activity-dependent neurotransmitter switching. Neuron *82*, 1004–1016.

Gunaydin, L.A., Yizhar, O., Berndt, A., Sohal, V.S., Deisseroth, K., and Hegemann, P. (2010). Ultrafast optogenetic control. Nat. Neurosci. *13*, 387–392.

Harrell, L.E., Decastro, J.M., and Balagura, S. (1975). A critical evaluation of body weight loss following lateral hypothalamic lesions. Physiol. Behav. *15*, 133–136.

Harris, H.W., and Nestler, E.J. (1996). Immunohistochemical studies of mesolimbic dopaminergic neurons in Fischer 344 and Lewis rats. Brain Res. *706*, 1–12.

Heimer, L., Zahm, D.S., Churchill, L., Kalivas, P.W., and Wohltmann, C. (1991). Specificity in the projection patterns of accumbal core and shell in the rat. Neuroscience *41*, 89–125.

Herbert, H., Klepper, A., and Ostwald, J. (1997). Afferent and efferent connections of the ventrolateral tegmental area in the rat. Anat. Embryol. (Berl.) *196*, 235–259.

Hernandez, L., and Hoebel, B.G. (1988). Feeding and hypothalamic stimulation increase dopamine turnover in the accumbens. Physiol. Behav. *44*, 599–606.

Hikosaka, O., Sesack, S.R., Lecourtier, L., and Shepard, P.D. (2008). Habenula: crossroad between the basal ganglia and the limbic system. J. Neurosci. Off. J. Soc. Neurosci. *28*, 11825–11829.

Hnasko, T.S., Chuhma, N., Zhang, H., Goh, G.Y., Sulzer, D., Palmiter, R.D., Rayport, S., and Edwards, R.H. (2010). Vesicular glutamate transport promotes dopamine storage and glutamate corelease in vivo. Neuron *65*, 643–656.

Hnasko, T.S., Hjelmstad, G.O., Fields, H.L., and Edwards, R.H. (2012). Ventral tegmental area glutamate neurons: electrophysiological properties and projections. J. Neurosci. Off. J. Soc. Neurosci. *32*, 15076–15085.

Hoebel, B.G., and Teitelbaum, P. (1962). Hypothalamic Control of Feeding and Self-Stimulation. Science *135*, 375–377.

Hong, S., Jhou, T.C., Smith, M., Saleem, K.S., and Hikosaka, O. (2011). Negative reward signals from the lateral habenula to dopamine neurons are mediated by rostromedial tegmental nucleus in primates. J. Neurosci. Off. J. Soc. Neurosci. *31*, 11457–11471.

Howland, J.G., Taepavarapruk, P., and Phillips, A.G. (2002). Glutamate receptor-dependent modulation of dopamine efflux in the nucleus accumbens by basolateral, but not central, nucleus of the amygdala in rats. J. Neurosci. Off. J. Soc. Neurosci. *22*, 1137–1145.

Ihalainen, J.A., Riekkinen, P., Jr, and Feenstra, M.G. (1999). Comparison of dopamine and noradrenaline release in mouse prefrontal cortex, striatum and hippocampus using microdialysis. Neurosci. Lett. *277*, 71–74.

Ikemoto, S., and Panksepp, J. (1999). The role of nucleus accumbens dopamine in motivated behavior: a unifying interpretation with special reference to reward-seeking. Brain Res. Brain Res. Rev. *31*, 6–41.

Jacobs, B.L., and Azmitia, E.C. (1992). Structure and function of the brain serotonin system. Physiol. Rev. *72*, 165–229.

Jaffe, E.H., Marty, A., Schulte, A., and Chow, R.H. (1998). Extrasynaptic vesicular transmitter release from the somata of substantia nigra neurons in rat midbrain slices. J. Neurosci. Off. J. Soc. Neurosci. *18*, 3548–3553.

Jennings, J.H., and Stuber, G.D. (2014). Tools for Resolving Functional Activity and Connectivity within Intact Neural Circuits. Curr. Biol. CB *24*, R41–R50.

Jennings, J.H., Sparta, D.R., Stamatakis, A.M., Ung, R.L., Pleil, K.E., Kash, T.L., and Stuber, G.D. (2013a). Distinct extended amygdala circuits for divergent motivational states. Nature *advance online publication*.

Jennings, J.H., Rizzi, G., Stamatakis, A.M., Ung, R.L., and Stuber, G.D. (2013b). The inhibitory circuit architecture of the lateral hypothalamus orchestrates feeding. Science *341*, 1517–1521.

Jhou, T.C., Geisler, S., Marinelli, M., Degarmo, B.A., and Zahm, D.S. (2009a). The mesopontine rostromedial tegmental nucleus: A structure targeted by the lateral habenula that projects to the ventral tegmental area of Tsai and substantia nigra compacta. J. Comp. Neurol. *513*, 566–596.

Jhou, T.C., Fields, H.L., Baxter, M.G., Saper, C.B., and Holland, P.C. (2009b). The Rostromedial Tegmental Nucleus (RMTg), a GABAergic Afferent to Midbrain Dopamine Neurons, Encodes Aversive Stimuli and Inhibits Motor Responses. Neuron *61*, 786–800.

Jhou, T.C., Good, C.H., Rowley, C.S., Xu, S.-P., Wang, H., Burnham, N.W., Hoffman, A.F., Lupica, C.R., and Ikemoto, S. (2013). Cocaine drives aversive conditioning via delayed activation of dopamine-responsive habenular and midbrain pathways. J. Neurosci. Off. J. Soc. Neurosci. *33*, 7501–7512.

Ji, H., and Shepard, P.D. (2007). Lateral habenula stimulation inhibits rat midbrain dopamine neurons through a GABA(A) receptor-mediated mechanism. J. Neurosci. Off. J. Soc. Neurosci. *27*, 6923–6930.

Kalivas, P.W., Churchill, L., and Klitenick, M.A. (1993). GABA and enkephalin projection from the nucleus accumbens and ventral pallidum to the ventral tegmental area. Neuroscience *57*, 1047–1060.

Kaufling, J., Veinante, P., Pawlowski, S.A., Freund-Mercier, M.-J., and Barrot, M. (2009). Afferents to the GABAergic tail of the ventral tegmental area in the rat. J. Comp. Neurol. *513*, 597–621.

Kaufling, J., Waltisperger, E., Bourdy, R., Valera, A., Veinante, P., Freund-Mercier, M.-J., and Barrot, M. (2010). Pharmacological recruitment of the GABAergic tail of the ventral tegmental area by acute drug exposure. Br. J. Pharmacol. *161*, 1677–1691.

Kempadoo, K.A., Tourino, C., Cho, S.L., Magnani, F., Leinninger, G.-M., Stuber, G.D., Zhang, F., Myers, M.G., Deisseroth, K., de Lecea, L., et al. (2013). Hypothalamic neurotensin projections promote reward by enhancing glutamate transmission in the VTA. J. Neurosci. Off. J. Soc. Neurosci. *33*, 7618–7626.

Kim, U., and Lee, T. (2012). Topography of descending projections from anterior insular and medial prefrontal regions to the lateral habenula of the epithalamus in the rat. Eur. J. Neurosci. *35*, 1253–1269.

Kim, K.M., Baratta, M.V., Yang, A., Lee, D., Boyden, E.S., and Fiorillo, C.D. (2012). Optogenetic mimicry of the transient activation of dopamine neurons by natural reward is sufficient for operant reinforcement. PloS One *7*, e33612.

Klemm, W.R. (2004). Habenular and interpeduncularis nuclei: shared components in multiple-function networks. Med. Sci. Monit. Int. Med. J. Exp. Clin. Res. *10*, RA261–RA273.

Knable, M.B., and Weinberger, D.R. (1997). Dopamine, the prefrontal cortex and schizophrenia. J. Psychopharmacol. Oxf. Engl. *11*, 123–131.

Koob, G.F. (2013). Addiction is a Reward Deficit and Stress Surfeit Disorder. Front. Psychiatry *4*, 72.

Koob, G.F., and Volkow, N.D. (2010). Neurocircuitry of addiction. Neuropsychopharmacol. Off. Publ. Am. Coll. Neuropsychopharmacol. *35*, 217–238.

Korotkova, T.M., Sergeeva, O.A., Eriksson, K.S., Haas, H.L., and Brown, R.E. (2003). Excitation of ventral tegmental area dopaminergic and nondopaminergic neurons by orexins/hypocretins. J. Neurosci. Off. J. Soc. Neurosci. *23*, 7–11.

Kowski, A.B., Veh, R.W., and Weiss, T. (2009). Dopaminergic activation excites rat lateral habenular neurons in vivo. Neuroscience *161*, 1154–1165.

Kranz, G.S., Kasper, S., and Lanzenberger, R. (2010). Reward and the serotonergic system. Neuroscience *166*, 1023–1035.

Kravitz, A.V., Tye, L.D., and Kreitzer, A.C. (2012). Distinct roles for direct and indirect pathway striatal neurons in reinforcement. Nat. Neurosci. *15*, 816–818.

Kudo, T., Uchigashima, M., Miyazaki, T., Konno, K., Yamasaki, M., Yanagawa, Y., Minami, M., and Watanabe, M. (2012). Three types of neurochemical projection from the bed nucleus of the stria terminalis to the ventral tegmental area in adult mice. J. Neurosci. Off. J. Soc. Neurosci. *32*, 18035–18046.

Lammel, S., Hetzel, A., Häckel, O., Jones, I., Liss, B., and Roeper, J. (2008). Unique properties of mesoprefrontal neurons within a dual mesocorticolimbic dopamine system. Neuron *57*, 760–773.

Lammel, S., Ion, D.I., Roeper, J., and Malenka, R.C. (2011). Projection-specific modulation of dopamine neuron synapses by aversive and rewarding stimuli. Neuron *70*, 855–862.

Lammel, S., Lim, B.K., Ran, C., Huang, K.W., Betley, M.J., Tye, K.M., Deisseroth, K., and Malenka, R.C. (2012). Input-specific control of reward and aversion in the ventral tegmental area. Nature *491*, 212–217.

Lau, C.-I., Wang, H.-C., Hsu, J.-L., and Liu, M.-E. (2013). Does the dopamine hypothesis explain schizophrenia? Rev. Neurosci. *24*, 389–400.

Lecourtier, L., Defrancesco, A., and Moghaddam, B. (2008). Differential tonic influence of lateral habenula on prefrontal cortex and nucleus accumbens dopamine release. Eur. J. Neurosci. *27*, 1755–1762.

Lein, E.S., Hawrylycz, M.J., Ao, N., Ayres, M., Bensinger, A., Bernard, A., Boe, A.F., Boguski, M.S., Brockway, K.S., Byrnes, E.J., et al. (2007). Genome-wide atlas of gene expression in the adult mouse brain. Nature *445*, 168–176.

Li, B., Piriz, J., Mirrione, M., Chung, C., Proulx, C.D., Schulz, D., Henn, F., and Malinow, R. (2011). Synaptic potentiation onto habenula neurons in the learned helplessness model of depression. Nature *470*, 535–539.

Li, K., Zhou, T., Liao, L., Yang, Z., Wong, C., Henn, F., Malinow, R., Yates, J.R., and Hu, H. (2013). βCaMKII in Lateral Habenula Mediates Core Symptoms of Depression. Science *341*, 1016–1020.

Li, S., Cullen, W.K., Anwyl, R., and Rowan, M.J. (2003). Dopamine-dependent facilitation of LTP induction in hippocampal CA1 by exposure to spatial novelty. Nat. Neurosci. *6*, 526–531.

Lisman, J.E., and Grace, A.A. (2005). The hippocampal-VTA loop: controlling the entry of information into long-term memory. Neuron *46*, 703–713.

Lisoprawski, A., Herve, D., Blanc, G., Glowinski, J., and Tassin, J.P. (1980). Selective activation of the mesocortico-frontal dopaminergic neurons induced by lesion of the habenula in the rat. Brain Res. *183*, 229–234.

Liu, Z., Zhou, J., Li, Y., Hu, F., Lu, Y., Ma, M., Feng, Q., Zhang, J.-E., Wang, D., Zeng, J., et al. (2014). Dorsal Raphe Neurons Signal Reward through 5-HT and Glutamate. Neuron *81*, 1360–1374.

Livak, K.J., and Schmittgen, T.D. (2001). Analysis of Relative Gene Expression Data Using Real-Time Quantitative PCR and the 2−ΔΔCT Method. Methods *25*, 402–408.

Lobo, M.K., Covington, H.E., Chaudhury, D., Friedman, A.K., Sun, H., Damez-Werno, D., Dietz, D.M., Zaman, S., Koo, J.W., Kennedy, P.J., et al. (2010). Cell type-specific loss of BDNF signaling mimics optogenetic control of cocaine reward. Science *330*, 385–390.

Lodge, D.J., and Grace, A.A. (2006a). The laterodorsal tegmentum is essential for burst firing of ventral tegmental area dopamine neurons. Proc. Natl. Acad. Sci. U. S. A. *103*, 5167–5172.

Lodge, D.J., and Grace, A.A. (2006b). The hippocampus modulates dopamine neuron responsivity by regulating the intensity of phasic neuron activation. Neuropsychopharmacol. Off. Publ. Am. Coll. Neuropsychopharmacol. *31*, 1356–1361.

Lu, X.Y., Ghasemzadeh, M.B., and Kalivas, P.W. (1998). Expression of D1 receptor, D2 receptor, substance P and enkephalin messenger RNAs in the neurons projecting from the nucleus accumbens. Neuroscience *82*, 767–780.

Lüscher, C., and Malenka, R.C. (2011). Drug-evoked synaptic plasticity in addiction: from molecular changes to circuit remodeling. Neuron *69*, 650–663.

Maeda, H., and Mogenson, G.J. (1981). A comparison of the effects of electrical stimulation of the lateral and ventromedial hypothalamus on the activity of neurons in the ventral tegmental area and substantia nigra. Brain Res. Bull. *7*, 283–291.

Margolis, E.B., Lock, H., Hjelmstad, G.O., and Fields, H.L. (2006). The ventral tegmental area revisited: is there an electrophysiological marker for dopaminergic neurons? J. Physiol. *577*, 907–924.

Margules, D.L., and Olds, J. (1962). Identical “feeding” and “rewarding” systems in the lateral hypothalamus of rats. Science *135*, 374–375.

Markakis, E.A. (2002). Development of the neuroendocrine hypothalamus. Front. Neuroendocrinol. *23*, 257–291.

Matsui, A., and Williams, J.T. (2011). Opioid-sensitive GABA inputs from rostromedial tegmental nucleus synapse onto midbrain dopamine neurons. J. Neurosci. Off. J. Soc. Neurosci. *31*, 17729–17735.

Matsumoto, M., and Hikosaka, O. (2007). Lateral habenula as a source of negative reward signals in dopamine neurons. Nature *447*, 1111–1115.

Matsumoto, M., and Hikosaka, O. (2009a). Representation of negative motivational value in the primate lateral habenula. Nat. Neurosci. *12*, 77–84.

Matsumoto, M., and Hikosaka, O. (2009b). Two types of dopamine neuron distinctly convey positive and negative motivational signals. Nature *459*, 837–841.

Matsuno-Yagi, A., and Mukohata, Y. (1977). Two possible roles of bacteriorhodopsin; a comparative study of strains of Halobacterium halobium differing in pigmentation. Biochem. Biophys. Res. Commun. *78*, 237–243.

Matsushita, N., Okada, H., Yasoshima, Y., Takahashi, K., Kiuchi, K., and Kobayashi, K. (2002). Dynamics of tyrosine hydroxylase promoter activity during midbrain dopaminergic neuron development. J. Neurochem. *82*, 295–304.

McCulloch, J., Savaki, H.E., and Sokoloff, L. (1980). Influence of dopaminergic systems on the lateral habenular nucleus of the rat. Brain Res. *194*, 117–124.

McDonald, A.J. (1992). Projection neurons of the basolateral amygdala: a correlative Golgi and retrograde tract tracing study. Brain Res. Bull. *28*, 179–185.

Meier, C., and Herrling, P. (1993). N-Methyl-D-Asparate induces regular firing patterns in the cat lateral habenula in vivo. Neuroscience *52*, 951–959.

Meister, B. (2007). Neurotransmitters in key neurons of the hypothalamus that regulate feeding behavior and body weight. Physiol. Behav. *92*, 263–271.

Mena-Segovia, J., Winn, P., and Bolam, J.P. (2008). Cholinergic modulation of midbrain dopaminergic systems. Brain Res. Rev. *58*, 265–271.

Mercuri, N.B., Bonci, A., Calabresi, P., Stefani, A., and Bernardi, G. (1995). Properties of the Hyperpolarization-activated Cation Current Ih in Rat Midbrain Dopaminergic Neurons. Eur. J. Neurosci. *7*, 462–469.

Mogenson, G.J., Jones, D.L., and Yim, C.Y. (1980). From motivation to action: Functional interface between the limbic system and the motor system. Prog. Neurobiol. *14*, 69–97.

Morris, J.S., Smith, K.A., Cowen, P.J., Friston, K.J., and Dolan, R.J. (1999). Covariation of activity in habenula and dorsal raphé nuclei following tryptophan depletion. NeuroImage *10*, 163–172.

Nagel, G., Szellas, T., Huhn, W., Kateriya, S., Adeishvili, N., Berthold, P., Ollig, D., Hegemann, P., and Bamberg, E. (2003). Channelrhodopsin-2, a directly light-gated cation-selective membrane channel. Proc. Natl. Acad. Sci. U. S. A. *100*, 13940–13945.

Nair, S.G., Strand, N.S., and Neumaier, J.F. (2012). DREADDing the lateral habenula: A review of methodological approaches for studying lateral habenula function. Brain Res.

Nair-Roberts, R.G., Chatelain-Badie, S.D., Benson, E., White-Cooper, H., Bolam, J.P., and Ungless, M.A. (2008). Stereological estimates of dopaminergic, GABAergic and glutamatergic neurons in the ventral tegmental area, substantia nigra and retrorubral field in the rat. Neuroscience *152*, 1024–1031.

Nauta, W.J., Smith, G.P., Faull, R.L., and Domesick, V.B. (1978). Efferent connections and nigral afferents of the nucleus accumbens septi in the rat. Neuroscience *3*, 385–401.

Nestler, E.J. (2005). Is there a common molecular pathway for addiction? Nat. Neurosci. *8*, 1445–1449.

Nestler, E.J., and Carlezon, W.A., Jr (2006). The mesolimbic dopamine reward circuit in depression. Biol. Psychiatry *59*, 1151–1159.

Newman-Tancredi, A., Cussac, D., Quentric, Y., Touzard, M., Verrièle, L., Carpentier, N., and Millan, M.J. (2002). Differential Actions of Antiparkinson Agents at Multiple Classes of Monoaminergic Receptor. III. Agonist and Antagonist

Properties at Serotonin, 5-HT1 and 5-HT2, Receptor Subtypes. J. Pharmacol. Exp. Ther. *303*, 815–822.

Nirenberg, M.J., Chan, J., Liu, Y., Edwards, R.H., and Pickel, V.M. (1996). Ultrastructural Localization of the Vesicular Monoamine Transporter-2 in Midbrain Dopaminergic Neurons: Potential Sites for Somatodendritic Storage and Release of Dopamine. J. Neurosci. *16*, 4135–4145.

Nishikawa, T., Fage, D., and Scatton, B. (1986). Evidence for, and nature of, the tonic inhibitory influence of habenulointerpeduncular pathways upon cerebral dopaminergic transmission in the rat. Brain Res. *373*, 324–336.

Oakman, S.A., Faris, P.L., Kerr, P.E., Cozzari, C., and Hartman, B.K. (1995). Distribution of pontomesencephalic cholinergic neurons projecting to substantia nigra differs significantly from those projecting to ventral tegmental area. J. Neurosci. Off. J. Soc. Neurosci. *15*, 5859–5869.

O'Connell, L.A., and Hofmann, H.A. (2011). Genes, hormones, and circuits: an integrative approach to study the evolution of social behavior. Front. Neuroendocrinol. *32*, 320–335.

Oertel, W.H., Nitsch, C., and Mugnaini, E. (1984). Immunocytochemical demonstration of the GABA-ergic neurons in rat globus pallidus and nucleus entopeduncularis and their GABA-ergic innervation. Adv. Neurol. *40*, 91–98.

OLDS, J., and MILNER, P. (1954). Positive reinforcement produced by electrical stimulation of septal area and other regions of rat brain. J. Comp. Physiol. Psychol. *47*, 419–427.

Olds, J., and Milner, P. (1954). Positive reinforcement produced by electrical stimulation of septal area and other regions of rat brain. J. Comp. Physiol. Psychol. *47*, 419–427.

Oleson, E.B., Gentry, R.N., Chioma, V.C., and Cheer, J.F. (2012). Subsecond dopamine release in the nucleus accumbens predicts conditioned punishment and its successful avoidance. J. Neurosci. Off. J. Soc. Neurosci. *32*, 14804–14808.

Overton, P., and Clark, D. (1992). Iontophoretically administered drugs acting at the N-methyl-D-aspartate receptor modulate burst firing in A9 dopamine neurons in the rat. Synap. N. Y. N *10*, 131–140.

Packard, M.G., and White, N.M. (1991). Dissociation of hippocampus and caudate nucleus memory systems by posttraining intracerebral injection of dopamine agonists. Behav. Neurosci. *105*, 295–306.

Pan, W.-X., and Hyland, B.I. (2005). Pedunculopontine tegmental nucleus controls conditioned responses of midbrain dopamine neurons in behaving rats. J. Neurosci. Off. J. Soc. Neurosci. *25*, 4725–4732.

Perrotti, L.I., Bolaños, C.A., Choi, K.-H., Russo, S.J., Edwards, S., Ulery, P.G., Wallace, D.L., Self, D.W., Nestler, E.J., and Barrot, M. (2005). DeltaFosB accumulates in a GABAergic cell population in the posterior tail of the ventral tegmental area after psychostimulant treatment. Eur. J. Neurosci. *21*, 2817–2824.

Phend, K.D., Weinberg, R.J., and Rustioni, A. (1992). Techniques to optimize post-embedding single and double staining for amino acid neurotransmitters. J. Histochem. Cytochem. Off. J. Histochem. Soc. *40*, 1011–1020.

Phillips, P.E.M., Robinson, D.L., Stuber, G.D., Carelli, R.M., and Wightman, R.M. (2003a). Real-time measurements of phasic changes in extracellular dopamine concentration in freely moving rats by fast-scan cyclic voltammetry. Methods Mol. Med. *79*, 443–464.

Phillips, P.E.M., Stuber, G.D., Heien, M.L.A.V., Wightman, R.M., and Carelli, R.M. (2003b). Subsecond dopamine release promotes cocaine seeking. Nature *422*, 614–618.

Phillipson, O.T., and Griffith, A.C. (1980). The neurones of origin for the mesohabenular dopamine pathway. Brain Res. *197*, 213–218.

Poller, W.C., Madai, V.I., Bernard, R., Laube, G., and Veh, R.W. (2013). A glutamatergic projection from the lateral hypothalamus targets VTA-projecting neurons in the lateral habenula of the rat. Brain Res.

Rebec, G.V., Christensen, J.R., Guerra, C., and Bardo, M.T. (1997). Regional and temporal differences in real-time dopamine efflux in the nucleus accumbens during free-choice novelty. Brain Res. *776*, 61–67.

Ren, J., Qin, C., Hu, F., Tan, J., Qiu, L., Zhao, S., Feng, G., and Luo, M. (2011). Habenula “cholinergic” neurons co-release glutamate and acetylcholine and activate postsynaptic neurons via distinct transmission modes. Neuron *69*, 445–452.

Robinson, D.L., Phillips, P.E., Budygin, E.A., Trafton, B.J., Garris, P.A., and Wightman, R.M. (2001). Sub-second changes in accumbal dopamine during sexual behavior in male rats. Neuroreport *12*, 2549–2552.

Root, D.H., Mejias-Aponte, C.A., Zhang, S., Wang, H.-L., Hoffman, A.F., Lupica, C.R., and Morales, M. (2014). Single rodent mesohabenular axons release glutamate and GABA. Nat. Neurosci.

Rosin, D.L., Weston, M.C., Sevigny, C.P., Stornetta, R.L., and Guyenet, P.G. (2003). Hypothalamic orexin (hypocretin) neurons express vesicular glutamate transporters VGLUT1 or VGLUT2. J. Comp. Neurol. *465*, 593–603.

Schallert, T., and Whishaw, I.Q. (1978). Two types of aphagia and two types of sensorimotor impairment after lateral hypothalamic lesions: observations in normal weight, dieted, and fattened rats. J. Comp. Physiol. Psychol. *92*, 720–741.

Schmidt, E.R.E., Brignani, S., Adolfs, Y., Lemstra, S., Demmers, J., Vidaki, M., Donahoo, A.-L.S., Lilleväli, K., Vasar, E., Richards, L.J., et al. (2014). Subdomain-Mediated Axon-Axon Signaling and Chemoattraction Cooperate to Regulate Afferent Innervation of the Lateral Habenula. Neuron *83*, 372–387.

Schultz, W. (2007). Multiple dopamine functions at different time courses. Annu. Rev. Neurosci. *30*, 259–288.

Schultz, W., Dayan, P., and Montague, P.R. (1997). A Neural Substrate of Prediction and Reward. Science *275*, 1593–1599.

Schweimer, J.V., and Ungless, M.A. (2010). Phasic responses in dorsal raphe serotonin neurons to noxious stimuli. Neuroscience *171*, 1209–1215.

Scott, B.B., Brody, C.D., and Tank, D.W. (2013). Cellular Resolution Functional Imaging in Behaving Rats Using Voluntary Head Restraint. Neuron *80*, 371–384.

Sesack, S.R., and Pickel, V.M. (1992). Prefrontal cortical efferents in the rat synapse on unlabeled neuronal targets of catecholamine terminals in the nucleus accumbens septi and on dopamine neurons in the ventral tegmental area. J. Comp. Neurol. *320*, 145–160.

Shabel, S.J., Proulx, C.D., Trias, A., Murphy, R.T., and Malinow, R. (2012). Input to the lateral habenula from the basal ganglia is excitatory, aversive, and suppressed by serotonin. Neuron *74*, 475–481.

Shabel, S.J., Proulx, C.D., Piriz, J., and Malinow, R. (2014). Mood regulation. GABA/glutamate co-release controls habenula output and is modified by antidepressant treatment. Science *345*, 1494–1498.

Shen, X., Ruan, X., and Zhao, H. (2012). Stimulation of midbrain dopaminergic structures modifies firing rates of rat lateral habenula neurons. PloS One *7*, e34323.

Shin, L.M., and Liberzon, I. (2010). The Neurocircuitry of Fear, Stress, and Anxiety Disorders. Neuropsychopharmacology *35*, 169–191.

Shumake, J., Edwards, E., and Gonzalez-Lima, F. (2003). Opposite metabolic changes in the habenula and ventral tegmental area of a genetic model of helpless behavior. Brain Res. *963*, 274–281.

Skagerberg, G., Lindvall, O., and Björklund, A. (1984). Origin, course and termination of the mesohabenular dopamine pathway in the rat. Brain Res. *307*, 99–108.

Sohal, V.S., Zhang, F., Yizhar, O., and Deisseroth, K. (2009). Parvalbumin neurons and gamma rhythms enhance cortical circuit performance. Nature *459*, 698–702.

Sparta, D.R., Stamatakis, A.M., Phillips, J.L., Hovelsø, N., van Zessen, R., and Stuber, G.D. (2012). Construction of implantable optical fibers for long-term optogenetic manipulation of neural circuits. Nat. Protoc. *7*, 12–23.

Stamatakis, A.M., and Stuber, G.D. (2012). Activation of lateral habenula inputs to the ventral midbrain promotes behavioral avoidance. Nat. Neurosci. *15*, 1105–1107.

Stamatakis, A.M., Jennings, J.H., Ung, R.L., Blair, G.A., Weinberg, R.J., Neve, R.L., Boyce, F., Mattis, J., Ramakrishnan, C., Deisseroth, K., et al. (2013). A unique population of ventral tegmental area neurons inhibits the lateral habenula to promote reward. Neuron *80*, 1039–1053.

Steinberg, E.E., Keiflin, R., Boivin, J.R., Witten, I.B., Deisseroth, K., and Janak, P.H. (2013). A causal link between prediction errors, dopamine neurons and learning. Nat. Neurosci. *16*, 966–973.

Steinberg, E.E., Boivin, J.R., Saunders, B.T., Witten, I.B., Deisseroth, K., and Janak, P.H. (2014). Positive Reinforcement Mediated by Midbrain Dopamine Neurons Requires D1 and D2 Receptor Activation in the Nucleus Accumbens. PLoS ONE *9*, e94771.

Stephenson, D.T., Li, Q., Simmons, C., Connell, M.A., Meglasson, M.D., Merchant, K., and Emborg, M.E. (2005). Expression of GAD65 and GAD67 immunoreactivity in MPTP-treated monkeys with or without L-DOPA administration. Neurobiol. Dis. *20*, 347–359.

Stephenson-Jones, M., Floros, O., Robertson, B., and Grillner, S. (2012). Evolutionary conservation of the habenular nuclei and their circuitry controlling the dopamine and 5-hydroxytryptophan (5-HT) systems. Proc. Natl. Acad. Sci. U. S. A. *109*, E164–E173.

Sternson, S.M. (2013). Hypothalamic survival circuits: blueprints for purposive behaviors. Neuron *77*, 810–824.

Sternson, S.M., Nicholas Betley, J., and Cao, Z.F.H. (2013). Neural circuits and motivational processes for hunger. Curr. Opin. Neurobiol. *23*, 353–360.

Stuber, G.D., Roitman, M.F., Phillips, P.E.M., Carelli, R.M., and Wightman, R.M. (2005). Rapid dopamine signaling in the nucleus accumbens during contingent and noncontingent cocaine administration. Neuropsychopharmacol. Off. Publ. Am. Coll. Neuropsychopharmacol. *30*, 853–863.

Stuber, G.D., Klanker, M., de Ridder, B., Bowers, M.S., Joosten, R.N., Feenstra, M.G., and Bonci, A. (2008). Reward-predictive cues enhance excitatory synaptic strength onto midbrain dopamine neurons. Science *321*, 1690–1692.

Stuber, G.D., Hnasko, T.S., Britt, J.P., Edwards, R.H., and Bonci, A. (2010). Dopaminergic terminals in the nucleus accumbens but not the dorsal striatum corelease glutamate. J. Neurosci. Off. J. Soc. Neurosci. *30*, 8229–8233.

Stuber, G.D., Sparta, D.R., Stamatakis, A.M., van Leeuwen, W.A., Hardjoprajitno, J.E., Cho, S., Tye, K.M., Kempadoo, K.A., Zhang, F., Deisseroth, K., et al. (2011). Excitatory transmission from the amygdala to nucleus accumbens facilitates reward seeking. Nature *475*, 377–380.

Sulzer, D., Joyce, M.P., Lin, L., Geldwert, D., Haber, S.N., Hattori, T., and Rayport, S. (1998). Dopamine neurons make glutamatergic synapses in vitro. J. Neurosci. Off. J. Soc. Neurosci. *18*, 4588–4602.

Swanson, L.W. (1982). The projections of the ventral tegmental area and adjacent regions: a combined fluorescent retrograde tracer and immunofluorescence study in the rat. Brain Res. Bull. *9*, 321–353.

Takahashi, Y.K., Roesch, M.R., Stalnaker, T.A., Haney, R.Z., Calu, D.J., Taylor, A.R., Burke, K.A., and Schoenbaum, G. (2009). The Orbitofrontal Cortex and Ventral Tegmental Area Are Necessary for Learning from Unexpected Outcomes. Neuron *62*, 269–280.

Tan, K.R., Yvon, C., Turiault, M., Mirzabekov, J.J., Doehner, J., Labouèbe, G., Deisseroth, K., Tye, K.M., and Lüscher, C. (2012). GABA neurons of the VTA drive conditioned place aversion. Neuron *73*, 1173–1183.

Taylor, S.R., Badurek, S., Dileone, R.J., Nashmi, R., Minichiello, L., and Picciotto, M.R. (2014). GABAergic and Glutamatergic Efferents of the Mouse Ventral Tegmental Area. J. Comp. Neurol.

Tecuapetla, F., Patel, J.C., Xenias, H., English, D., Tadros, I., Shah, F., Berlin, J., Deisseroth, K., Rice, M.E., Tepper, J.M., et al. (2010). Glutamatergic signaling by mesolimbic dopamine neurons in the nucleus accumbens. J. Neurosci. Off. J. Soc. Neurosci. *30*, 7105–7110.

Telese, F., Gamliel, A., Skowronska-Krawczyk, D., Garcia-Bassets, I., and Rosenfeld, M.G. (2013). “Seq-ing” Insights into the Epigenetics of Neuronal Gene Regulation. Neuron *77*, 606–623.

Tobler, P.N., Fiorillo, C.D., and Schultz, W. (2005). Adaptive Coding of Reward Value by Dopamine Neurons. Science *307*, 1642–1645.

Tripathi, A., Prensa, L., Cebrián, C., and Mengual, E. (2010). Axonal branching patterns of nucleus accumbens neurons in the rat. J. Comp. Neurol. *518*, 4649–4673.

Tritsch, N.X., Ding, J.B., and Sabatini, B.L. (2012). Dopaminergic neurons inhibit striatal output through non-canonical release of GABA. Nature *490*, 262–266.

Tsai, H.-C., Zhang, F., Adamantidis, A., Stuber, G.D., Bonci, A., de Lecea, L., and Deisseroth, K. (2009). Phasic firing in dopaminergic neurons is sufficient for behavioral conditioning. Science *324*, 1080–1084.

Tye, K.M., and Deisseroth, K. (2012). Optogenetic investigation of neural circuits underlying brain disease in animal models. Nat. Rev. Neurosci. *13*, 251–266.

Tye, K.M., Prakash, R., Kim, S.-Y., Fenno, L.E., Grosenick, L., Zarabi, H., Thompson, K.R., Gradinaru, V., Ramakrishnan, C., and Deisseroth, K. (2011). Amygdala circuitry mediating reversible and bidirectional control of anxiety. Nature *471*, 358–362.

Tye, K.M., Mirzabekov, J.J., Warden, M.R., Ferenczi, E.A., Tsai, H.-C., Finkelstein, J., Kim, S.-Y., Adhikari, A., Thompson, K.R., Andalman, A.S., et al. (2013). Dopamine neurons modulate neural encoding and expression of depression-related behaviour. Nature *493*, 537–541.

Ungless, M.A., Magill, P.J., and Bolam, J.P. (2004). Uniform inhibition of dopamine neurons in the ventral tegmental area by aversive stimuli. Science *303*, 2040–2042.

Usuda, I., Tanaka, K., and Chiba, T. (1998). Efferent projections of the nucleus accumbens in the rat with special reference to subdivision of the nucleus: biotinylated dextran amine study. Brain Res. *797*, 73–93.

Vertes, R.P. (1991). A PHA-L analysis of ascending projections of the dorsal raphe nucleus in the rat. J. Comp. Neurol. *313*, 643–668.

Viggiano, D., Vallone, D., Ruocco, L.A., and Sadile, A.G. (2003). Behavioural, pharmacological, morpho-functional molecular studies reveal a hyperfunctioning mesocortical dopamine system in an animal model of attention deficit and hyperactivity disorder. Neurosci. Biobehav. Rev. *27*, 683–689.

Wanat, M.J., Willuhn, I., Clark, J.J., and Phillips, P.E.M. (2009). Phasic dopamine release in appetitive behaviors and drug addiction. Curr. Drug Abuse Rev. *2*, 195–213.

Wang, H.-L., and Morales, M. (2009). Pedunculopontine and laterodorsal tegmental nuclei contain distinct populations of cholinergic, glutamatergic and GABAergic neurons in the rat. Eur. J. Neurosci. *29*, 340–358.

Warden, M.R., Selimbeyoglu, A., Mirzabekov, J.J., Lo, M., Thompson, K.R., Kim, S.-Y., Adhikari, A., Tye, K.M., Frank, L.M., and Deisseroth, K. (2012). A prefrontal cortex-brainstem neuronal projection that controls response to behavioural challenge. Nature *492*, 428–432.

Watabe-Uchida, M., Zhu, L., Ogawa, S.K., Vamanrao, A., and Uchida, N. (2012). Whole-brain mapping of direct inputs to midbrain dopamine neurons. Neuron *74*, 858–873.

Winn, P., Brown, V.J., and Inglis, W.L. (1997). On the relationships between the striatum and the pedunculopontine tegmental nucleus. Crit. Rev. Neurobiol. *11*, 241–261.

Wise, R.A. (2004). Dopamine, learning and motivation. Nat. Rev. Neurosci. *5*, 483–494.

Wise, R.A. (2005). Forebrain substrates of reward and motivation. J. Comp. Neurol. *493*, 115–121.

Wise, R.A. (2008). Dopamine and reward: the anhedonia hypothesis 30 years on. Neurotox. Res. *14*, 169–183.

Wise, R.A., and Koob, G.F. (2014). The Development and Maintenance of Drug Addiction. Neuropsychopharmacology *39*, 254–262.

Witten, I.B., Lin, S.-C., Brodsky, M., Prakash, R., Diester, I., Anikeeva, P., Gradinaru, V., Ramakrishnan, C., and Deisseroth, K. (2010). Cholinergic interneurons control local circuit activity and cocaine conditioning. Science *330*, 1677–1681.

Witten, I.B., Steinberg, E.E., Lee, S.Y., Davidson, T.J., Zalocusky, K.A., Brodsky, M., Yizhar, O., Cho, S.L., Gong, S., Ramakrishnan, C., et al. (2011). Recombinase-driver rat lines: tools, techniques, and optogenetic application to dopamine-mediated reinforcement. Neuron *72*, 721–733.

Woulfe, J., and Beaudet, A. (1992). Neurotensin terminals form synapses primarily with neurons lacking detectable tyrosine hydroxylase immunoreactivity in the rat substantia nigra and ventral tegmental area. J. Comp. Neurol. *321*, 163–176.

Xia, Y., Driscoll, J.R., Wilbrecht, L., Margolis, E.B., Fields, H.L., and Hjelmstad, G.O. (2011). Nucleus accumbens medium spiny neurons target non-dopaminergic neurons in the ventral tegmental area. J. Neurosci. Off. J. Soc. Neurosci. *31*, 7811–7816.

Yamaguchi, T., Sheen, W., and Morales, M. (2007). Glutamatergic neurons are present in the rat ventral tegmental area. Eur. J. Neurosci. *25*, 106–118.

Yamaguchi, T., Wang, H.-L., Li, X., Ng, T.H., and Morales, M. (2011). Mesocorticolimbic Glutamatergic Pathway. J. Neurosci. *31*, 8476–8490.

Yizhar, O., Fenno, L.E., Davidson, T.J., Mogri, M., and Deisseroth, K. (2011a). Optogenetics in neural systems. Neuron *71*, 9–34.

Yizhar, O., Fenno, L.E., Prigge, M., Schneider, F., Davidson, T.J., O'Shea, D.J., Sohal, V.S., Goshen, I., Finkelstein, J., Paz, J.T., et al. (2011b). Neocortical excitation/inhibition balance in information processing and social dysfunction. Nature *477*, 171–178.

Young, A.M., Joseph, M.H., and Gray, J.A. (1993). Latent inhibition of conditioned dopamine release in rat nucleus accumbens. Neuroscience *54*, 5–9.

Zahm, D.S. (2010). Pharmacotherapeutic approach to the treatment of addiction: persistent challenges. Mo. Med. *107*, 276–280.

Van Zessen, R., Phillips, J.L., Budygin, E.A., and Stuber, G.D. (2012). Activation of VTA GABA neurons disrupts reward consumption. Neuron *73*, 1184–1194.

Zhang, F., Gradinaru, V., Adamantidis, A.R., Durand, R., Airan, R.D., de Lecea, L., and Deisseroth, K. (2010). Optogenetic interrogation of neural circuits: technology for probing mammalian brain structures. Nat. Protoc. *5*, 439–456.

Zhao, S., Ting, J.T., Atallah, H.E., Qiu, L., Tan, J., Gloss, B., Augustine, G.J., Deisseroth, K., Luo, M., Graybiel, A.M., et al. (2011). Cell type–specific channelrhodopsin-2 transgenic mice for optogenetic dissection of neural circuitry function. Nat. Methods *8*, 745–752.